Composite hydrogel - nanofibre vessels for vascular graft applications

by

Yurong Liu (M.Eng.)

Thesis presented to Dublin City University

in fulfilment of the requirements for the degree of

Doctor of Philosophy

Dublin City University

School of Mechanical and Manufacturing Engineering

Supervisor: Dr. Garrett B. McGuinness

Prof. Paul A. Cahill

2010

Declaration

I hereby certify that this material, which I now submit for assessment on the programme of study leading to the award of Doctor of Philosophy is entirely my own work, that I have excercised reasonable care to ensure that the work is original, and does not to the best of my knowledge breach any law of copyright, and has not been taken from the work of others save and to the extent that such work has been cited and acknowledged within the text of my work.

Signed:_____(Yurong Liu)

ID No.:_____ Date:_____

Acknowledgements

First and foremost I would like to thank my supervisors, Dr. Garrett B. McGuinness and Prof. Paul A. Cahill. I am heartily thankful to Garrett for his patience, guidance and support throughout my three-year project. His comments and technical discussions were also invaluable. I am grateful to Paul for his support and discussion in cell culture.

I also want to express my gratitude to the staff of the School of Mechanical and Manufacturing Engineering. Dr. Lisa Looney, Dr. Dermot Brabazon, Dr. Joseph Stokes and Dr. Sumsun Naher have dedicated their time to the management of the Marie Curie project. Dr. Triona Lally offered me access to the compliance test system. I am also appreciative of technicians, Liam Dominican, Michael May, Cian Merne and Eoin Tuohy for their support in ordering research materials and manufacturing hydrogel moulds.

I enjoyed working and having fun with my dear Marie Curie Research Fellows, Diana Garcia Alonso Garcia, Nihal Engin Vrana, Szilvia Eosoly, Marcin Lipowiecki, Irina Pascu and Tamas Szucs. Diana is always like a lovely kid. Engin gave me frequent technical support and he is talent in writing and speaking. Szilvia and Tamas always comes with warm smiles. Marcin and Irina always present their sense of humour. Without them, my life in DCU would not be so enjoyable. I am also happy to work with other fellow PhD students in the School of Mechanical and Manufacturing and Vascular Health Research Centre. Especially, Houman Zahedmanesh gave me great help in the compliance test.

Sincere thanks to Dr. Clement L. Higginbotham, Dr. Luke Geever and Dr. James Kennedy in Athlone Institute of Technology for their assistant in studying the physical

properties of hydrogels.

I wish to thank The Putian Lee Wang Se Al Mei Scholarship. It gave my family great support to prepare my first trip to Ireland.

Thanks also to my Chinese folks, especially Dengli Wang, Qiang Zeng, Jie Zhu and Yan Zhu, for your unforgettable friendship. All of you have made me accomodate better to Ireland.

I would like to express my big thanks to my girlfriend, Juhong Li. She supported me with endless patience and encouragement. It is my luck to have her with me.

Finally, I am forever indebted to my parents for their understanding and unwavering support all my life.

This research has been supported by a Marie Curie Early Stage Research Training Fellowship of the European Community's Sixth Framework Programme under contract number MEST-CT-2005-020621.

Publications and Presentations

Publications

1. Yurong Liu, Luke M. Geever, James E. Kennedy, Clement L. Higginbotham, Paul A. Cahill, Garrett B. McGuinness, Thermal behaviour and mechanical properties of physically crosslinked PVA/Gelatin hydrogels, Journal of the Mechanical Behavior of Biomedical Materials, 2010, volume 3, Pages 203-209.

2. Yurong Liu, Nihal E. Vrana, Paul A. Cahill, Garrett B. McGuinness, Physical crosslinked composite hydrogels of PVA with natural macromolecules: structure, mechanical properties, and endothelial cell compatibility, Journal of Biomedical Materials Research Part B: Applied Biomaterials, 2009, Volume 90B, Pages 492-502.

3. Yurong Liu, Brian Bolger, Paul A. Cahill, Garrett B. McGuinness, Water resistance of photocrosslinked polyvinyl alcohol based fibers, Materials letters, 2009, Volume 63, Issues 3-4, Pages 419-421.

4. Nihal E. Vrana, Yurong Liu, Garrett B. McGuinness, Paul A. Cahill, Characterization of poly(vinyl alcohol)/chitosan hydrogels as vascular tissue engineering scaffolds, Macromolecular Symposia, 2008, Volume 269, Pages 106-110.

5. Garrett B. McGuiness, Nihal E. Vrana, Yurong Liu, Hydrogel processing and fabrication technologies, Chapter in *Novel biomedical hydrogels: biochemistry, manufacture and medical applications*, Woodhead publishing. (In press)

Presentations

1. Yurong Liu, Nihal E. Vrana, Paul A. Cahill, Garrett B. McGuinness, Characterisation of PVA based cryogels with natural polymeric additives for vascular tissue engineering applications, Northern Ireland Biomedical Engineering Society, Belfast, Northern Ireland, 2008.

2. Yurong Liu, Paul A. Cahill, Garrett B. McGuinness, Study on the structure of poly(vinyl alcohol) based hydrogels, 8th World Biomaterials Congress, Amsterdam, Netherlands, 2008.

3. Yurong Liu, Brian Bolger, Paul A. Cahill, Garrett B. McGuinness, Controlled assembly of electrospun tubular scaffolds, 15th Bioengineering in Ireland Conference, Limerick, Ireland, 2009.

4. Yurong Liu, Luke M. Geever, James E. Kennedy, Clement L. Higginbotham, Paul A. Cahill, Garrett B. McGuinness, Thermal behavior and mechanical property of PVA/Gelatin hydrogel scaffolds prepared by freeze-thaw technique and coagulation, TERMIS World Congress, Seoul, South Korea, 2009.

5. Yurong Liu, Paul A. Cahill, Garrett B. McGuinness, Photocrosslinked electrospun PVA-SbQ fibers for vascular tissue engineering scaffolds, TERMIS World Congress, Seoul, South Korea, 2009.

6. Yurong Liu, Paul A. Cahill, Garrett B. McGuinness, Photocrosslinked electrospun PVA-SbQ fibers and its potential as vascular graft, Marie Curie Cutting Edge Practical Training Course: Tissue engineering, stem cells and biocompatibility testing of biomaterials, Aachen, Germany, 2009.

Abstract

A vascular graft should mimic the structure and properties of the native artery which has a layered structure. The media layer of native arteries contributes the main mechanical support to the vessel and the intima layer, lined with endothelial cells, provides a smooth antithrombogenic surface for circulating blood. To mimic this arterial structure and property, this study focused on fabricating a layered vascular graft with hydrogel and fibre layers to match the compliance properties of native arteries, which is a critical property to smooth the pulsatile blood flow in circulation.

Firstly, the feasibility of preparing polyvinyl alcohol (PVA) based hydrogels with controllable mechanical property was investigated. Three PVA based hydrogels were prepared by blending PVA with chitosan, gelatin or starch and by treatment with freeze-thaw cycles and coagulation. The synergistic crosslinking with the freeze-thaw technique and coagulation was found as a versatile method to control the structure and mechanical properties of PVA-based hydrogels.

A further study was focused on the microstructure formation of PVA/Gelatin hydrogel. The results showed that the freeze-thaw cycles increased the strength of hydrogels by growing the crystal domains in the PVA matrix. The coagulation treatment strengthened the mechanical properties of the hydrogels by increasing the overall polymer fraction of the hydrogels.

Polyvinyl alcohol with styrylpyridinium pendent groups (PVA-SbQ) is a photosensitive polymer. PVA-SbQ fibres were fabricated by electrospinning and photocrosslinking techniques. The photocrosslinked PVA-SbQ fibre presented water-insoluble properties. Priliminary endothelial cell culture result showed evidence that the PVA-SbQ fibres could potentially act as a cell lining substrate.

Finally, a duo-layer vascular graft was constructed with one outer layer composed of a PVA based hydrogel and one inner layer of composed of PVA-SbQ fibres. The mechanical properties, especially the compliance, of the as-prepared duo-layer graft were shown to closely match with that of selected native arteries.

Contents

Declaration ii

Acknowledgements iii

Publications and Presentations v

Abstract vii

Table of Contents viii

Nomenclature xiv

List of Figures xvi

List of Tables xxiii

1 Introduction 1

1.1 Bypass surgery 2

1.2 Vascular grafts 2

1.3 PVA hydrogels 4

1.4 Research objectives and methodology 4

2 Literature Review 6

2.1 Introduction 6

2.2 Vascular architecture and biomechanics 6

2.2.1 Vascular architecture 6

2.2.1.1 Intima layer 7
2.2.1.2 Media layer 8
2.2.1.3 Adventitia layer 9
2.2.2 Vascular biomechanics 10
2.3 Vascular grafts 12
2.3.1 Grafts from natural materials 12
2.3.2 Synthetic grafts 12
2.3.3 Compliance mismatch of conventional vascular grafts 14
2.3.4 Comparison of mechanical properties of PVA hydrogel with native vessel 15
2.4 Poly(vinyl alcohol) hydrogel 17
2.4.1 Structure and property of Poly(vinyl alcohol) 17
2.4.2 Synthesis methods of PVA hydrogels 18
2.4.2.1 Crosslinking by chemical agents 19
2.4.2.2 Crosslinking by high energy radiation 19
2.4.2.3 Physical crosslinking 20
2.4.3 Preparation of PVA hydrogels 20
2.4.4 Factors to control the structure and properties of PVA hydrogels 21
2.4.5 Structure of PVA hydrogels 21
2.4.5.1 Characterization techniques 21
2.4.5.2 Structure model 23
2.5 Electrospinning 24
2.5.1 Fundamentals of electrospinning 25
2.5.2 Electrospinning conditions 26
2.5.3 Guided assembly of electrospinning fibres 26
2.5.4 Electrospun fibres as vascular grafts 28
2.5.5 Challenges and approaches 29
2.6 Thesis layout 31

3 Materials and Methods **34**

3.1 Materials 34

3.1.1 Chemicals 34

3.1.2 Equipment 35

3.2 Methods 36

3.2.1 Preparation of hydrogels and fibres 36

3.2.1.1 Preparation of hydrogels 36

3.2.1.2 Preparation of PVA and PVA-SbQ fibres 37

3.2.2 Structural and mechanical properties of PVA based hydrogels 38

3.2.2.1 Equilibrium swelling study 38

3.2.2.2 Rehydration study 41

3.2.2.3 Uniaxial tensile tests 42

3.2.3 The structure formation of PVA/Gelatin hydrogels 42

3.2.3.1 Attenuated total reflectance fourier transform infrared spectroscopy (ATR-FTIR) 42

3.2.3.2 Modulated differential scanning calorimetry (MDSC) 44

3.2.3.3 Dynamic mechanical thermal analysis (DMTA) . . 45

3.2.3.4 Low strain rheological measurements 45

3.2.4 PVA-SbQ fibres 46

3.2.4.1 Photoactivation of PVA-SbQ 46

3.2.4.2 Weight loss measurement 46

3.2.4.3 Scanning electron microscopy (SEM) 46

3.2.4.4 Endothelial cell culture on PVA-SbQ fibres 47

3.2.4.5 Immunofluoresence Staining 47

3.2.4.6 Cell morphology 48

3.2.5 Study on hydrogel/fibre duo-layer construct 48

3.2.5.1 Fabrication of hydrogel/fibre duo-layer film 48

3.2.5.2 Fabrication of hydrogel/fibre duo-layer vessel . . . 49

3.2.5.3 Uniaxial tensile test 50
3.2.5.4 Compliance test 51
3.2.6 Statistical Analysis 53

4 Composite hydrogels of PVA with natural macromolecules 54
4.1 Introduction 54
4.1.1 PVA and chitosan/gelatin/starch blending system 54
4.1.2 Freeze-thawing and coagulation 55
4.1.3 Objective of this study 56
4.2 Results 56
4.2.1 Equilibrium swelling study 56
4.2.2 PVA hydrogel structure 57
4.2.3 Rehydration study and reequilibrium ratio 59
4.2.4 Mechanical properties 60
4.3 Discussion 62
4.3.1 Preconditioning cycle 62
4.3.2 Nonlinearity 64
4.3.3 Reswelling ratio 67
4.4 Summary 69

5 Structure formation of PVA/Gelatin hydrogels 71
5.1 Introduction 71
5.2 Results 72
5.2.1 ATR-FTIR analysis of PVA/Gelatin hydrogels 72
5.2.2 Thermal analysis of the hydrogel systems 74
5.2.3 Crystallinity analysis of the hydrogel systems 74
5.2.4 DMTA analysis of the hydrogel systems 76
5.2.5 Polymer fraction analysis 77
5.2.6 Mechanical analysis of the hydrogel systems 77

5.3 Discussion . . . 79
5.3.1 The effect of thermal treatment . . . 79
5.3.2 The effect of coagulation treatment . . . 80
5.4 Summary . . . 82

6 Fabrication of PVA-SbQ fibres by electrospinning and photocrosslinking 83
6.1 Introduction . . . 83
6.2 Results and discussion . . . 84
6.2.1 Preliminary experiment of electrospun fibres . . . 84
6.2.2 Photosensitivity of PVA-SbQ . . . 85
6.2.2.1 UV-VIS Spectrum . . . 85
6.2.2.2 FTIR . . . 87
6.2.3 Weight loss measurement . . . 87
6.2.4 Fibre morphology . . . 90
6.2.5 Optimization of electrospinning parameters . . . 90
6.2.5.1 Effect of the applied voltage . . . 92
6.2.5.2 Effect of feeding rate . . . 93
6.2.6 Cell attachment on PVA-SbQ fibres . . . 93
6.3 Summary . . . 99

7 PVA based hydrogel and fibres duo-layer construct 100
7.1 Introduction . . . 100
7.2 Results . . . 101
7.2.1 Uniaxial tensile test . . . 101
7.2.2 Compliance test . . . 103
7.3 Discussion . . . 107
7.3.1 Nonlinearity . . . 107
7.3.2 Effect of coagulation treatment . . . 109
7.3.3 Effect of fibres layer . . . 111

7.3.4 Compliance test 112
7.4 Summary 115

8 Conclusions and future work **117**
8.1 Conclusions 117
8.2 Perspectives and future work 118
8.2.1 Duo-layer constructs as vascular grafts 118
8.2.2 PVA based hydrogel developments 120
8.2.3 Alignment of electrospun fibres 121
8.2.4 Biocompatibility testing 121

Bibliography **123**

Appendix **147**

Nomenclature

1-bcb	1 freeze-thaw cycle and before coagulation bath
3-acb	3 freeze-thaw cycles and after coagulation bath
ANOVA	Analysis of variance
BSA	Bovine serum albumin
C	compliance
CPU	Poly(carbonate) polyurethane
CVD	Cardiovascular disease
Dacron	Polyethylene terepthalate
DAPI	4'-6-Diamidino-2-phenylindole
DMTA	Dynamic mechanical thermal analysis
DSC	Differential Scanning Calorimetry
EC	Endothelial cells
ePTFE	Expanded polytetrafluoroethylene
f-actin	Filamentous actin
FCS	Fetal calf serum
FITC	Fluorescein isothiocyanate
FT	Freeze-thaw cycle
FTIR	Fourier Transform Infrared
G'	Storage modulus
KOH	Potassium Hydroxide
Na2SO4	Sodium Sulphate

P	polyvinyl alcohol
PC	Polyvinyl alcohol/Chitosan hydrogels
PG	Polyvinyl alcohol/Gelatin hydrogels
PS	Polyvinyl alcohol/Starch hydrogels
PTFE	polytetrafluoroethylene
PVA	Polyvinyl alcohol
PU	Polyurethane
SbQ	4-styrylpyridinium groups
SEM	Scanning electron microscope
SMC	Smooth muscle cells
Tg	Glass transition temperature
Tm	Melting temperature
UV	Ultraviolet
cm	Centimetre
h	Hour
kV	Kilovolt
M	Molar
ml	Millilitre
mm	Millimetre
um	Micrometre
W	Watt

List of Figures

1.1 Schematics of bypass surgeries. (A) Coronary artery bypass (Image obtained from www.medmovie.com); (B) Femoral popliteal bypass (Image obtained from Healthwise, Incorporated) 3

2.1 Structure of literature review. 7

2.2 Diagram of the major components of a healthy elastic artery composed of three layers: intima, media, adventitia. 8

2.3 Mechanical separation of the layers of human external iliac artery into a stiff media-intima tube (left) and a limp adventitia (right). 9

2.4 Illustration of the J-shape stress-strain curve of blood vessel. 11

2.5 Compliance-pressure curves of artery, vein, CPU, Dacron and ePTFE. (Dacron–polyethylene terepthalate, ePTFE–expended polytetrafluoroethylene, CPU–polycarbonate polyurethanes). 15

2.6 Stress-strain curves of PVA hydrogels and porcine aorta. PVA hydrogels were prepared with 1, 2, 3, 4, 5 and 10 freeze-thaw cycles. Data from a fresh porcine aorta are plotted as dashed lines. The inset shows the low strain range of the same stress-strain curve. 16

2.7 The stress-strain curves of anisotropic PVA hydrogels and aorta. PVA hydrogels were prepared with 75% initial strain and 3 freeze-thaw cycles which closely match the stress-strain curve of aorta in both the circular and axial direction. 17

2.8 PVA chemical structure. 18

2.9 Crosslinking by high energy radiation. 19
2.10 The crystallites generated within network structure of freeze/thawed PVA gels 21
2.11 General thermogram of the formation of PVA hydrogel. T_i–initial temperature; T_0–freezing point; T_s-temperature at which the sample is stored in frozen state. 23
2.12 Schematic of the structure formation of the PVA hydrogels. The dimension of the crystallites is about 3nm, and the average distance between crystallites is about 19nm. 24
2.13 Schematic of the setup of electrospinning system. 25
2.14 Diagrams of fibre formation during electrospinning. A) The drop shape without presence of a high voltage; B) Jet initiated; C) Jet instability and elongation; D) Dried fibre deposited on collector. Image A and B are adapted from a review by Greiner et al. Image C is adapted from a study by Yarin et al. 26
2.15 Parameters of electrospinning process. Adapted from Ramakrishna et al. 27
2.16 The effect of processing parameters on the diameter of fibres based on systematic parameter study by Tan et al. 27
2.17 Schematics of electrospinning set-ups for fibre assembly. (A) Parallel electrodes collector; (B) Rotating drum collector; (C) Rotating wire drum collector; (D) Rotating drum collector wires wound circumferentially; (E) Rotating tube collector with knife-edge electrodes below; (F) Rotating tube collector with knife-edge bar below and blade attached to needle. 28
2.18 Micrographs of smooth muscle cell growth on aligned electrospun fibres and tissue culture plate. (A) aligned electrospun fibres; (B) tissue culture plate. 29

2.19 SEM images of fibre alignment over various durations of electrospinning. (A) 5min; (B) 15min; (C) 2.5h. 30
2.20 Structure of literature review and the thesis layout. 33

3.1 Preparation of PVA based hydrogels. 37
3.2 Hydrogel casting moulds. (A) Flat plastic mould; (B) Plane glass mould with spacers; (C) Tubular mould to prepare hydrogel vessel graft. 38
3.3 Electrospinning set-up. Collector-1, square collector covered with Aluminium foil; Collector-2, Glass slides collector; Collector-3, Collector assembled by metal wires; Collector-4: Rotating mandrel as collector. 39
3.4 Photocrosslinking set-up. 39
3.5 Hydrogels samples for uniaxial tensile test. (A) Dog-bone hydrogel samples; (B) Dog-bone sample before and after tensile test. Note that the hydrogel samples were griped with abrasive paper to prevent slippage during loading. 43
3.6 Stretching of hydrogel samples in uniaxial tensile test. 43
3.7 Schematic diagram of fabrication of hydrogel/fibre duo-layer film. . . 49
3.8 Schematic diagram of fabrication of hydrogel/fibre duo-layer vessel.Note that the PVA-SbQ fibres were manually covered onto the stainless steel mandrel in this study. 50
3.9 Typical profile of pressure versus time and displacement versus time in compliance test. The control on the frequency of pusatile flow was of concern and therefore the profiles were ploted without specific time on x-axis. 52

4.1 The equilibrium swelling of PVA based hydrogels (n=4). 57
4.2 The rehydration profiles of PVA based hydrogels (n=3). 59
4.3 The effect of freeze-thaw cycles and coagulation treatments on PVA hydrogels (n=6). 61

4.4 The effect of freeze-thaw cycles and coagulation treatments on PVA/Chitosan hydrogels (n=6). 62
4.5 The effect of freeze-thaw cycles and coagulation treatments on PVA/Gelatin hydrogels (n=6). 63
4.6 The effect of freeze-thaw cycles and coagulation treatments on PVA/Starch hydrogels (n=6). 63
4.7 Preconditioning cycles in tensile test on a hydrogel sample. Arrows represent loading and unloading. 65
4.8 The tension-length profile of human iliac artery and its main components, elastin and collagen. Trypsin digestion removed elastin and remained collagen fibres. Formic-acid digestion removed collagen and remained elastin fibres. 65
4.9 Secant modulus of PVA based hydrogels at 40% strain (n=6). 67
4.10 The reequilibrium swelling ratio of PVA based hydrogels. 68

5.1 FTIR spectra of PVA, gelatin and PVA/Gelatin hydrogels. 72
5.2 MDSC thermograms of PVA and PVA/Gelatin hydrogels with 1 freeze-thaw cycle. 75
5.3 DSC thermograms of PVA/Gelatin dried hydrogels. 75
5.4 Tan delta of PVA/Gelatin dried hydrogels. 76
5.5 The polymer fraction of PVA/Gelatin hydrogels (n=4). 77
5.6 Storage modulus of PVA/Gelatin hydrogels in rheological measurement (n=3). 78
5.7 The ultimate strengths of PVA/Gelatin hydrogels in uniaxial tensile test (n=6). 79

6.1 Schematic of the [2+2] cycloaddition reation of PVA-SbQ 84
6.2 Morphology of PVA electrospun fibres. (A) Without contact with water; (B) Briefly immersed in water and dried out immediately. 85
6.3 Absorption spectra of 3.3% PVA-SbQ and 10% PVA-SbQ. 86

6.4 ATR-FTIR spectra of PVA fibre exposed to UV light for 0 min, 5 min and 10 min. PVA has been shown as control. (A) IR spectra in 4000-400 cm^{-1}; (B) IR spectra in 1500-900 cm^{-1}. The band of at 1626 cm^{-1} was assigned to the C=C bonds of styrylpyridinium pendent groups and the enhancement at band 1652 cm^{-1} indicated the reaction of [2+2] cycloaddition. 88

6.5 Mass loss of PVA, PVA-SbQ and PVA-SbQ-hv fibres (n=4). Data are presented as mean ± S.D. *p<0.001, significant differences from the PVA and PVA-SbQ fibres. 89

6.6 SEM micrographs of PVA, PVA-SbQ and PVA-SbQ-hv fibres. (A) PVA fibres with a trace of water drop, (B) PVA-SbQ fibres with a trace of water drop, (C) PVA-SbQ-hv fibres during water immersion (label "W" refers to the position of the trace of water drop) 91

6.7 The schematic of wired assembled collector. Solid lines are wires and the dot line represent the edge of collector. 92

6.8 SEM micrographs of each run of the design of experiment, bar=100μm. (A)Run 2, 10kV, 0.2 mL/h; (B) Run 3, 15kV, 0.2 mL/h; (C) Run 5, 10kV, 0.35mL/h; (D) Run 6, 15kV, 0.35mL/h; (E) Run 8, 10kV, 0.5 mL/h; (F) Run 9, 15kV, 0.5 mL/h. 94

6.9 SEM micrographs showing the effect of applied voltage on the structure in the electrospun PVA-SbQ fibres. (A) 10kV; (B) 15kV. 95

6.10 Immunofluoresence staining of endothelial cell attachment on PVA-SbQ fibres (bar=50 μm). (A) Immunofluoresence stainning image, DAPI stains cell nucleus in blue and Phalloidin-FITC stains F-actin and electrospun fibre in green. (B) Light microscope image, as control. 96

6.11 Morphology of endothelial cell attached on PVA-SbQ fibres. (A) light microscope image; (B) scanning electronic microscopy image. 97

6.12 Morphology of the endothelial cell attached on PVA-SbQ electrospun fibres. (A) Cell-cell contact on fibres; (B) Cell hanging on fibres. . . . 98

7.1 Stress-strain profile of 1mm thick PG hydrogel with 1freeze-thaw cycle and 15 min coagulation. 102
7.2 Stress-strain profile of 1mm thick PG hydrogel with 1 freeze-thaw cycle and 30 min coagulation. 102
7.3 Stress-strain profile of 1 mm thick PG hydrogel with 1 freeze-thaw cycle and 60 min coagulation. 103
7.4 Stress-strain profile of 2 mm thick PG hydrogel with1 freeze-thaw cycle and 15 min coagulation. 104
7.5 Stress-strain profile of 2 mm thick PG hydrogel with 1 freeze-thaw cycle and 30 min coagulation. 104
7.6 Stress-strain profile of 2 mm thick PG hydrogel with 1 freeze-thaw cycle and 60 min coagulation. 105
7.7 Stress-strain profile of 2 mm hydrogel/fibre duo-layer construct with 1 freeze-thaw cycle and 60 min coagulation. 105
7.8 Compliance-mean pressure profile of PG hydrogel with 1freeze-thaw cycle and 60 min dynamic coagulation. 106
7.9 Compliance-mean pressure profile of PG hydrogel and hydrogel/fibre duo-layer vessels. 108
7.10 Stress-strain profile of five pig aortas. (data redrawn from Prendergast et al. 109
7.11 Thickness of hydrogel changed when increasing coagulation duration. The thickness of hydrogel before submerging in coagulation bath was 2 mm (dash-dot line). 110
7.12 The relationship between the compliance of various vascular grafts versus patency rate. 112

7.13 The comparison of compliance-mean pressure profile of the hydrogel/fibre duo-layer graft, human femoral artery and PTFE graft. (A) PG hydrogel / PVA-SbQ fibre duo-layer graft. (B) Human femoral artery and PTFE graft (this data is adapted from Salacinski et al.). . . 114

7.14 Creeping of statically coagulated PG hydrogel at the mean pressure of 140 mmHg. The control on the frequency of pusatile flow was of concern and therefore the displacement-time profile were ploted without specific time on x-axis. 115

8.1 VWR thermal circulator 1187P. 120

8.2 Aligned fibres on wire collector of electrospinning. (A) 200 magnification; (B) 5000 magnification. 122

8.3 A helically assembled stent. (Image obtained from www. bostonscientific. com) 122

List of Tables

2.1 Compliance and cumulative patency of arterial grafts. 14

2.2 Factors to tune the final properties of PVA hydrogels. Adapted from Lozinsky's review. 22

3.1 Percentage weight per volume ratio of the composition of polymer solutions. 37

3.2 Samples for uniaxial tensile test. 50

4.1 Network structure properties of PVA hydrogels 58

5.1 Assignment of the FTIR peak of PVA. 73

5.2 Assignment of the FTIR peak of gelatin. 73

5.3 A summary of testing results. 80

Chapter 1

Introduction

Cardiovascular disease (CVD) refers to the class of diseases related to heart or blood vessels. It remains as one of the most significant health challenges. In USA, the mortality rate from CVD was 278.9 per 100,000 population in 2005, which can be translated as 1 American death from CVD every 37 seconds [1]. Mortality from CVD in Ireland was 214.0 per 100,000 population in 2002 [2]. In European countries, each year there were over 4.35 million deaths resulting from CVD, which account for 49% of all deaths [3]. It was estimated that CVD costs the European Union (EU) economy €169 billion every year [3]. The burden of CVD remains high despite the fact that a decline of mortality rate of CVD was reported from 1995 to 2005 [1].

Many of the patients with CVD had other cocurrent arterial diseases, such as peripheral arterial disease and cerebrovascular disease. It was reported that about 29% of patients with CVD had cocurrent peripheral arterial disease and 20% had cocurrent cerebrovascular disease [4].

Nowadays an increasing number of patients with arterial diseases can be treated by pharmaceuticals and minimally invasive techniques. However, the demand for vessel reconstruction by grafting methods remains significant, especially in treating complex arterial disease or cases in which minimal invasive treatments have failed [5].

1.1 Bypass surgery

The arteries that serve the heart muscle and other parts of human body can be blocked by plaque build-up. This can slow or stop the flow of oxygen-rich blood to heart muscle and organs, leading to muscle necrosis and ischemia. When long lesion of arteries happens, a bypass surgery is necessary. The bypass surgery uses vessel grafts to bypass the obstruction and improve the blood supply to the heart muscle and organs. In each surgery, several arteries may need to be bypassed. A schematic of a coronary artery bypass and a femoral popliteal bypass is shown in Figure 1.1.

1.2 Vascular grafts

The gold standard for vessel graft is the autologous saphenous vein taken from another part the body, most often from the leg. Although successful, grafting with autologous grafts faces a supply deficit due to limited donor locations in the body and also a lack of suitable vessels in elderly or diseased patients. The increasing demand for vascular grafts has driven the development of grafts from synthetic materials, such as polyethylene terepthalate (PET, Dacron), polytetrafluoroethylene (PTFE, Teflon) and polyurethanes (PU). However, the elastic or compliance properties of commercially available synthetic grafts are significantly different from those of native vessels. This mismatch of compliance at the junction of graft and artery has been postulated to cause the formation of neointimal hyperplasia or thrombosis [6], which leads to the disappointing long-term patency and eventual failure of grafting. Consequently, the development of new vascular grafts is aimed at achieving a compliant graft to mimic native arteries.

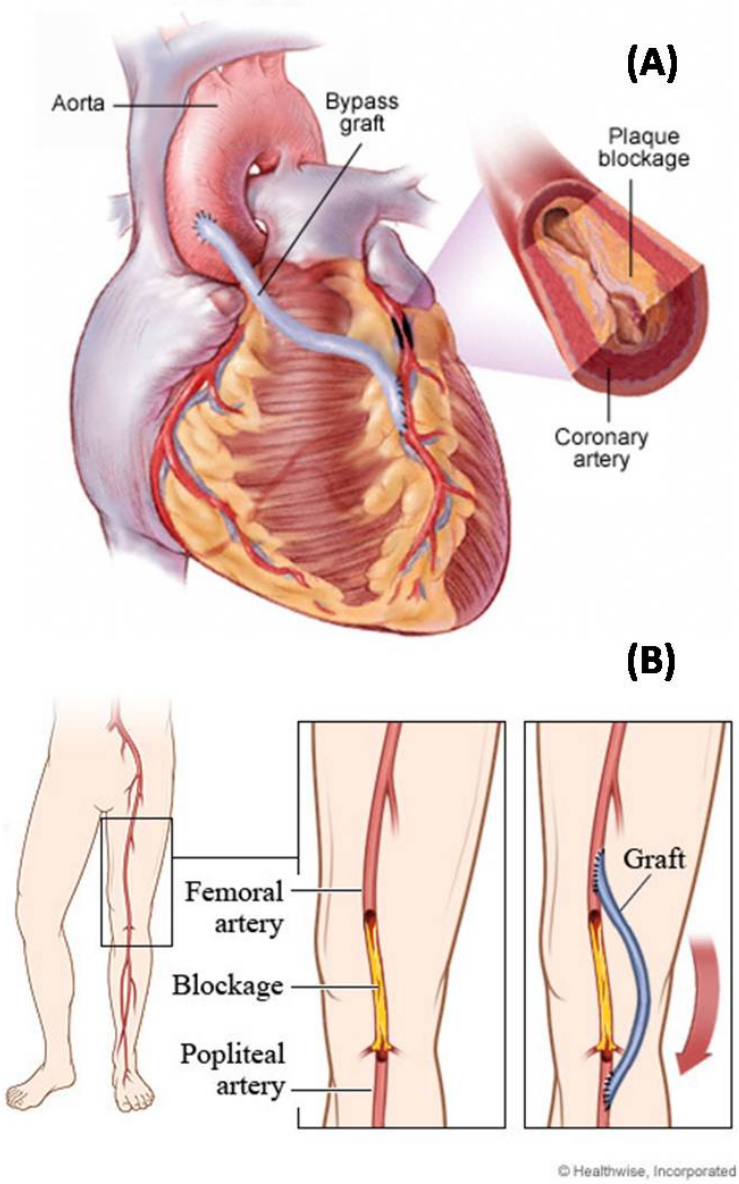

Figure 1.1: Schematics of bypass surgeries. (A) Coronary artery bypass (Image obtained from www.medmovie.com); (B) Femoral popliteal bypass (Image obtained from Healthwise, Incorporated)

1.3 PVA hydrogels

Polyvinyl alcohol (PVA), as a synthetic polymer, has attracted attention as a potential biomaterial for artificial blood vessels because it can be fabricated as a hydrogel, and can match the mechanical properties of the vascular system. For example, Wan et al. [7] have optimized the tensile properties of PVA hydrogels to match those of the porcine aortic root. Chu and Rutt [8] have applied PVA hydrogel structures as vessel phantoms due to the similarity of mechanical and acoustic properties between the PVA hydrogel and porcine aortas. Millon et al. [9] demonstrated that the mechanical properties of the porcine aorta can be closely matched by an anisotropic PVA conduit. These studies have established PVA hydrogels as potentially good vessel substitute candidates in terms of mechanical characteristics.

1.4 Research objectives and methodology

PVA hydrogels formed by cryogelation have poor cell attachment properties. Hence, previous work has investigated the development of PVA/Chitosan hydrogel as a candidate for vascular grafts. PVA/Chitosan hydrogels have been reported to be suitable for the adherence of endothelial cells and their mechanical properties are comparable to porcine arteries[10, 11].

Healthy native arteries are composed of three layers: intima, media, and adventia [12, 13]. In the intima layer, the lining of endothelial cells provides a smooth antithrombogenic surface for circulating blood. A subendothelial tissue plays a critical role in the attachment of endothelial cells. The media layer provides the necessary structural integrity and strength of blood vessels. In contrast, the adventia layer contributes much less mechanical support to the vessel in comparison with the media layer. Accordingly, a vascular graft would preferably be fabricated into a layered construct. Multiple layered tissue engineered blood vessels have been constructed using fibrin hydrogels [14], and also using sequential electrospinning techniques [15].

Based on the previous work on PVA/Chitosan hydrogels and the concept of multilayer artery construction, the main concern of this research was to combine both the merits of PVA based hydrogels and nanofibres by constructing hydrogel/fibres duo-layer graft for vascular applications. The PVA based hydrogel was to mimic the media layer which supplies the mechanical properties for native blood vessel and the PVA-based fibres were to conduct endothelial cell attachment. Thereafter, a two-layer vascular graft, PVA based hydrogel as outer layer and PVA based fibre as inner layer, were constructed.

To accomplish this design of vascular graft, some hypotheses are listed as follow.

1. That the mechanical and structural properties of composite hydrogels of PVA with a selection of candidate natural macromolecules (which, unlike PVA, are conducive to cell attachment) can be closely controlled by the freeze-thaw and coagulation bath parameters.

2. That PVA-based fibres, fabricated by the electrospinning technique, would be stable in aqueous environments and be conducive to endothelial cell attachment.

3. That a final duo-layer construct vessel can be fabricated whose mechanical properties (specifically compliance) closely match those of native arteries over a wide range of mean blood pressures.

Chapter 2

Literature Review

2.1 Introduction

This literature review is structured as into four main sections as shown in Figure 2.1. These are (i) vascular architecture and biomechanics, (ii) vascular grafts, (iii) polyvinyl alcohol hydrogels and (iv) electrospinning.

2.2 Vascular architecture and biomechanics

2.2.1 Vascular architecture

The common strategies of vascular tissue engineering involve developing vascular grafts by mimicking the structure and function of native vessels. It is therefore important to understand the architecture of the vessel wall.

All healthy arteries are composed of three distinct tissue layers, the intima, media and adventitia [12, 13], Figure 2.2 shows a diagram of the major components of arteries. Generally, there are two categories of arteries; elastic and muscular [16]. Elastic arteries are those arteries with media containing both smooth muscle cells and many elastic laminae. Often, elastic arteries are large in diameter. Arteries located more peripherally have smaller diameters and contain less elastic laminae, and are therefore

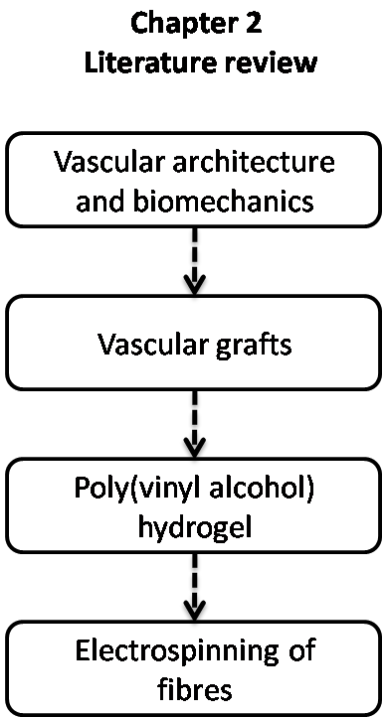

Figure 2.1: Structure of literature review.

called muscular arteries. A brief description of each tissue layer of the arterial vessel is included below to introduce the overall structure of arterial vessel wall. More detailed studies on the macroscopic and microscopic structure of vessel wall have been published by Clark and Glagov [17], Rhodin and Bohr [16] and Silver et al. [18].

2.2.1.1 Intima layer

The intima is the innermost layer of the vessel wall. It consists of monolayer endothelial cells, a basal membrane and subendothelial connective tissue [18]. Endothelial cells are in direct contact with blood and rest on the basal membrane. These cells are flat and elongated to the direction of blood flow. They are held together by junction complexes, which ensure blood flow without thrombosis. Beneath the basal membrane is the subendothelial connective tissue, which develops gradually with age or pathologically with disease. In infants or young adults, the intima plays an insignificant role in the mechanical properties of vessel walls. In middle age, the internal elastic lamina becomes thicker and affects mechanical properties [16]. The pathological changes

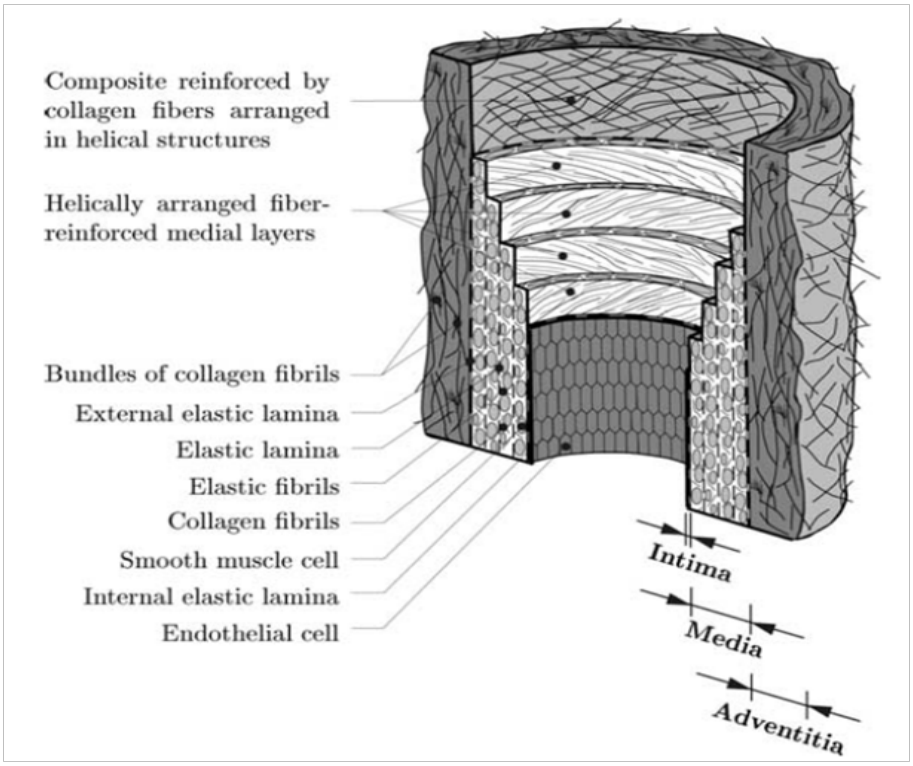

Figure 2.2: Diagram of the major components of a healthy elastic artery composed of three layers: intima, media, adventitia[12].

in the intima layer tends to result in deposition of fatty substances, calcium, collagen fibres, cellular waste products and fibrin, which is consequently associated with the most common artery disease, atherosclerosis [12].

2.2.1.2 Media layer

The media is the middle layer of the vessel wall. It can be distinguished from the intima and adventitia by the internal elastic lamina and external elastic lamina, respectively. The media consists of smooth muscle cells, a number of elastic lamina, bundles of collagen fibrils and a network of elastic fibrils [12]. Rhodin and Bohr [16] further conclude that smooth muscle cells are the only cells present in the media, and that they closely contact with collagen fibrils, elastic fibrils and elastic laminae, and form together a continuous fibrous helix. The helix has different pitch in different elastic lamina. Therefore, these helically arranged fibre-reinforced medial layers can resist forces acting in both the longitudinal and circumferential directions. The media is the

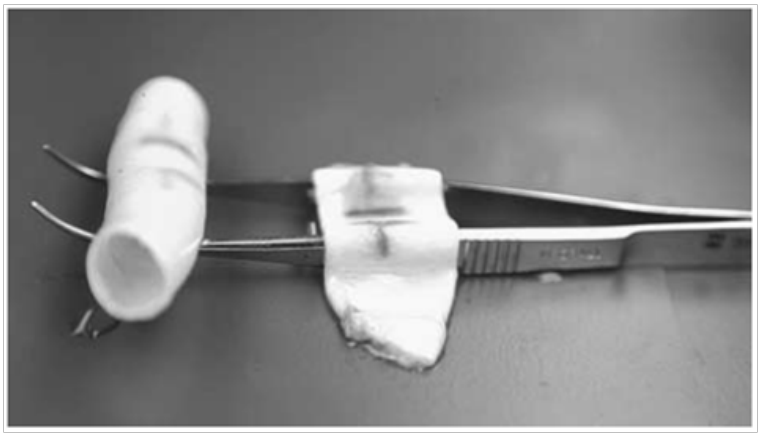

Figure 2.3: Mechanical separation of the layers of human external iliac artery into a stiff media-intima tube (left) and a limp adventitia (right) [12].

layer which primarily determines the mechanical properties of healthy arteries. In the aorta, the media can reach 500 μm in thickness and this reduces as arteries become more peripheral.

2.2.1.3 Adventitia layer

The adventitia is the outermost layer of the vessel wall. It is composed of fibroblasts, fibrocytes, large-diameter collagen fibrils, the micro-vascular supply, and a neural network that regulates the vasotone of the blood vessel [18, 19]. Clark and Glagov [17] reported a collagen network which is interlaced in the manner of a helix, the so-called "Chinese finger trap". The helically arranged collagen fibrils serve to stabilize vessel structure [12]. At low blood pressure, the adventitia layer contributes much less to the mechanical resistance of the vessel wall in comparison with the medial layer. However, when reaching higher pressure levels, the adventitia helps to increase vessel stiffness and prevent the vessel from overstretch and rupture. Schulze-Bauer [12] was able to separate the layers of the human external iliac artery into a media-intima tube and a limp adventitia (see Figure 2.3).

2.2.2 Vascular biomechanics

The artery is the conduit to maintain the pressure of pulsatile blood flow and distribute blood to the various tissues in the body. The mechanical properties of the vessel are of great importance to energy-efficient pulsatile blood flow and to withstanding the stress and strain imparted [6, 18]. To design a vascular graft requires a fundamental understanding of the mechanical properties of vessels.

Viscoelasticity and nonlinearity are the most significant mechanical properties of arterial walls. Elastic solids strain instantaneously when extended and regain their original dimensions when the stress is removed. Viscous fluids exhibit a constant rate of strain when a constant stress is applied, and do not retract when the stress is removed. The vessel walls exhibit a combination of the properties of an elastic solid and a viscous fluid [20], a behaviour known as viscoelasticity. When this property is plotted as stress versus strain, it has a non-linear profile. The elastic component of this property is responsible for the ability of the artery to store a part of the pulsatile energy in systole and restore it to the circulation in diastole. Consequently, blood vessels convert the heart pulsatile ejection into a smoother, more continuous blood flow [21].

Investigators [22, 23, 24, 25, 26] agree that the stress-strain relationships of blood vessels are not linear. This nonlinearity is dependent on the mechanical characteristics of the main components of arteries, such as elastin and collagen. Elastin is a highly elastic component which undergoes a large strain under small loads, whereas collagen exhibits higher stiffness and strength properties than elastin [25]. A schematic of this nonlinearity is shown in Figure 2.4. The stress-strain response displays a J-shape which demonstrates it does not abide by Hooke's law over the whole stress range. Within an initial low stress (region A), the stress-strain line is nearly straight with a low slope (low modulus) and only elastin is recruited to withstand extension in this region. With further extension (region B), load bearing is gradually taken over by collagen fibres, which is a relatively inelastic but stiffer component [21, 27]. Holzapfel et al. [26] have also confirmed that the adventitia, where large-diameter collagen bundles are located,

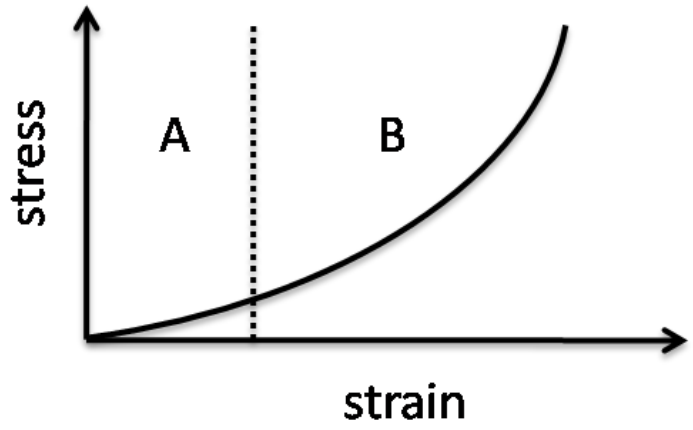

Figure 2.4: Illustration of the J-shape stress-strain curve of blood vessel.

shows pronounced stiffening behaviour in larger strain regions.

The stress-strain nonlinearity of materials is mainly measured by uniaxial tensile tests. In this method, dumbbell-shaped vessel samples are gripped between two flat plate clamps with sandpaper to prevent sample slippage during the test. One end of the sample is pulled away from the other at the required extension rates or loads. The stress-strain relationship is recorded continuously with extension. The width and thickness of dumbbell-shaped sample can be measured with a micrometer at the narrow section. A more detail test method can be obtained from the standard ASTM D638-00 [28].

The other method commonly used to access the elastic property of vessels is the compliance measurement. Vessel compliance is defined as the ratio of change in vessel diameter over the change in blood pressure [20]. It can be calculated by the following equation [6]:

$$Compliance = \frac{D_s - D_d}{D_d \times (P_s - P_d)} \times 10^4$$

where D and P are vessel diameter and blood pressure, and the d and s subscripts refer to the diastole and systole respectively. The unit of compliance is % per mmHg $\times 10^{-2}$.

2.3 Vascular grafts

2.3.1 Grafts from natural materials

Native vessels can be utilised in a number of ways [29], including decellularized autologous and allologous blood vessels [30], decellularized xenogenic blood vessels [31, 32, 33], decellularized non-vascular conduits [34, 35, 36] and prefabricated ECMs [37, 38]. These grafts can be decellularized by chemical methods, which generally use a combination of enzymatic and detergent treatments [29]. Enzymtatic treatment is used for cell lysis and detergent treatment is used to remove cell membrane lipids and nuclear debris, which can invoke calcification and graft degeneration [30, 31, 38]. The apparent advantages of these grafts are that intact collagen [39] and elastin [40] fibres are preserved to withstand wall extension and the cell signalling components [41, 42, 43] are retained for control of cell behaviours like adhesion, migration, proliferation and differentiation. Natural grafts generally have good outcomes in surgical applications [44]. However, this is offset by the supply deficit in autologous and allologous grafts, and the concern on the cross-species infection of xenogenic grafts. Although the contamination risk of porcine endogenous retrovirus (PERV) can be reduced in decellularization processes, a remaining up to 2% donor DNA in grafts should be taken into account [45], especially when primary human cells are reported to be infected by PERV [46]. A cell-sheet-based tissue engineering approach is able to solve this issue by using autologous human cell sheets to fabricate tissue engineering blood vessels [38, 47]. Even so, matching the elastic properties of native arteries remains as a challenging topic for as-engineering natural blood vessels.

2.3.2 Synthetic grafts

Synthetic grafts to replace natural blood vessels have been explored for more than 50 years [19]. There is an extensive list of synthetic materials employed for vascular grafts. Here, the focus is on the three dominant synthetic vascular grafts, namely

polyethylene terepthalate (PET, Dacron), polytetrafluoroethylene (PTFE, Teflon) and polyurethanes (PU), which have been commercialized in industry.

PET is commonly available in a standard fibre form which can be readily fabricated into textile and mesh. It has been successfully applied in large-diameter vessel grafts. However, blood responds actively with PET implants, which stimulates the release of macrophage TGF-beta [48] and consequently leads to high inflammation, neointimal proliferation and inhibition of endothelialization. Impregnation of albumin [49], hyaluronic acid, fibronectin and growth factors [50] have shown promise in enhancing the vascularisation within PET grafts.

PTFE is the most widely used fluorocarbon for biomaterials applications due to its long term biostability and biocompatibility in vivo. It has been applied extensively in various vessels, such as the femoral [51], carotid [52] and infrapopliteal [53] arteries. The patency rates of these implants are closely related to their diameters. Generally, larger diameter would have higher patency following implantations [54]. The expanded form of PTFE (ePTFE) can be produced by an extrusion and sintering process and fabricated into a tube with a porous wall [55], which improved cell adhesion characteristics in comparison with plain PTFE [54]. One concern with PTFE is that other materials can have difficulty binding to its surface which is a beneficial declotting function but, however, limits the adherence of endothelial cells. This issue has been addressed and investigated with coating of adhesion molecules to improve endothelialisation on the inner surface of the tubular graft [55, 56].

Polyurethanes (PU) are a large family of polymers which are commonly comprised of hard and soft segments. The diversity in hard and soft segments assigns PU a range of physical properties and they have been considered as soft, tough and rigid polymers [55]. The soft segments in PU are sites mainly related to its biodegradation property. Conventional polyester soft segments exhibit biodegradation potentials [57, 58], however, which also resulted in occlusion in vivo [59]. This issue can be addressed by replacing polyester with polycarbonate, so-called polycarbonate polyurethane (CPU),

Table 2.1: Compliance and cumulative patency of arterial grafts. (Adapted from Walden et al. [70])

Grafts	Compliance *	Patency, % (1-year)	Patency, % (2-year)
Host artery (N=8)	5.9 ± 0.5	-	-
Saphenous vein (N=5)	4.4 ± 0.8	88	84
Umbilical vein (N=16)	3.7 ± 0.5	83	80
Bovine heterograft (N=3)	2.6 ± 0.3	65	59
Dacron (N=16)	1.9 ± 0.3	65	42
ePTFE (N=5)	1.6 ± 0.2	60	42

*percent radial change per mmHg × 10^{-2}.

which has shown high resistance to degradation [60, 61, 62, 63]. However, a minor intrinsic hydrolytic effect is detectable in CPU one-year after implantation [59]. Although the biostability of CPU can be improved by manipulating the degree of hydrogen bonding among hard segments [64], the progressive degradation has laid a challenge for its use as long-term or "permanent" vascular grafts.

2.3.3 Compliance mismatch of conventional vascular grafts

The mismatch of elastic properties between vascular grafts and native vessel, called compliance mismatch, has been reported to be primarily responsible for intimal hyperplasia (IH) [21, 65], a major causes of long term failure of vascular grafts [66]. The fluid mechanics at the junction between the graft and the native arterie could also affect the success rate of vascular grafts. There could also be two main factors affecting the fluid mechanics at the junction: (1) matching of the geometry and properties of grafts and native arteries; (2) sewing technique. Compliance mismatch causes an alternation to fluid flow in the arterial system [66, 67], which subsequently affects the wall shear distribution [68], damages endothelial cells [69], changes histological features [65], and consequently results in formation of IH and poor patency rates of vascular grafts. Walden et al. [70] showed a positive correlation between compliance and patency rates and the results have been listed in Table 2.1.

Tai et al. [6] has compared the compliance of a prosthetic graft with the native

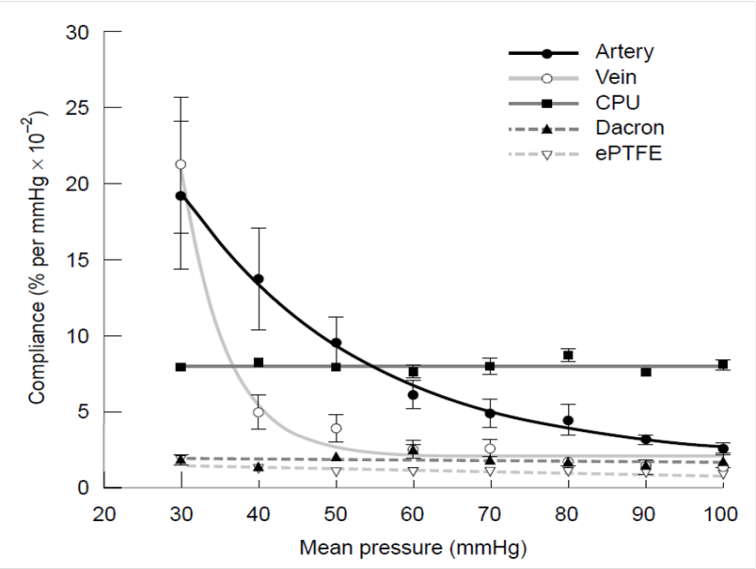

Figure 2.5: Compliance-pressure curves of artery, vein, CPU, Dacron and ePTFE. (Dacron–polyethylene terepthalate, ePTFE–expended polytetrafluoroethylene, CPU–polycarbonate polyurethanes)[6] .

artery. The compliances of Dacron, ePTFE, CPU, vein and artery were calculated over mean pressures in the range of 30-100 mmHg with 10 mmHg increments and the results are shown in Figure 2.5 [6]. It is apparent that the ePTFE and Dacron are rigid grafts, CPU is more compliant and veins exhibit a compliance-pressure profile closer to that of an artery. However, the compliance mismatch between these grafts and artery is apparent.

2.3.4 Comparison of mechanical properties of PVA hydrogel with native vessel

Addressing the issue of compliance mismatch, an alternative to ePTFE, Dacron and CPU would preferably exhibit viscoelastic properties to match the native artery. A PVA hydrogel is an attractive material for vascular graft applications due to its suitable elastic properties, in terms of the nonlinear stress-strain relationship. PVA cyrogels are fabricated by a thermal treatment, freeze-thaw cycles. The stiffness of these hydrogels can be enhanced by increasing the number of freeze-thaw cycles [71].

Chu and Rutt [8] have compared the stress-strain property of PVA hydrogels with

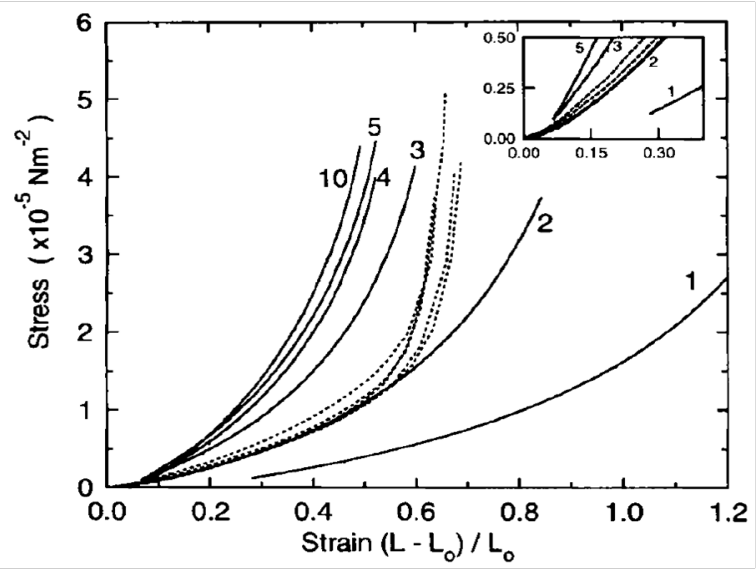

Figure 2.6: Stress-strain curves of PVA hydrogels and porcine aorta. PVA hydrogels were prepared with 1, 2, 3, 4, 5 and 10 freeze-thaw cycles. Data from a fresh porcine aorta are plotted as dashed lines. The inset shows the low strain range of the same stress-strain curve [8].

that of porcine aorta (Figure 2.6). The PVA hydrogels were prepared by 1,2,3,4,5 and 10 freeze-thaw cycles. It was found that there is no longer a change in the shape of stress-strain curve after 5 freeze-thaw cycles. At the low stress level where corresponding strain values are less than 0.2, the secant modulus of PVA hydrogel with 2 freeze-thaw cycles is $1.9 \pm 0.3 \times 10^5 Nm^{-2}$ which matched closely with that of porcine aorta, $1.75 \pm 0.03 \times 10^5 Nm^{-2}$.

Wan et al. [7] reported that the stress-strain curve of PVA hydrogels with 4 freeze-thaw cycles was comparable to that of porcine aortic root in the physiological strain range. This stress-strain relationship of PVA hydrogel is advantageous compared to commercial products, such as ePTFE and Dacron.

Millon et al. [72] prepared anisotropic PVA hydrogel by applying initial strain during thermal cycles. It was found that the stress-strain properties of anisotropic PVA hydrogels with 3 freeze-thaw cycles and 75% initial strain was able to match closely that of porcine aorta (Figure 2.7).

A previous study in our group prepared PVA and chitosan blended hydrogels [10]. The PVA/chitosan hydrogels with 1 freeze-thaw cycle and 3 freeze-thaw cycles exhib-

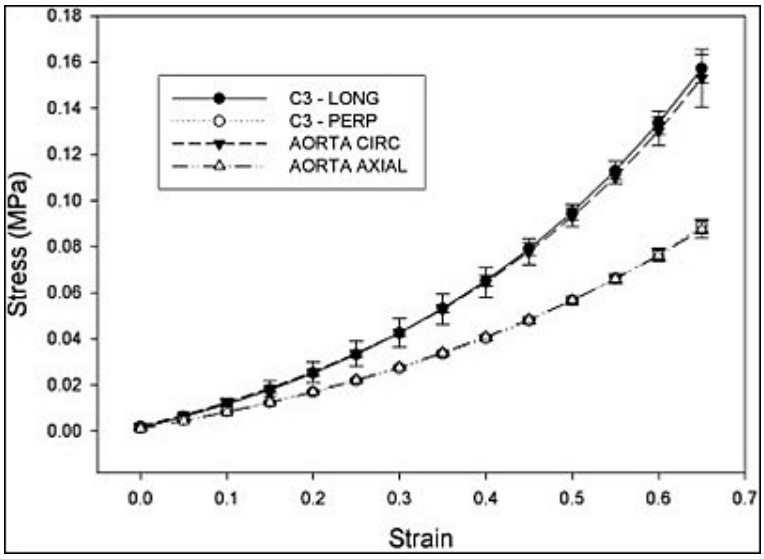

Figure 2.7: The stress-strain curves of anisotropic PVA hydrogels and aorta. PVA hydrogels were prepared with 75% initial strain and 3 freeze-thaw cycles which closely match the stress-strain curve of aorta in both the circular and axial direction [72].

ited the bounds of the softer and stiffer porcine aortic tissue respectively.

2.4 Poly(vinyl alcohol) hydrogel

2.4.1 Structure and property of Poly(vinyl alcohol)

Poly(vinyl alcohol) (PVA) is a synthetic water-soluble polymer with a number of pendant hydroxyl groups (Figure 2.8). It is commercially produced by the hydrolysis of poly(vinyl acetate) (PVAc). The manufacturing process can be viewed as two segments, a polymerization of vinyl acetate and a following hydrolysis of poly(vinyl acetate) to PVA. The hydrolysis reaction does not go to completion and therefore the term PVA refers to a copolymer of vinyl acetate and vinyl alcohol. The molecular weight and the degree of hydrolysis have an overall impact on the physical properties of PVA. It is possible to purchase PVA with various molecular weights and degrees of hydrolysis.

PVA has been broadly used in industry due to its excellent chemical resistance and physical properties. It can be produced as an adhesive with resistance to solvent, oil and

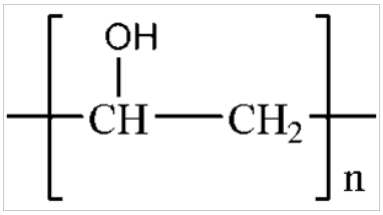

Figure 2.8: PVA chemical structure.

grease. The polymer films also exhibit high tensile strength and abrasion resistance.

The crystallization of PVA is one of the most important mechanical properties of PVA as it controls water sensitivity, tensile strength, oxygen barrier properties, and thermoplastic properties [73]. PVA is able to dissolve in solvents with high polarity, such as water, dimethyl sulfoxide (DMSO), glycols, and dimethylformamide. The solubility of PVA depends on the degree of polymerization (DP) and hydrolysis. The hydroxyl groups along PVA molecular chain promote strong hydrogen bonding which reduces the solubility of PVA in water. This hydrogen bonding can be weakened by the presence of residual acetate groups in PVA molecules and consequently allow a solubility of PVA at lower temperature. As a polyhydric alcohol, PVA is able to participate in various reactions, such as esterification with boric acid and borax, etherification with ethylene oxide, acetalization with aldehydes [73]. These reactions can be applied to cross-link PVA and form specific materials, like hydrogels.

Some other properties of PVA, such as solution viscosity, solvent resistance and biodegradation, have been investigated in detail by Marten [73] and Sundararajan et al. [74].

2.4.2 Synthesis methods of PVA hydrogels

A hydrogel is a hydrophilic polymer network where the loose cross-links prevents solubility but allows for swelling in water. They are in high demand in a number of applications, especially in biomedical and pharmaceutical sectors. PVA can be prepared as a hydrogel by either chemical or physical cross-linking.

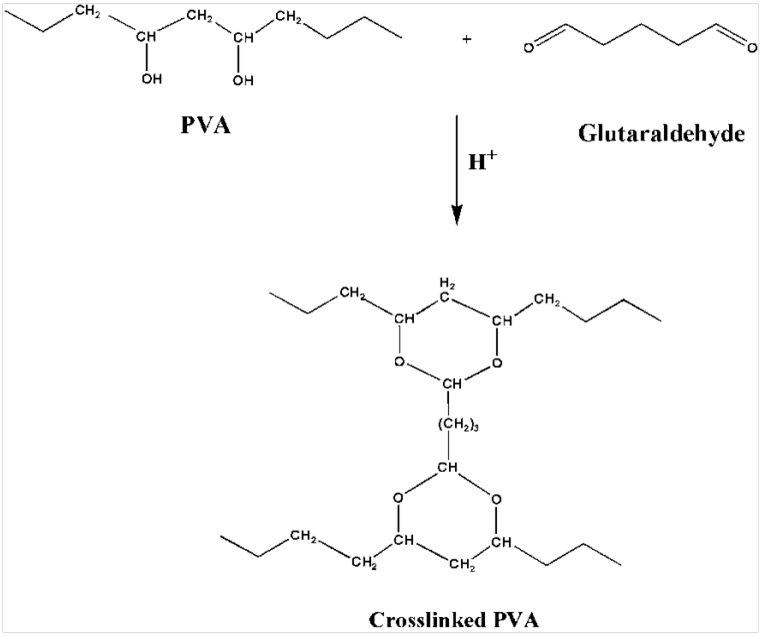

Figure 2.9: Crosslinking by high energy radiation [75].

2.4.2.1 Crosslinking by chemical agents

PVA is able to be cross-linked by a multifunctional crosslinking agent that reacts with hydroxyl groups. The most widely used cross-linking agents are glutaraldehyde (Figure 2.9), formaldehyde, acetaldehyde, glyoxal, boric acid, and isocyanates [73]. However, these cross-linking agents are often toxic compounds and can result in unwanted reactions with bioactive substances. The residue of these agents has to be extracted before the hydrogel can be applied in the area of biomaterials and medicine.

2.4.2.2 Crosslinking by high energy radiation

High energy radiation on polymer enables numerous applications in industry, such as crosslinking of plastics, curing of coating, surface modification, sterilization and hydrogel formation [76]. High energy radiation, in particular Gamma–irradiation and electron beam radiation, can be applied as another physical cross-linking method to prepare PVA hydrogels. This method is better than the use of chemical cross-linking agents as no chemical residue would be left behind. In the procedure of irradiation, radicals can be formed both from the scission of chemical groups on polymer chains

and from the radiolysis of water molecules [77]. The radiation is generally performed in an inert atmosphere since the radical is sensitive to oxygen. Peppas and Merrill prepared transparent PVA hydrogels with irradiation by electron beam [78]. This hydrogel showed low mechanical properties, including elastic moduli, tensile strength and extensibility to break. Zhao et al. [79] prepared a PVA and carboxymethylated chitosan blend hydrogel by electron beam. The hydrogel exhibited satisfying antibacterial activity, but relatively weak mechanical properties. Another technical issue is the formation of bubbles which resulted in difficulties to form homogeneous hydrogels [80]. Moreover, the radicals generated by irradiation might potentially attack and damage bioactive substances.

2.4.2.3 Physical crosslinking

To avoid the residue of cross-linking agents and the generation of radicals, physical cross-link methods are of increasing interest in recent years. A variety of physical methods has been applied to form hydrogels, including ionic interaction, crystallization, hydrogen bonds or even protein interaction [77]. The crystallization is the most feasible physical method to produce a PVA hydrogel as crystallites can be generated within hydrogel network by repeated freezing and thawing cycles (Figure 2.10). This physically formed PVA hydrogel has unusual mechanical characteristics, such as visco-elasticity and high mechanical strength which is very attractive to be a drug carrier or a tissue substitute in biomedical application.

2.4.3 Preparation of PVA hydrogels

The thermogram (Figure 2.11) of PVA hydrogel formation can be divided into three parts, freezing (A to B), storing (B to C) and thawing (C to D). In the freezing stage, PVA solution is cooled from initial temperature (Ti) down to temperature at which the sample is stored in frozen state (Ts). Upon storage at the frozen state, the specimen is subject to a thawing process, raising the temperature to the initial temperature of this

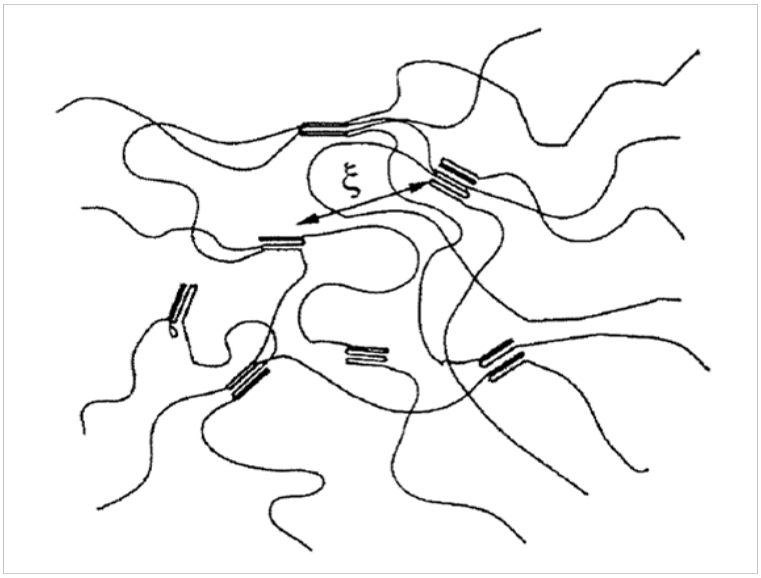

Figure 2.10: The crystallites generated within network structure of freeze/thawed PVA gels [80].

system.

2.4.4 Factors to control the structure and properties of PVA hydrogels

There are a number of factors which can be considered to control the final physical properties of PVA hydrogels, including the characteristics of the PVA polymer, thermal treatment and the nature of solvents for PVA. These factors have been reviewed by Lozinsky [81] and Table 2.2 has been adapted from that review to overview how the factors would influence final physical properties of PVA hydrogels. The comment and the rating of factors within this table should be considered as a guideline, and for a more detailed description the reader is referred to the original review.

2.4.5 Structure of PVA hydrogels

2.4.5.1 Characterization techniques

The outstanding elastic properties of PVA hydrogel, as shown in the section 2.3.4, is strongly depending on the structure [78, 80, 81] formed during freeze-thaw cycles. The

Table 2.2: Factors to tune the final properties of PVA hydrogels. Adapted from Lozinsky's review [81].

Category of factor	Subcategory of factor	Comments	Rate of factor
Polymer characteristics	OAc residues	OAc residues hindered the generation of hydrogen bonds between alcohol groups. Only PVA with highly deacylated backbones have the possibility to form strong gels.	+
	Tacticity	PVA with syndiotactic fragment has higher degree of crystallinity compared to the PVA with atactic fragments.	+
	Molecular mass	PVA with molecular mass higher than 50,000 is preferable to form strong gels.	+
	PVA concentration	An increase in the PVA concentration results in a more thermostable but less compliant gel.	+
Thermal treatment	Freezing process	Freezing process (i.e. freezing rate) has no significant influence on gel property.	-
	Storing temperature and duration	The compliance of gel changes with various temperatures and durations when storing the frozen sample.	+
	Rate of thawing	Stronger gel can be formed with slower thawing process. More specifically, there is a temperature range optimum for the formation of gel network, around -2.5 °C for PVA cryogel. The longer the temperature resides in this range, the stronger gel will be.	++
	Number of freeze-thaw cycles	An increase in the number of freeze-thaw cycles results in higher strength for PVA cryogels.	++
Nature of solvents	DMSO-water	The properties of PVA cryogel depend on the DMSO content of the solvents and the freezing rate.	+

Legend: important and significant factor ++; important but less significant factor +; non-significant factor -;

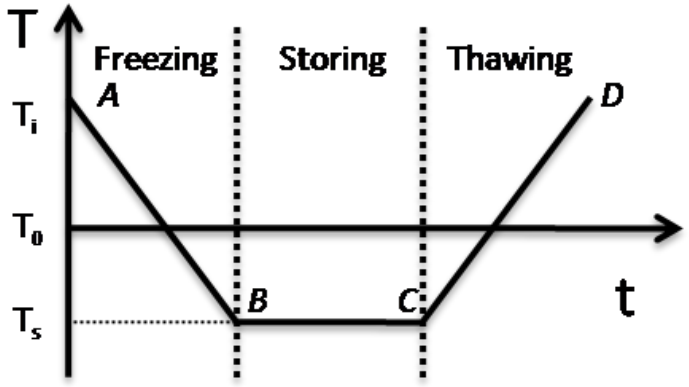

Figure 2.11: General thermogram of the formation of PVA hydrogel. T_i–initial temperature; T_0–freezing point; T_s-temperature at which the sample is stored in frozen state.

structure of PVA hydrogels has been extensively studied by swelling behavior [82, 83]. Other techniques can also be applied to the structural characterizations: including confocal microscopy [84], transmission electron microscopy (TEM) [85], differential scanning calorimetry (DSC) [86], 13C nuclear magnetic resonance (13C NMR) [85], solid-state 1H nuclear magnetic resonance (NMR) [86, 87, 88], wide-angle X-ray diffractioin (WXRD) [86, 89, 90], small-angle X-ray scattering (SAXS) [85], light scattering [91, 92, 93], small-angle neutron scattering (SANS) [72, 90, 91, 92] and ultrasmall-angle neutron scattering (USANS)[92, 94].

2.4.5.2 Structure model

Based on these characterizations, a model of the structure of PVA hydrogels has been proposed by Yokoyama et al. [89], Willcox et al. [85] and Millon et al [9]. The structure of PVA hydrogels is a porous network, in which polymer crystallites act as junction points for dangling chains [80, 85, 89, 91, 92, 93, 94, 95]. These crystallites ensure the dimensional stability and elastic property of PVA hydrogels. Three phases are present within PVA hydrogel, including PVA crystallites phase, amorphous PVA phase and free water phase [89]. Before freeze-thaw cycles, a PVA solution is composed of polymer chains randomly spread in the solvent. Upon the first free-thaw cycle, polymer chains are concentrated by either phase separation or the formation of ice crystals, and

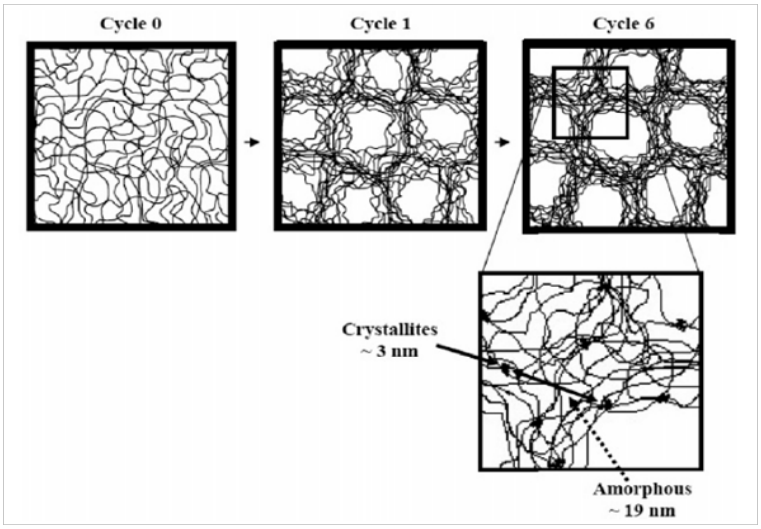

Figure 2.12: Schematic of the structure formation of the PVA hydrogels. The dimension of the crystallites is about 3nm, and the average distance between crystallites is about 19nm. [9]

held together by hydroxyl bonds to form a folded chain structure, which leads to small crystallites scattered in an amorphous polymer matrix. Successive freeze-thaw cycles results in further crystallization by the growth of previously-formed crystallites and the formation of new crystallites. A schematic of the structure formation of the PVA hydrogels has been proposed by Millon et al. [9] and shown in Figure 2.12. It is reported that crystallites are about 3 nm in size and the space in between crystallites is about 19 nm, based on the characterization technique of small-angle neutron scattering.

2.5 Electrospinning

Electrospinning is a simple and versatile technique to produce fibres with dimensions down to the micro- or nano-meter scale. The electrospun fibres have large surface-to-volume ratio, controllable porosity, morphology and assembly and a relatively high production rate, which invoke applications in biomedical engineering, environmental engineering, energy storage, healthcare and protective clothing [96, 97]. A large number of polymers have been electrospun in solution form, and these have been reviewed extensively by Huang et al. [97] and Greiner et al [98].

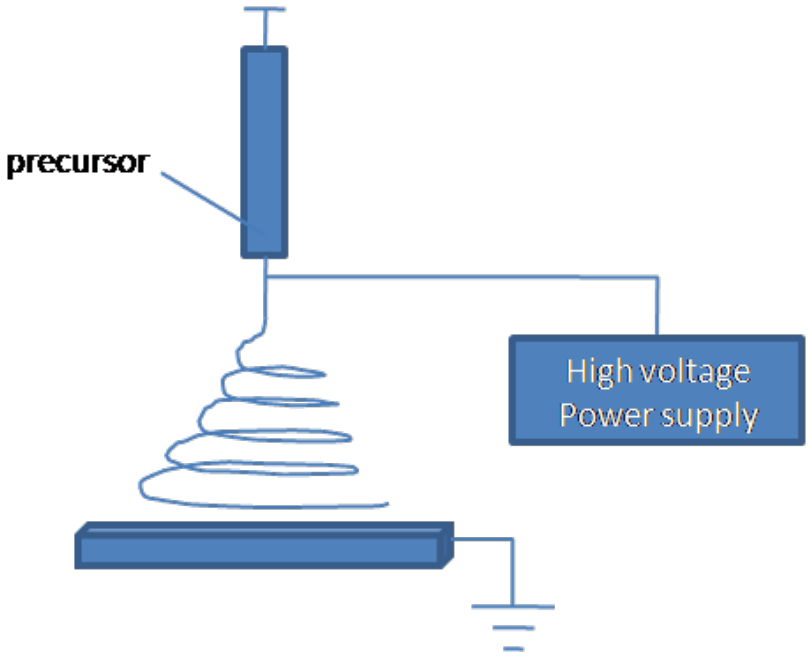

Figure 2.13: Schematic of the setup of electrospinning system.

2.5.1 Fundamentals of electrospinning

In principle, there are only three components required in this system, namely a high voltage power supply, a capillary tube and a collector (Figure 2.13). The capillary tube, such as a syringe with a metal needle tip, is firstly filled with fibre precursor, such as polymer, metal, ceramic or glass. When a high voltage is applied to the capillary tube, the fibre precursor is therefore charged and subject to a repulsive force as resulting in the electrical field generated in between the capillary tube and collector. The repulsive force is opposite to the intrinsic surface tension of the fibre precursor and can be enhanced by increasing the applied voltage. Upon reaching a critical point that the repulsive force overcomes the surface tension, a further increase of voltage gives rise to a charged jet ejected from the capillary tube (Figure 2.14 B) [98, 99]. The jet is then subject to bending instability [100] in the electric field and subsequently elongates into a fibre form (Figure 2.14 C) [101]. The as-formed fibres dry on travelling towards the lower potential, and deposits onto the collector (Figure 2.14 D) which is generally grounded.

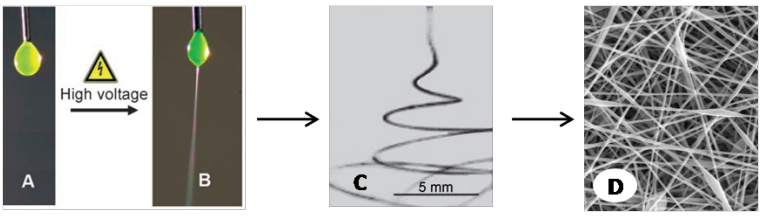

Figure 2.14: Diagrams of fibre formation during electrospinning. A) The drop shape without presence of a high voltage; B) Jet initiated; C) Jet instability and elongation; D) Dried fibre deposited on collector. Image A and B are adapted from a review by Greiner et al. [98]. Image C is adapted from a study by Yarin et al. [100]. Image D is the PVA electrospun fibres.

2.5.2 Electrospinning conditions

The parameters which affect the electrospinning process and the resultant fibre diameter and morphology have been investigated extensively by some researchers [102, 103, 104, 105]. Ramakrishna et al. [102] have classified these parameters into three categories: polymer solution parameters, processing conditions, and ambient parameters. Operating parameter are classified which have been listed in Figure 2.15. The main parameters that affect fibre diameter have been systematically studied by Tan et al. [103] and divided into two groups. One is the parameters that affect the electrical force. The other group is the parameters that affect the mass of polymer that can be brought into the jet. The effects of these parameters have been summarized as a processing map (Figure 2.16). Generally, when fibre morphology is dominated by the effects of mass of polymer, a lower polymer concentration, feed rate and applied voltage can result in fibres with smaller diameter. Alternatively, when the fibre morphology is controlled by the effects of electrical force, a higher applied voltage and solution electrical conductivity can result in fibres with smaller diameters.

2.5.3 Guided assembly of electrospinning fibres

Teo and Ramakrishna [106] have reviewed various concepts for guided assembly of fibres in electrospinning by using dynamic collection devices and by manipulating the electric field. The concepts related to assembling aligned fibrous mesh have been

Polymer solution properties	Processing conditions	Ambient parameters
• Molecular weight • Viscosity • Surface tension • Solution conductivity	• Applied voltage • Feed rate • Temperature • Effect of collector • Diameter of needle • Distance between tip and collector	• Humidity • Type of atmosphere • Pressure

Figure 2.15: Parameters of electrospinning process. Adapted from Ramakrishna et al. [102].

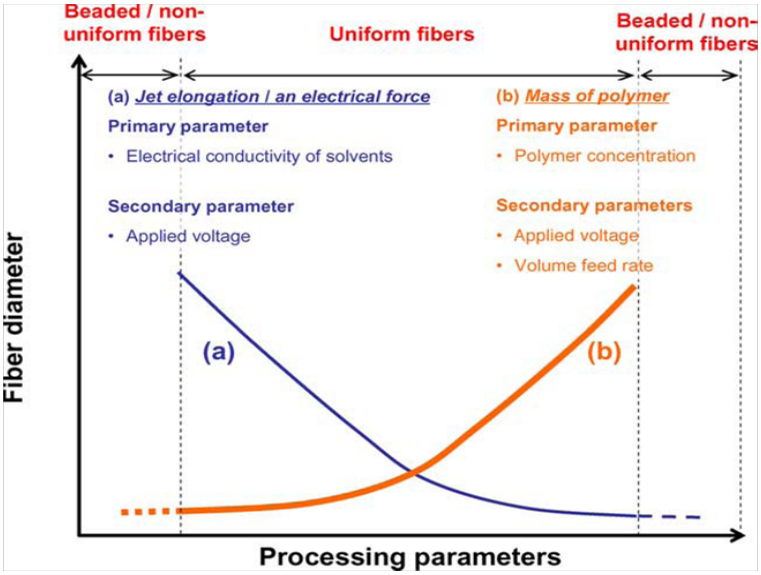

Figure 2.16: The effect of processing parameters on the diameter of fibres based on systematic parameter study by Tan et al. [103]

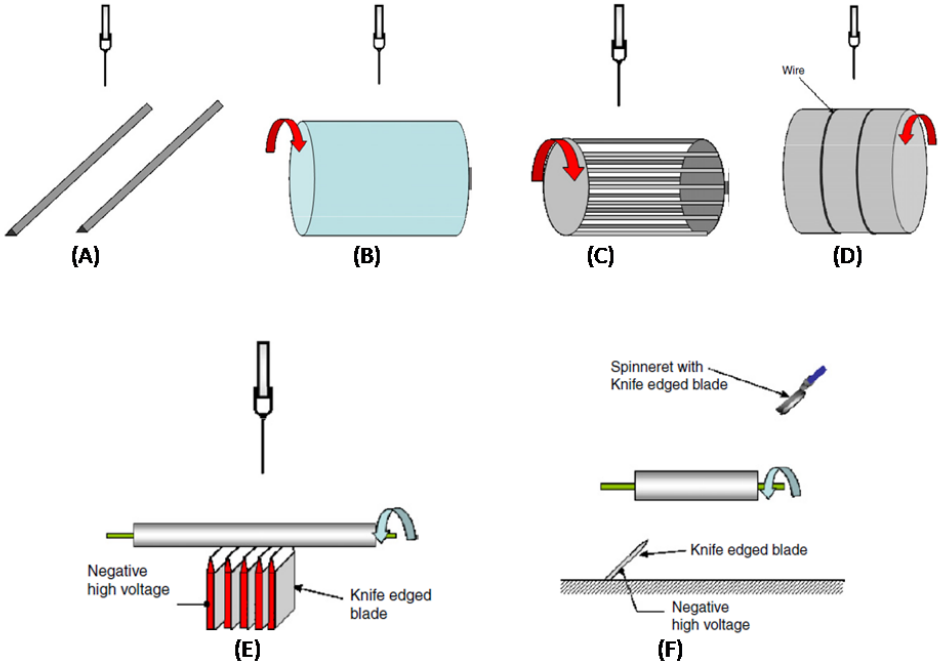

Figure 2.17: Schematics of electrospinning set-ups for fibre assembly [106]. (A) Parallel electrodes collector [107]; (B) Rotating drum collector [108, 109, 110, 111]; (C) Rotating wire drum collector [112]; (D) Rotating drum collector wires wound circumferentially [113]; (E) Rotating tube collector with knife-edge electrodes below [114]; (F) Rotating tube collector with knife-edge bar below and blade attached to needle [114].

shown in Figure 2.17.

2.5.4 Electrospun fibres as vascular grafts

The electrospinning technique can easily produce tubular fibrous constructs which directly inspire its use as a method to fabricate vascular grafts [115, 116, 117, 118, 58, 119]. The alignment of electrospun fibres could act as guidance for the migration of smooth muscle cells (Figure 2.18 [115]) and endothelial cells [115, 120]. An innovative method of forming electrospun fibrous tube with diagonal alignment could help in designing a fibrous construct to match the helical arrangement of elastin in the media layer of vessel wall [114].

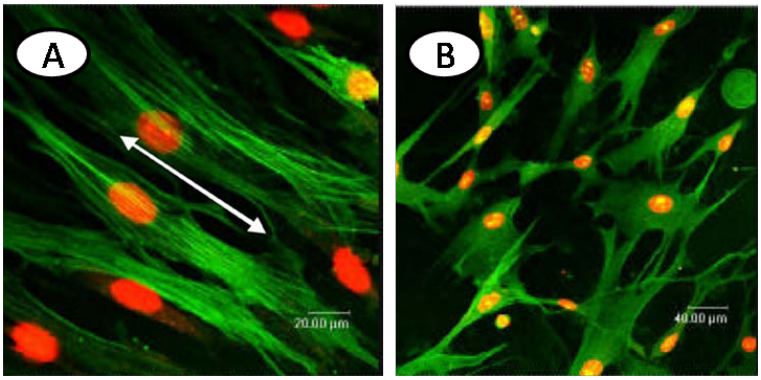

Figure 2.18: Micrographs of smooth muscle cell growth on aligned electrospun fibres and tissue culture plate [115]. (A) aligned electrospun fibres; (B) tissue culture plate.

2.5.5 Challenges and approaches

There has been much effort and great progress in the design of electrospinning systems for controllable assembly of fibres. Nevertheless, we are still facing some challenges.

Firstly, alignment of fibres over a substantial thickness is generally difficult to achieve. Katta et al. [112] clearly showed that the alignment of fibres tend to be diminished over electrospinning duration (Figure 2.19). Two solutions can be considered to fabricate fibres with greater alignment. One is to reduce the chaotic whipping of liquid jets. Sun et al. [121] have designed a near-field electrospinning method to deposit nanofibres with a controllable manner. The electrode-to-collector distance has been reduced to a range of between 500 microns and 3 mm. A tungsten spinneret of 25 microns tip diameter was used to intensify the electrical field and generate small-diameter jets in a stable region. The chaotic whipping effect is therefore reduced and the fibres are able to deposit directly to controllable positions. The other solution is to reduce the build-up of surface charge on deposited fibres. Kessick et al. [122] have replaced the conventional direct-current (DC) power supply with the alternating-current (AC) power supply. Fibres with significantly higher alignment have been detected under AC potential, which is accounted for by the reduction of net charge on deposited fibres.

Electrospun fibres are generally produced into two-dimensional mats. The only three-dimensional form that has been widely studied is the fibrous tube which can

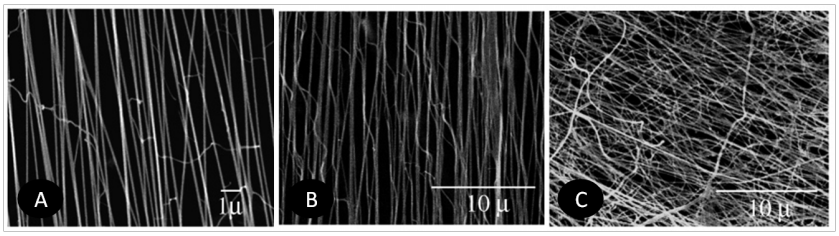

Figure 2.19: SEM images of fibre alignment over various durations of electrospinning [112]. (A) 5min; (B) 15min; (C) 2.5h.

be fabricated with columnar collectors. Zhang et al. [123] has prepared tubes with multiple patterns, different shapes, sizes and structures by designing 3D collectors, which give the possibility to control the 3D configuration of electrospun fibrous tubes. This technique is versatile to fabricate fibres in the form of tube. However, more complicated 3D structures are still necessary for further investigation to match various applications. A technique for targetted deposition of fibres with controllable fibre-fibre distance would help to fabricate 3D fibrous structures.

As for biomedical applications, a fibrous construct with pores large enough for cell penetration is often not easy to prepare. A dissolvable polymer can be incorporated into fibrous structures, which can be prepared by simultaneously electrospraying hydrogels with the electrospinning process and then leaching hydrogels to form electrospun fibrous constructs with macroporous structures [124]. Im et al. [125] also reported the possibility to form macro-meso pores by dissolving polyacrylonitrile (PAN) with N,N-dimethyl formamide (DMF). Another alternative way to directly incorporate cells into fibrous constructs is electrospraying cell solutions simultaneously with polymer solution in the electrospinning process or coaxial electrospinning cell solution with polymer solution [126]. It is evident that elecrospinning process, with its high voltage, has no significant effect on the cell function at cytogenetic or physiological level [127]. Stankus et al. [58] have constructed vascular grafts by electrospraying smooth muscle cell (SMC) solutions simultaneously with electrospinning poly(ester urethane) urea (PEUU). A compliant tubular matrix with SMC incorporated is thereby fabricated.

2.6 Thesis layout

As a summary, PVA hydrogels and electrospun nanofibres have been investigated intensively. However, there is a gap in the literature to combine both the merits of hydrogels and nanofibres by constructing hydrogel/fibres duo-layer graft for vascular applications.

To address the design of composite duo-layer vessels, the following studies will be described:

1. Composite hydrogels of PVA with one of three macromolecules (chitosan, starch and gelatin) were physically crosslinked by freeze-thaw thermal cycles followed by coagulation treatment. The mechanical properties of the hydrogels were characterized by uniaxial tensile tests. The structure profile of the hydrogels was investigated by equilibrium swelling and rehydration tests to show the relationship between network structure and mechanical properties.

2. A more detailed investigation was performed on PVA/Gelatin hydrogels to study how the freeze-thaw thermal cycles and coagulation treatment influence the structure and consequently the control over the mechanical properties of the hydrogels. Infrared Spectroscopy was applied to investigate the presence of gelatin in the matrix of the PVA hydrogel. Differential Scanning Calorimetry was employed to calculate the crystallinity of hydrogels. The glass transition temperatures were studied by DMA. Rheological properties and uniaxial tensile tests were applied to characterize the mechanical properties of hydrogels.

3. PVA-SbQ was selected as a photocross-linkable PVA based polymer. PVA-SbQ has not previously been fabricated into fibres by the electrospinning process. Firstly, Infrared Spectroscopy and Ultraviolet-Visible spectroscopy were employed to track the photoreaction of PVA-SbQ. Also, the water resistance of photocrossliked PVA-SbQ was assessed by weight loss experiments, and the morphology was assessed by Scanning Electronic Microscopy (SEM). Finally,

endothelial cells were cultured on PVA-SbQ fibres. Immunofluoresence staining and SEM were applied to determine whether the PVA-SbQ fibre support the attachment of Endothelial Cells.

4. Based on the above studies, a duo-layer vascular graft was construct by fabricating a PVA/Gelatin hydrogel vessel as an outer layer to provide the main mechanical support and PVA-SbQ fibres as an inner layer to provide a favourable surface for endothelial cell attachment. Both uniaxial tensile tests and compliance tests were employed to compare the mechanical properties between the duo-layer construct and with published results for the native artery.

The structure of the thesis is shown in Figure 2.20. Chapter 3 describes materials and methods. Chapter 4 and 5 contains studies on the structure-property relationships of PVA based hydrogels. Chapter 6 describes electrospinning of PVA-SbQ fibrous mat. Chapter 7 presents a duo-layer vessel graft and study the mechanical properties of the duo-layer construct. Chapter 8 summarises the conclusions from this study and discusses potential future work.

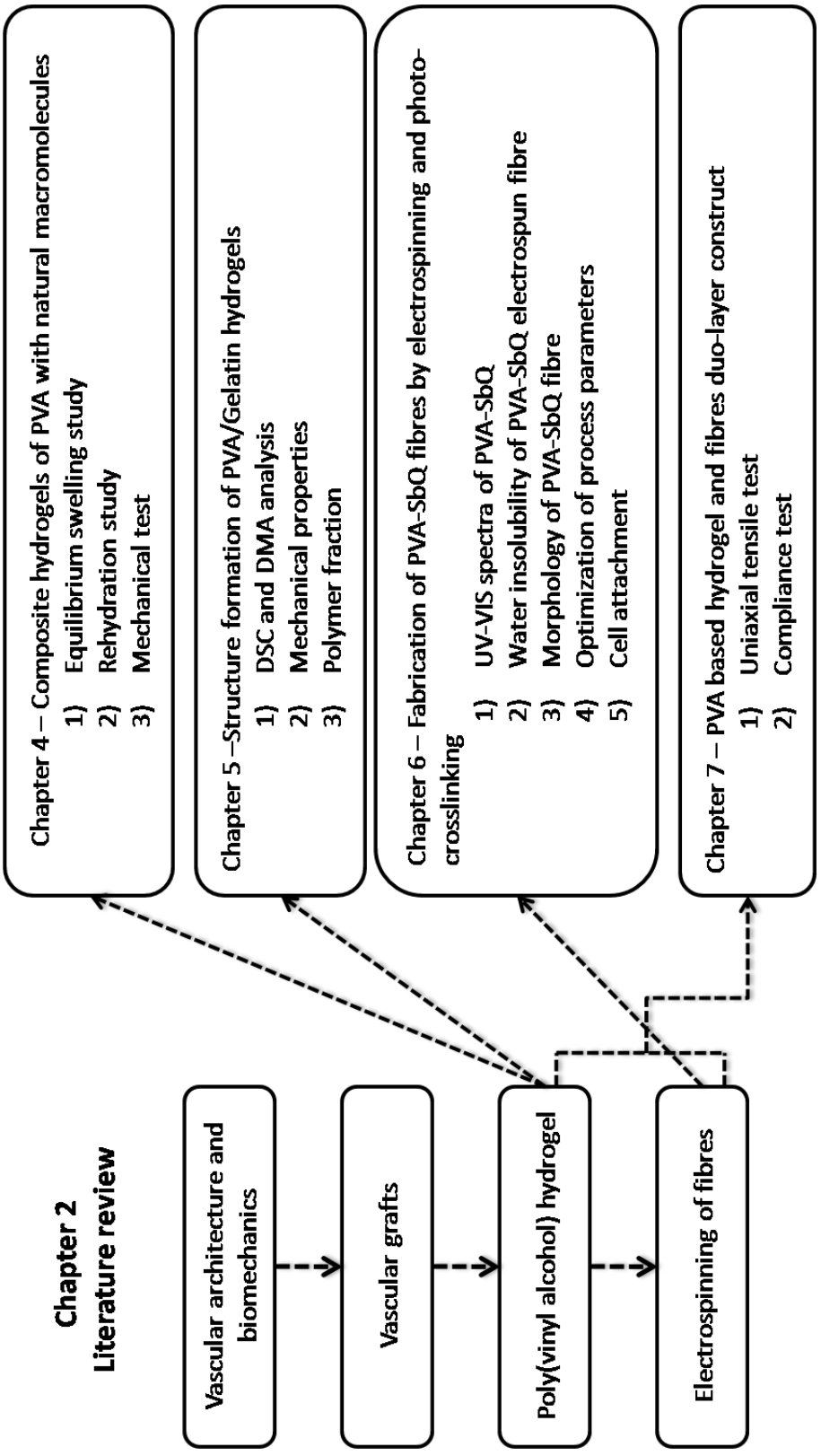

Figure 2.20: Structure of literature review and the thesis layout.

Chapter 3

Materials and Methods

3.1 Materials

3.1.1 Chemicals

PVA with an average molecular weight (M_n) of 78,400 g/mol was purchased from Vassar Brothers Medical Center (New York, USA) to prepare PVA hydrogels. Another PVA with molecular weight of 89,000~98,000 was obtained from Sigma-Aldrich (Germany) and applied as a control material in the electrospinning process.

Water soluble chitosan with a de-acetylation degree of 85% was bought from Jinan Haidebei Marine Bioengineering Co. (China). Starch, from potato, and gelatin, type B from bovine skin, were supplied by Sigma-Aldrich, Germany.

PVA-SbQ was ordered from Polysciences Inc. (USA) with a concentration of 13.3%, 45,000 molecular weight and 4.1 mol% SbQ content.

Other chemicals used were:

- Potassium Hydroxide (KOH) (Sigma, Germany)
- Sodium Sulphate (Na_2SO_4) (Sigma, Germany)
- Iso-octane (Fisher, Ireland)
- DAPI (Sigma D9542, USA)

- Phalloidin-FITC (Sigma P5282, USA)
- Rat collagen type I (Sigma, Germany)
- RPMI 1640 cell culture medium (Sigma, Germany)
- Fetal Calf Serum (Sigma, Germany)

3.1.2 Equipment

The following scientific instruments were used in the study:

- YDK 01 LP Density Measurement Kit (Sartorius AG, Germany)
- Labconco Freeze Dry Freezone System (Labconco, USA)
- Zwick Z005 Tensile Test Machine (Zwick-Roell, Germany)
- DTA/TGA STA 1500 (PL Thermal Sciences Ltd., UK)
- Nicolet Avator 360 Fourier Transform Infrared Spectroscopy (Thermo Scientific, USA)
- DSC 2920 Modulated DSC (TA Instruments, UK)
- Rheometric Scientific Mark III DMTA (Rheometric Scientific, USA)
- Advanced Rheometer AR1000 (TA instruments, UK)
- UV-3100 UV-VIS Spectrophotometer (Shimadzu, Japan)
- BX51 Olympus Microscopy (Olympus, Japan)
- EVO LS15 Scanning Electron Microscopy (Zeiss, Germany)

3.2 Methods

3.2.1 Preparation of hydrogels and fibres

3.2.1.1 Preparation of hydrogels

PVA, PVA/Chitosan, PVA/Starch and PVA/Gelatin solutions were prepared by mixing polymer powders in deionized water and autoclaving at 121°C for 1h. Table 3.1 shows the percentage weight per volume ratio of the composition of each solution and Figure 3.1 shows the process of the preparation of hydrogels. After autoclaving, the solutions were immediately homogenized by magnetic stirrer to prevent aggregation of polymers. Air bubbles in the solutions were removed by settling at room temperature. After casting solutions in casting moulds (Figure 3.2), they were physically crosslinked by one or three freeze-thaw cycles which consisted of freezing at -20°C for 12h and thawing at 21°C for 12h. Those freeze-thawed hydrogels to be treated with the coagulation bath were submerged in a constantly stirred coagulation bath (7.5% KOH and 1M Na_2SO_4) for 1h. As-formed hydrogels were washed with deionized water several times and kept in deionized water until testing (storage duration 3-5 days). The names of samples are abbreviated as follows. These designations will be used throughout the thesis.

- P : PVA
- PC : PVA/Chitosan
- PS : PVA/Starch
- PG : PVA/Gelatin
- 1FT, 1 Cycle : 1 freeze-thaw cycle
- 3FT, 3 Cycles : 3 freeze-thaw cycles
- bcb: before coagulation bath

Table 3.1: Percentage weight per volume ratio of the composition of polymer solutions.

Solutions	Water (%, w/w)	PVA (%, w/w)	Chitosan (%, w/w)	Starch (%, w/w)	Gelatin (%, w/w)
PVA	**90**	**10**	-	-	-
PVA/Chitosan	**90**	**9**	1	-	-
PVA/Starch	**90**	**9**	-	1	
PVA/Gelatin	**90**	**9**	-	-	1

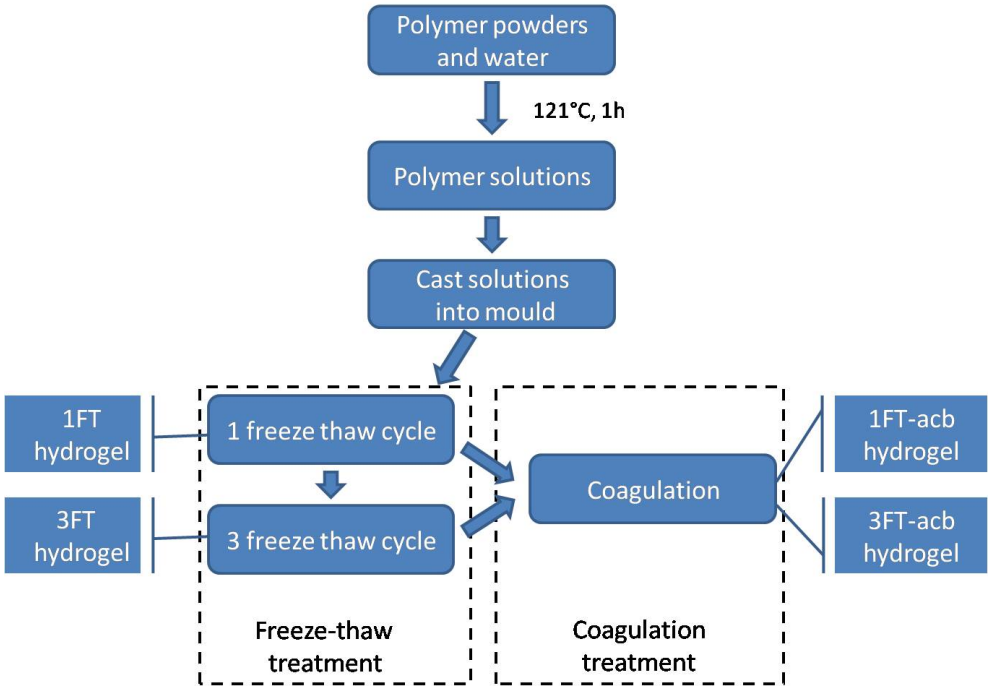

Figure 3.1: Preparation of PVA based hydrogels.

- acb : after coagulation bath
- 1-bcb: 1 freeze-thaw cycle before coagulation bath
- 3-acb: 3 freeze-thaw cycles after coagulation bath

3.2.1.2 Preparation of PVA and PVA-SbQ fibres

Electrospinning of PVA and PVA-SbQ fibres: 10 % PVA solution was prepared by dissolving PVA powder in distilled water and heating at 121 $^{\circ}C$ for 1 hour. The prepared 10% PVA and 13.3% PVA-SbQ solutions were then transferred into a syringe equipped

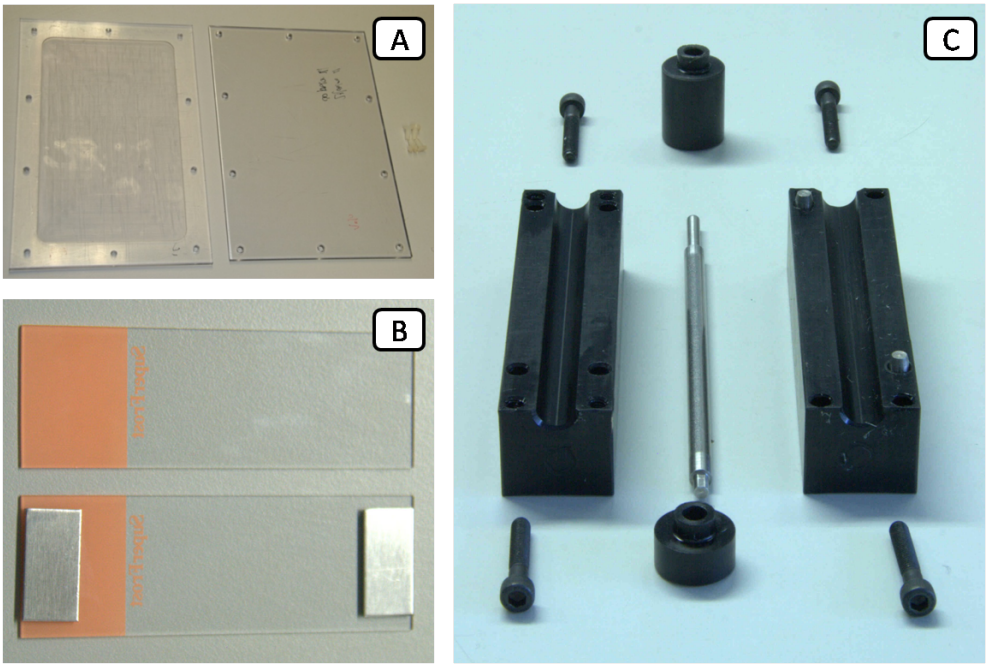

Figure 3.2: Hydrogel casting moulds. (A) Flat plastic mould; (B) Plane glass mould with spacers; (C) Tubular mould to prepare hydrogel vessel graft.

with a 19 gauge stainless blunt needle and infused at 0.35 ml/h with a syringe pump. A positive bias of 19 kV was applied to the needle. The collector position was placed 10 cm away from the needle to collect the as-formed PVA fibres and PVA-SbQ fibres. Figure 3.3 showed the set-up of electrospinning rigs. Collector-1 was the generally used collector and the other collectors are applied when it was specified.

For photocrosslinking of PVA-SbQ fibres, the electrospun PVA-SbQ was irradiated by a 100W UV lamp (B-100AP, UVP, Ireland) for 20 min (Figure 3.4). The PVA-SbQ fibres before and after irradiation were named as PVA-SbQ and PVA-SbQ-hv, respectively.

3.2.2 Structural and mechanical properties of PVA based hydrogels

3.2.2.1 Equilibrium swelling study

There are three main structural parameters for hydrogels, namely the polymer volume fraction in the swollen state, the number average molecular weight between cross-

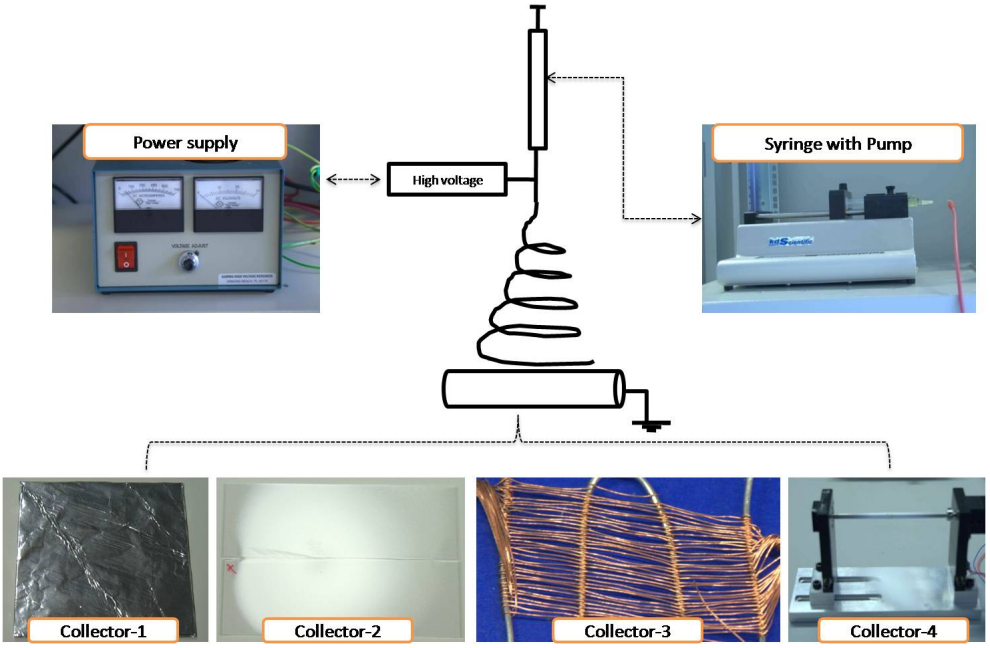

Figure 3.3: Electrospinning set-up. Collector-1, square collector covered with Aluminium foil; Collector-2, Glass slides collector; Collector-3, Collector assembled by metal wires; Collector-4: Rotating mandrel as collector.

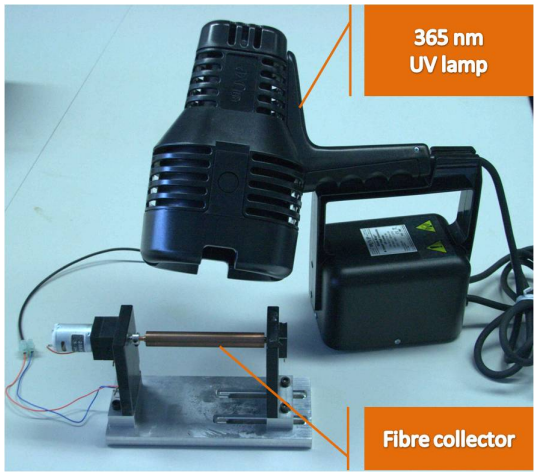

Figure 3.4: Photocrosslinking set-up.

links, and the network mesh size. These parameters can be determined or predicted by equilibrium swelling experiments [83] and the theory of hydrogel elastic networks reported by Peppas and Merrill [78].

The hydrogels formed by physical treatments were considered to be in a relaxed state. The weight and volume of the relaxed membranes were measured by a Density Measurement Kit. Briefly, the as-formed hydrogels were weighed in air and then immediately weighed in iso-octane. When weighing in iso-octane, the sample was put into the stainless steel mesh basket which was then suspended in iso-octane. To determine the equilibrium swelling ratio, Q (Eq. 3.6), the membranes in the relaxed state were placed in deionized water at room temperature for 4 days to swell to equilibrium and then were dried for 6 h with a freeze-dryer . Q indicates relative polymer volume fraction for a hydrogel.

The calculation method used for our equilibrium swelling studies was similar to that used by Peppas and Wright [83]. The polymer volume fraction in the relaxed state and swollen state were calculated using Eqs. 3.1 and 3.2.

$$V_{2,r} = \frac{V_d}{V_r} \tag{3.1}$$

$$V_{2,s} = \frac{V_d}{V_s} \tag{3.2}$$

where, V_d, V_r and V_s are the volume of the polymer samples in the dry, relaxed, and swollen states, respectively; $V_{2,r}$ and $V_{2,s}$ are the polymer volume fractions of the relaxed and swollen polymer gel, respectively.

The volumes were calculated using Eqs 3.3, 3.4 and 3.5. which utilize the weights of the dry polymer, W_d, the relaxed polymer, W_r, and the swollen polymer, W_s, in the air and iso-octane. a refers to the weight in the air and i refer to the weight in the iso-octane.

$$V_d = \frac{W_{a,d} - W_{i,d}}{\rho_i} \tag{3.3}$$

$$V_r = \frac{W_{a,r} - W_{i,r}}{\rho_i} \tag{3.4}$$

$$V_s = \frac{W_{a,s} - W_{i,s}}{\rho_i} \tag{3.5}$$

where $\rho_i$is the density of iso-octane (0.691 g/ml). The equilibrium swelling ratio, Q, in this study is defined as Eq. 3.6

$$Q = \frac{1}{V_{2,s}} \tag{3.6}$$

3.2.2.2 Rehydration study

Dehydrated PVA hydrogel is able to re-swell completely to the predehydrated level [88, 90]. This rehydration is a process of re-expanding the polymer structure by the diffusion of water, which indicated the stability of hydrogel structure.

Samples for the rehydration study were cut from the as-formed PVA-based hydrogels. The water was removed from samples by drying with the freeze-dryer for 6 h. The sample weight was monitored periodically to make sure the sample was completely dehydrated. The dry weight was recorded before immersing the dehydrated samples in deionized water. The sample weight was first measured half an hour after immersion, then taken out every hour for the next 4 h. As swelling approached the equilibrium, sample was taken out of the water for weighing after 12, 15.5, 20, and 36 h. The dry and wet weights of the samples were used to calculate the swelling ratio in rehydration.

3.2.2.3 Uniaxial tensile tests

The uniaxial tensile test is a commonly used test for evaluating the mechanical properties of materials. A programmed force or a specify strain rate is applied to specimen by the tensile test machine, resulting in the gradual elongation and eventual fracture of the specimen. The force-extension data are monitored and can be used to quantify some important mechanical properties, such as Young's modulus.

Two different types of samples were tested: hydrogels and laminates of hydrogels with electrospun fibres. The fabrication of the composite specimens is discussed in Section 3.2.5.1.

Uniaxial tensile tests were conducted on a Zwick Z005 displacement controlled tensile testing machine. All PVA/Gelatin hydrogel samples were cut in dog-bone shape (Figure 3.5 A) and swollen to the equilibrium state before tensile testing. Fixed grips were mounted onto the tensile testing machine. Abrasive paper was placed between the hydrogel sample and the grip surface to prevent slippage during loading. All tests followed the protocol established by Mathews et al. [10]. Briefly, a preconditioning cycle was performed firstly at 60% min^{-1} strain rate to 60% strain and the hydrogel samples were then loaded to failure (Figure 3.6). The preconditioning protocol is described in more detail in Section 4.3.1.The behavior of the material changes with the first cycle but does not change under any subsequent loading cycles. Six samples of each type of hydrogel were tested. The broken sample after tensile test is shown in Figure 3.5 B.

3.2.3 The structure formation of PVA/Gelatin hydrogels

3.2.3.1 Attenuated total reflectance fourier transform infrared spectroscopy (ATR-FTIR)

FTIR is a sensitive characterisation technique which can detect molecule interactions. This technique examine samples through the vibrations of the atoms and molecules. An infrared spectrum is a plot of the energy absorption over a range of wave numbers

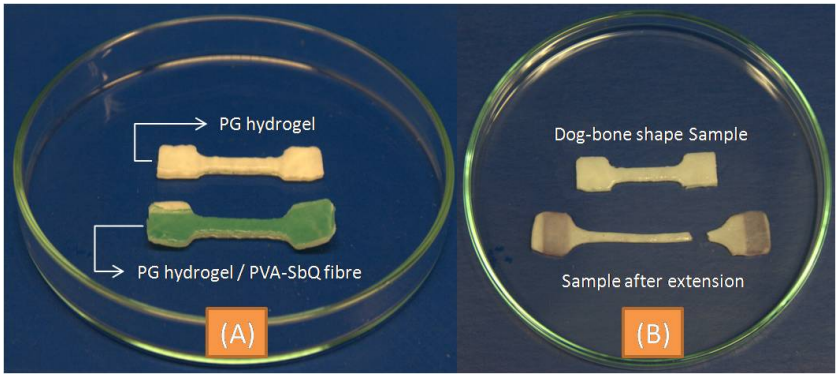

Figure 3.5: Hydrogels samples for uniaxial tensile test. (A) Dog-bone hydrogel samples; (B) Dog-bone sample before and after tensile test. Note that the hydrogel samples were griped with abrasive paper to prevent slippage during loading.

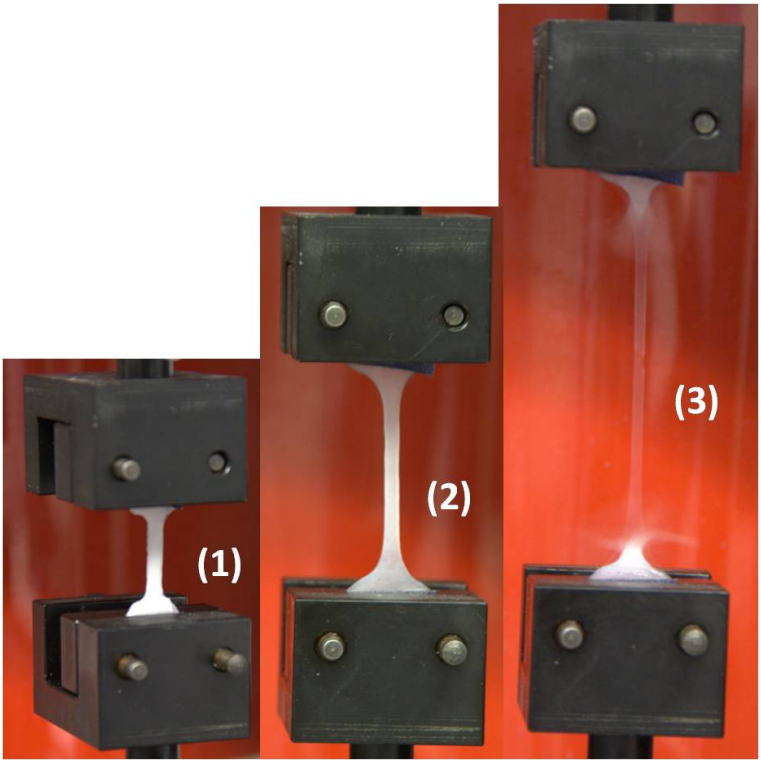

Figure 3.6: Stretching of hydrogel samples in uniaxial tensile test.

when infrared radiation passes through a sample. The energy absorption peak corresponds to the frequency of a vibration of the sample molecule [128]. Conventionally, potassium bromide (KBr) is grounded with a solid sample to make a die for analysis. The attenuated total reflectance (ATR) mode of the FTIR system provides a better and easier sampling technique for liquid and solid sample when compared with the conventional technique.

Fourier transform infrared spectroscopy was carried out on samples of PVA, gelatin and PVA/Gelatin hydrogels using the Attenuated Total Reflectance (ATR) mode on a Nicolet Avator 360 FTIR, with a 32 scan per sample cycle and a resolution of 8 cm^{-1}. The samples were scanned from 400 to 4000 cm^{-1}.

3.2.3.2 Modulated differential scanning calorimetry (MDSC)

Differential Scanning Calorimetry (DSC) is a technique most often used for characterizing the glass transition temperature, melting temperature, crystallization temperature and other phase transitions of materials. It measures the power (heat energy per unit time) differential between a sample and reference and is shown as a function of temperature [129]. Modulated DSC permits separation of overlapping events that are difficult to do by standard DSC and provides further information to have a better understanding of the thermal properties of materials.

MDSC analysis was performed on hydrogel samples with the DSC 2920 Modulated DSC (TA Instruments) containing a refrigerator cooling system. All samples were dried at 30 $°C$ for 20h before analysis. 8 – 12 mg of dry sample was placed in a hermetically sealed aluminum pan. An empty hermetically sealed aluminum pan was used as the reference cell. The samples were ramped from 10 to 120 $°C$ and isothermally held for five minutes. After this the sample was cooled and the calorimetry data was collected from 10 to 300 $°C$ (modulated +/- 1$°C$ every 60 seconds) with a heating rate of 10 $°C/min$ under nitrogen atmosphere. The instrument was calibrated using indium as standard.

3.2.3.3 Dynamic mechanical thermal analysis (DMTA)

DMTA is a versatile technique to have information linking chemical composition directly with mechanical properties in a single test. With an oscillatory mechanical deformation mode, DMTA measures the dynamic modulus of sample during a programmed temperature scan at controlled frequency [129]. It is more sensitive and yields more easily interpreted information in measuring glass transition temperature compared to another conventional measurement, DSC.

DMTA scans were performed using a Rheometric scientific mark III DMTA in tensile mode. Samples were dried in an LMS cooled incubator at 4 $°C$ for 7 days and the specimens for DMTA testing (7mm×3mm×0.5mm) were cut from the selected samples. The temperature profile ranged from -40 to 250$°C$ at a 2 $°C/min$ heating rate with a frequency of 1Hz.

3.2.3.4 Low strain rheological measurements

The Rheometric system is especially suitable for measuring the viscoelasticity of materials. It has the advantage of separating the moduli into the elastic component and the viscous component, which are represented by the dynamic storage modulus (G') and the dynamic loss modulus (G") respectively.

Oscillatory parallel plate rheological measurements were carried out on PVA/Gelatin hydrogels using an Advanced Rheometer AR1000 (TA instruments) fitted with a Peltier temperature controller to measure the dynamic storage modulus (G‘). Hydrated hydrogel samples were tested in triplicate (using individual samples) at a temperature of 20 $°C$ using a 6 cm parallel steel plate. A strain sweep was applied from 5×10^{-4} to 3×10^{-3} at a frequency of 1Hz, while a constant normal force of 10 ± 0.5 N was exerted on the samples. A low frequency and low strain range was adopted while all samples were blotted free of water using filter paper prior to testing in an attempt to minimize slippage.

3.2.4 PVA-SbQ fibres

3.2.4.1 Photoactivation of PVA-SbQ

- Ultraviolet-visible spectroscopy (UV-VIS)

UV-VIS is a technique to measure the light absorption of molecules which represent the electronic transitions from the ground state to the excited state. The use of Shimadzu UV-3100 ultraviolet-visible spectroscopy allows for evaluating the photoreaction of PVA-SbQ. PVA-SbQ was diluted from 13.3% to 3.3% and 10%, and then their UV absorbencies were measured in a UV disposable plastic cuvette. Distilled water was used as a control.

- Attenuated total reflectance Fourier transform infrared spectroscopy (ATR-FTIR)

PVA-SbQ fibres with varied exposure duration to the UV lamp were prepared for FTIR analysis to study the molecular structure change upon photocrosslinking. The FTIR analysis was carried out by using the Attenuated Total Reflectance (ATR) mode on a Nicolet Avator 360 FTIR, with a 32 scan per sample cycle and a resolution of 8 cm^{-1}. The samples were scanned from 400 to 4000 cm^{-1}.

3.2.4.2 Weight loss measurement

The water solubility of PVA, PVA-SbQ and PVA-SbQ-hv fibres was studied by mass loss measurement. The fibres were immersed in 37 $^{\circ}C$ distilled water for 5 days. All samples were vacuum dried before measuring mass loss.

3.2.4.3 Scanning electron microscopy (SEM)

The SEM is a technique to image the surface of samples. When high-energy electrons are applied to scan the sample surface, they interact with the atoms of samples and produce signals, such as secondary electrons, back scattered electrons and characteristic x-rays, which contain information of the sample surface, including the topography

and composition. The use of EVO LS15 scanning electron microscopy allows for observing the morphology PVA fibres and PVA-SbQ fibres. Prior to observation, fibres were dried at room temperature and coated with thin conducting material, gold, to prevent the accumulation of electrostatic charge during electron scanning. The fibres were collected onto carbon tape, which is able to improve the conductivity of sample and increase the contrast of image.

3.2.4.4 Endothelial cell culture on PVA-SbQ fibres

Bovine aortic endothelial cells (AG08504, Coriell Institute, NJ, USA) at passage 10 were cultured by RPMI 1640 medium with 10% fetal bovine serum. The medium was changed every 2-3 days and culture flasks or plates were maintained in a humidified incubator at 37 $°C$ with 5% CO_2. At 80-90% confluence, the endothelial cells were detached with 1% trypsin-EDTA and counted with a hemocytometer. Cells were then seeded onto scaffold in the density of 2×10^5 $cells/cm^2$. It is important that the cell suspension was concentrated by centrifuging and seeded on the scaffold for 20min to induce initial cell attachment. The additional culture medium was gently filled into 6-well culture plate along the well wall to prevent flushing cell away from scaffolds.

3.2.4.5 Immunofluoresence Staining

Immunofluoresence staining was performed to assess the cell attachment on PVA-SbQ fibre scaffolds. After 1 day of cell cultured, the fibre sample with cells on it were stained with DAPI and Phalloidin-FITC. DAPI is a blue fluorescent nucleic acid stain which shows the cell nucleus. Phalloidin is a fungal toxin with ability to bind to F-actin in liver and muscle cells and shows green color with FITC label. Phalloidin-FITC stains the cytoskeleton. Briefly, the scaffold samples were fixed with 3.7% formaldehyde for 30 minutes and rinsed with PBS. Then the cells were permeated by immersing in 0.1% triton-X solution for 2-3 minutes. After permeation, the samples were incubated in PBS containing 1% BSA at 37 $°C$ for 30 minutes to reduce nonspecific

background staining. 1: 1000 dilution of DAPI (1 mg/mL in stock) and 1:20 dilution of Phalloidin-FITC (0.5 mg/mL in stock) were then added onto the samples and they were incubated in the dark for 15 minutes. Rinsing with PBS several times, the samples were then viewed under fluorescence microscope with multiple fluorescence modes (Olympus BX51, Japan).

3.2.4.6 Cell morphology

The morphology of endothelial cells on fibres was observed by the use of EVO LS15 scanning electron microscopy (SEM). After 1-day cell culture, the fibre samples with endothelial cells attached were firstly fixed with 3.7% formaldehyde for 30 mins and then dried at room temperature for 1 week. Prior to SEM observation, the samples were coated with gold to reduce the accumulation of the electrostatic charge when the electrons scanned.

3.2.5 Study on hydrogel/fibre duo-layer construct

3.2.5.1 Fabrication of hydrogel/fibre duo-layer film

The duo-layer film samples were designed for the uniaxial tensile test. The fabrication process of hydrogel/fibre duo-layer film has been shown in Figure 3.7. Glass slides were applied as a casting mould for the duo-layer film. Briefly, one glass slide is firstly laminated with 5% PVA solution. Upon drying, PVA thin film is formed on the glass slide (Figure 3.7 A). PVA-SbQ fibres are deposited onto this glass slide by electrospinning technique (Figure 3.7 B). The process parameters in the electrospinning are 10cm as electrospinning distance, 10kv as positive potential, 0.3 mL/h as solution feeding rate and 20min as collecting duration. The collected fibres are then photocrosslinked by exposing to 365nm UV light for 20min. PVA/Gelatin solution is prepared as the same way of in section 3.2.1.1. The as-prepared PVA/Gelatin solution is casted onto fibres (Figure 3.7 C) and covered by another glass slide (Figure 3.7 D). Aluminium spacers are placed in between the glass slides to control the thickness of the film.

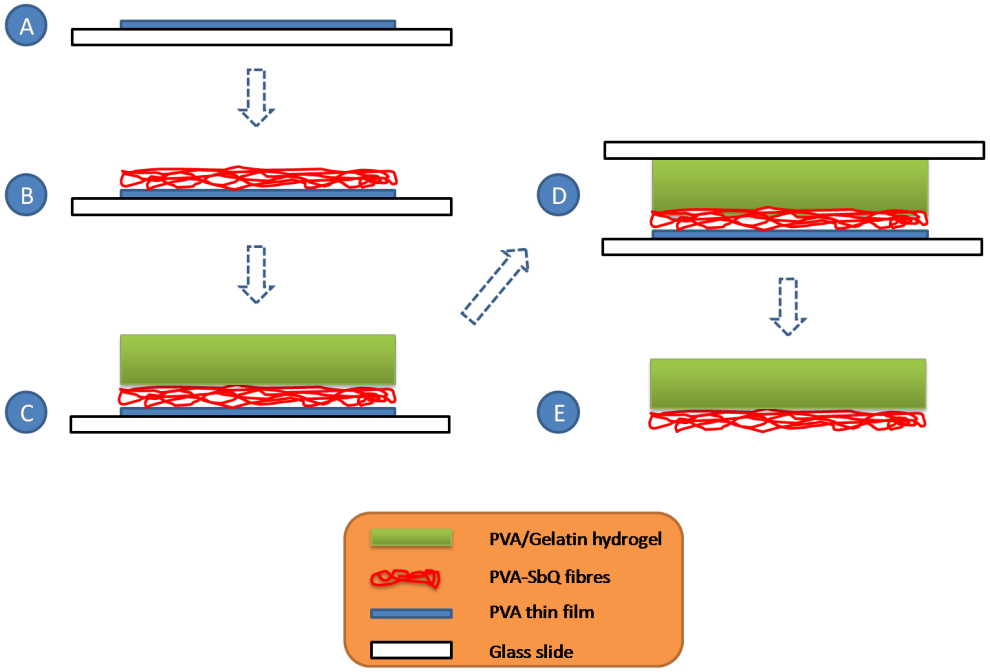

Figure 3.7: Schematic diagram of fabrication of hydrogel/fibre duo-layer film.

Upon 1 cycle freeze-thawing treatment and 1 h coagulation (dynamic coagulation bath stirred by magnetic stirrer), PVA/Gelatin hydrogel and PVA-SbQ fibres duo-layer film is therefore fabricated (Figure 3.7 E). Note that the PVA thin film eases the detachment of final duo-layer film from glass slide.

3.2.5.2 Fabrication of hydrogel/fibre duo-layer vessel

The concept of fabricating hydrogel/fibre duo-layer vessel is similar to that of duo-layer film. Figure 3.8 showed the schematic diagram of the fabrication process of the duo-layer vessel. The PVA-SbQ fibres and PVA/Gelatin solution were prepared with the same process parameters as in Section 3.2.5.1. The as-prepared PVA-SbQ fibres were manually covered onto a stainless steel mandrel. This mandrel is then placed in the graft casting mould (Figure 3.2 B). Upon injecting PVA/Gelatin solution, the mould was then subject to 1 freeze-thaw cycle. The as-formed hydrogel/fibre construct was further submerged into coagulation bath for 1h to obtain the final vessel graft. Coagulation treatment was performed in either static coagulation bath or dynamic coagulation bath as in section 3.2.1.1. Note that it is important to have the fibrous mat big enough

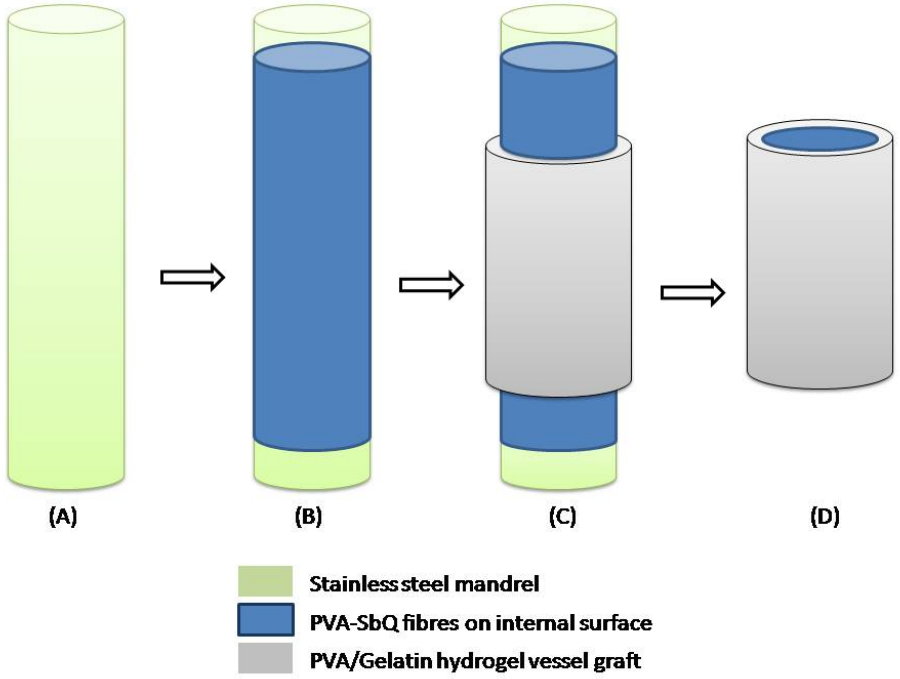

Figure 3.8: Schematic diagram of fabrication of hydrogel/fibre duo-layer vessel.Note that the PVA-SbQ fibres were manually covered onto the stainless steel mandrel in this study.

to cover the whole mandrel to ensure the reproducibility of the duo-layer vessel.

3.2.5.3 Uniaxial tensile test

Uniaxial tensile test was performed in the same parameters as in section 3.2.2.3. The duo-layer film samples tested were shown in table 3.2.

Table 3.2: Samples for uniaxial tensile test.

Coagulation duration	Thickness of PG1FT hydrogel		Thickness of PG1FT hydrogel/fibre construct
	1mm	2mm	2mm
15min	√	√	-
30min	√	√	-
60min	√	√	√

3.2.5.4 Compliance test

A system was set up to perform compliance tests by Dr. C. Lally's research group at Dublin City University. It mainly includes a pump to generate pulsatile cardiac pressure, a sensor to monitor pressure in the system and a video-extensometer to track the changes in the external diameter of vessel graft with respect to each pressure cycle. Two types of tubular samples were tested, including:

1. PVA/Gelatin hydrogel vessel with 1 freeze-thaw cycle and 1h coagulation treatment (static coagulation bath).

2. PVA/Gelatin Hydrogel / PVA-SbQ fibre duo-layer vessel with 1 freeze-thaw cycle and 1h coagulation treatment (static coagulation bath).

A typical pulsatile pressure over time (monitored by the pressure sensor) is shown in Fig 3.9A, and the corresponding displacement of vessel over time (tracked by video-extensometer) is shown Fig 3.9B. The pulse pressure was controlled over a range of mean pressures (40- 140 mmHg) with an increment of 10 mmHg. At each mean pressure, 60 mmHg was set to be the constant difference between end-diastolic pressure and end-systolic pressure. The end-systolic and end-systolic external diameters were measured from the waveform of displacement, like that shown in Fig 3.9B.

The compliance (C) of the vessel grafts is determined at each mean pressure as follows [6]:

$$Compliance = \frac{D_s - D_d}{D_d \times (P_s - P_d)} \times 10^4 \tag{3.7}$$

Where D_s and D_d are systolic and diastolic external diameter of grafts, and P_s and P_d are systolic and diastolic pressure, respectively. In the test, $P_s - P_d$ is maintained as 60 mmHg. The unit of compliance is % per mmHg $\times 10^{-2}$.

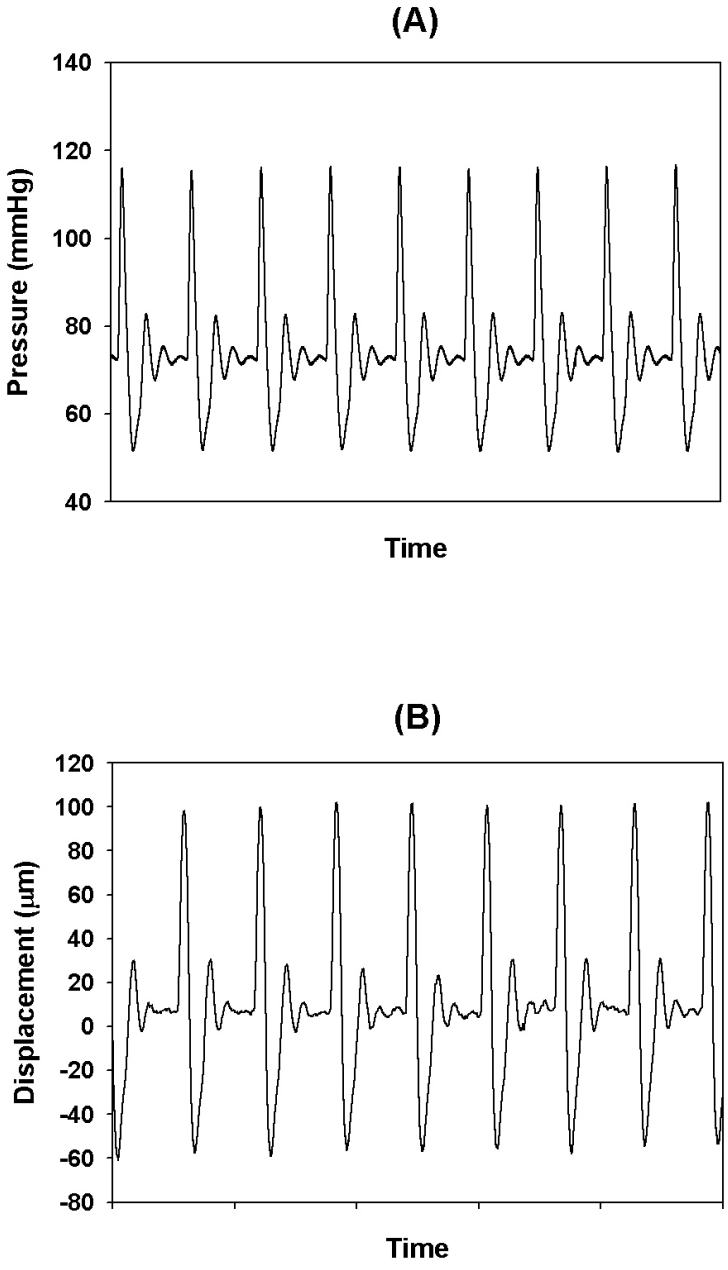

Figure 3.9: Typical profile of pressure versus time and displacement versus time in compliance test. The control on the frequency of pusatile flow was of concern and therefore the profiles were ploted without specific time on x-axis.

3.2.6 Statistical Analysis

Each experiment was performed three to six times. All quantitative data are presented as $Mean \pm S.D$. Statistic analysis was conducted by two-way analysis of variance (ANOVA). The statistical differences between the treatment and control were determined by Tukey's Honestly Significant Differences Test. The level of statistical significance was set to $p < 0.05$.

Chapter 4

Composite hydrogels of PVA with natural macromolecules

4.1 Introduction

4.1.1 PVA and chitosan/gelatin/starch blending system

Polyvinyl alcohol (PVA), as a synthetic polymer, has attracted attention as a potential biomaterial for artificial blood vessels because it can be fabricated as hydrogel, and can match the mechanical properties of the vascular system [7, 8, 9, 130]. However, PVA hydrogels by themselves are not suitable for cell adherence due to their highly hydrophilic nature. To tackle this issue, various biocompatible macromolecules have been blended with PVA to provide for cell attachment to the gel. Gelatin, dextran, collagen, starch, chitosan, and hyaluronic acid blended with PVA have been intensively studied by Cascone et al. [131, 132, 133, 134]

Chitosan is a cationic polysaccharide obtained by alkaline deacetylation of chitin. It has been widely used to improve the cell attachment of PVA hydrogels. Chuang et al. [135] and Koyano et al. [136] reported that chitosan blended with PVA is favorable for the attachment and growth of fibroblast cells. One previous study has shown that the chitosan blended with PVA allowed vascular smooth muscle and endothelial cells to

attach and grow on the hydrogel [10]. Gelatin, a natural protein derived from collagen denaturation, maintains functional groups to promote cell attachment [137, 138] and is known to exhibit biocompatibility in long term clinical applications [139]. Gelatin is widely used to fabricate tissue scaffolds in combination with various synthetic polymers for the purpose of improving the biocompatibility of synthetic polymers, [7, 140] including PVA[138]. Starch, a polysaccharide-based polymer, is a mixture of amylose and amylopectin and it has been blended with PVA in previous studies [141, 142].

4.1.2 Freeze-thawing and coagulation

PVA hydrogels can be prepared by chemical crosslinking, photocrosslinking, high-energy irradiation, or physical crosslinking (such as the freeze-thaw technique). Among these, the freeze-thaw technique has a remarkable advantage of being able to crosslink the polymer solution without leaving in the gel matrix any crosslink remnant which could leak out and evoke serious inflammatory response after implantation into the human body. The freeze-thaw process is capable of producing PVA hydrogels with a wide range of mechanical properties by controlling parameters such as the number of freeze-thaw cycles, the quenching temperature, and the thawing rate. An increase in the number of freeze-thaw cycles and a decrease in the thawing rate could result in a stiffer hydrogel. However, this would render the manufacturing process time-consuming. In manufacturing polymer product, a fast and cost-efficient processing route is required. Moreover, freeze-thawing cycles do not have the same effect on the substitutes as on PVA; thus the degradation of the substitutes would be faster than the PVA, which could compromise the hydrogel composition.

Polymer coagulation is an important technique in polymer solution processing. It involves quenching a polymer solution in an aqueous nonsolvent, which results in solvent-nonsolvent exchange and polymer precipitation [143]. This process would considerably simplify the manufacturing route and act as another physical crosslinking route for PVA-based hydrogels.

4.1.3 Objective of this study

In this study, PVA was blended with chitosan, gelatin and with starch, and treated with a combination of freeze-thaw and coagulation techniques to obtain hydrogels for evaluation with respect to artificial blood vessel applications. The structure-property reltionships were examined by measuring the swelling, rehydration, mechanical properties of PVA based hydrogels. In particular, the influence of the number of freeze-thaw cycles, coagulation and additive type on the structure on the structure and mechanical properties were investigatede.

4.2 Results

4.2.1 Equilibrium swelling study

The equilibrium swelling ratios of each PVA hydrogel sample are shown in Figure 4.1. For all the PVA hydrogels, the equilibrium swelling ratio decreases with increasing number of freeze-thaw cycle and with coagulation treatment, although some variation is observed. The highly swollen hydrogel represents a less tight structure and a lower degree of crosslinking compared to the hydrogels with lower swelling ratio. The crosslinks in the hydrogel hinder the mobility of polymer chain and resulted in a lower swelling ratio [144].

For PVA, PVA/Chitosan and PVA/Gelatin hydrogels, the samples treated for one freeze-thaw cycle without coagulation showed a much more swollen structure than others ($p < 0.05$). However, the "overshoot" in the volume swelling ratio is a strong indication of some initial instability due to the loss of crystallinity and chain dissolution [145].

Increasing the number of freeze-thaw cycles leads to further formation of crystals which act as crosslinking sites, therefore indicating a more stable network structure, which behaves like a less swollen structure. The equilibrium swelling decreases with the increasing number of freeze-thaw cycles, except for the PVA/starch hydrogels. Af-

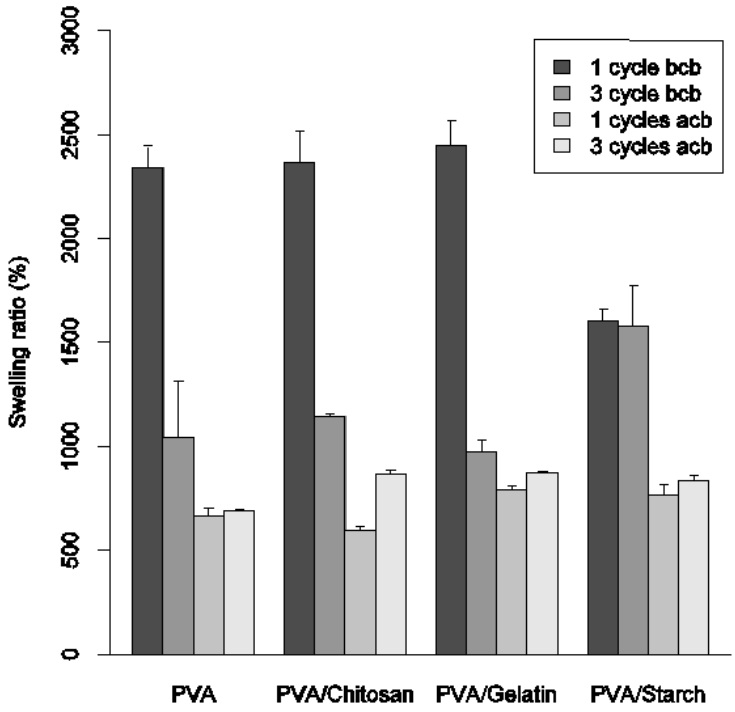

Figure 4.1: The equilibrium swelling of PVA based hydrogels (n=4).

ter submersion in the coagulation bath, the equilibrium swelling ratio of all hydrogels went through a significant decrease in their equilibrium swelling ratio ($p < 0.05$).

4.2.2 PVA hydrogel structure

The degree of equilibrium swelling is closely related to the hydrogel structure. A high degree of equilibrium swelling is generally associated with large pore or mesh size of gel network. A significant change in the structure of PVA based hydrogels can be qualitatively reflected by the changes in equilibrium swelling. Flory and Rehner [146] contributed to the early development of rubber elasticity theory for polymers. Peppas and Merrill et al. [78] further modified this theory and developed a new model suitable for studying the structural properties of hydrogels prepared in the presence of a solvent. Two structural properties, including the average molecular weight between crosslinks, M_c, and mesh size, ξ, were predicted by Eqs 4.1 and 4.2 [78].

Table 4.1: Network structure properties of PVA hydrogels

Hydrogels	$V_{2,s}$ ×10^{-2}	$V_{2,r}$ ×10^{-2}	M_c (g/mol)	ζ (Å)
1 Cycle bcb[a]	4.3	4.9	8200	230
3 Cycles bcb	9.6	9.5	3100	120
1 Cycle acb	15.0	19.6	500	40
3 Cycles acb[b]	14.5	19.1	500	40

[a] 1 cycle, 1 freeze-thaw cycle; bcb; before treatment of coagulation bath.
[b] 3 cycles, 3 freeze-thaw cycles; acb, after treatment of coagulation bath.

$$\frac{1}{M_c} = \frac{2}{M_n} - \frac{\frac{ln(1-V_{2,s})+V_{2,s}+\chi V_{2,s}^2}{\rho_2 V_1}}{V_{2,r}\left[\left(\frac{V_{2,s}}{V_{2,r}}\right)^{1/2} - \left(\frac{V_{2,s}}{2V_{2,r}}\right)\right]} \tag{4.1}$$

$$\xi = Q^{-1/3}\left[C_\infty\left(\frac{2M_c}{M_r}\right)\right]^{1/2} l \tag{4.2}$$

Where M_n is the average molecular weight of PVA, ρ_2 is the density of the dry polymer (1.269 g/cm^3 for atactic PVA), and V_1 is the molar volume of the solvent (18 cm^3/mol for water). C_∞ is the Flory characteristic ratio (8.4 for PVA), and l is the carbon-carbon bond length (1.54 Å). The Flory-Huggins interaction parameter, χ, is another important parameter. The χ of PVA and water is 0.494 [147]. This model will now be applied to PVA-only cryogels which have been processed by four different routes, and used to provide estimates of the molecular weight between crosslinks and mesh size. Even though the χ of chitosan, starch and gelatin have not been reported in literatures and some further determination of χ will be required in future works, the effect of the number of freeze-thaw cycles and coagulation on the network structure of PVA hydrogel can be clearly addressed from Table 4.1. The molecular weight between crosslinks (M_c) and mesh size (ξ) were remarkably decreased with the increasing number of freeze-thaw cycles and the treatment of coagulation bath. However, there is no significant different between PVA hydrogels with 1 cycle after coagulation bath (1Cycles-acb) and 3 cycles before coagulation bath (3Cycles-bcb).

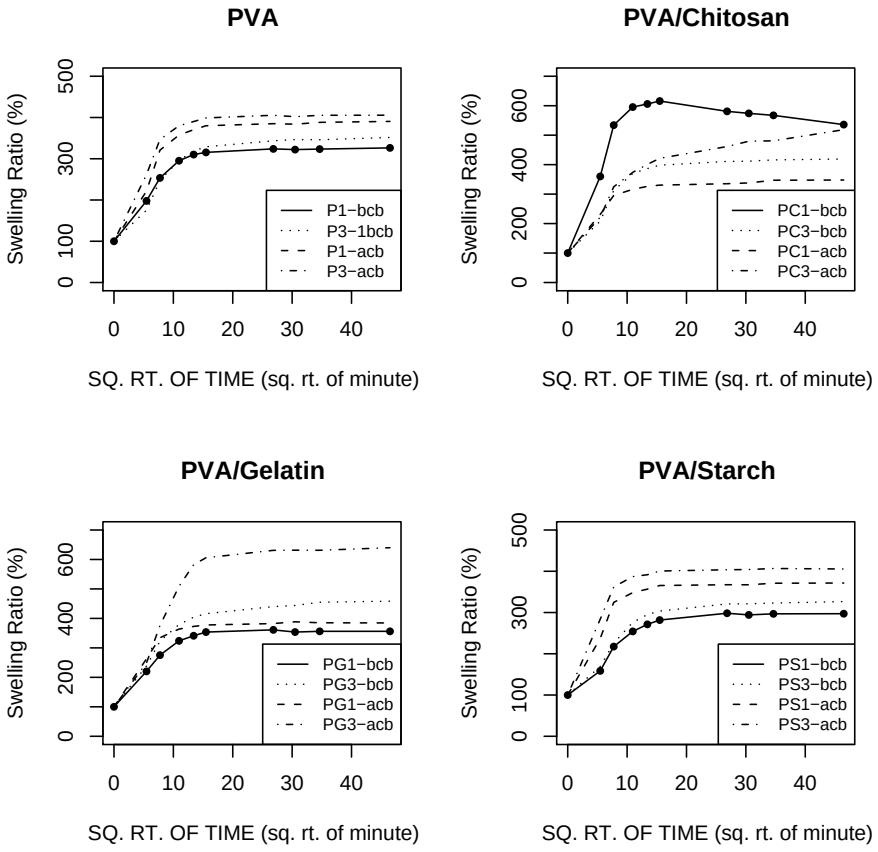

Figure 4.2: The rehydration profiles of PVA based hydrogels (n=3).

4.2.3 Rehydration study and reequilibrium ratio

When a dehydrated hydrogel sample is submerged into water, swelling occurs due to water absorption, which is induced by osmotic pressure. During the sorption process, diffusion of water into the sample matrix causes continuous changes in materials until equilibrium swelling is reached [148]. The sorption behavior of dehydrated PVA samples is shown in Figure 4.2. The swelling ratio is plotted against the square root of sorption time to aid interpretation. In general, sorption occurs rapidly within the first few hours, and then slows down after approximately 5 hours as equilibrium swelling is approached. The sorption curves in Figure 4.2 are close to sigmoid behavior, which is related to the diffusion behavior of water. The anomalous water sorption behavior of hydrophilic polymers including PVA has previously been reported [149], following a similar pattern to that shown here for short times.

4.2.4 Mechanical properties

The data obtained from tensile tests was in the form of load versus extension data, which was then converted into engineering stress versus engineering strain and further converted into true stress versus true strain, using the sample cross section area and the initial gauge length. The true stress and true strain were calculated by eqs. 4.3, 4.4, 4.5 and 4.6 as follows:

$$\sigma_E = \frac{F}{A_0} \tag{4.3}$$

$$\varepsilon_E = \frac{l - l_0}{l_0} \tag{4.4}$$

$$\sigma_T = \sigma_E(1 + \varepsilon_E) \tag{4.5}$$

$$\varepsilon_T = ln(1 + \varepsilon_E) \tag{4.6}$$

Where σ_E is engineering stress, F is force, A_0 is initial cross-section area, ε_E is engineering strain, l is final extension, and l_0 is intial gauge length, σ_T is true stress and ε_T is true strain. Even though the approximate average strain between diastole and systole of porcine aortic root is between 20 and 30% [9, 150], to provide a full characterization of the uniaxial mechanical response up to and beyond in vivo strain levels, data was shown up to 40% strain.

Figure 4.3 presents the effect of numbers of freeze-thaw cycles and the coagulation bath on the tensile property of PVA hydrogels. When ANOVA was applied to the stress reading of all PVA hydrogel samples at 40% strain, a stiffening effect is observed between p1-bcb and p3-bcb hydrogels (where p1 and p3 denote pure PVA hydrogels with one and three freeze-thaw cycles, respectively, and bcb signifies hydrogels tested before coagulation bath treatment). The coagulation bath enhanced the stiffness of

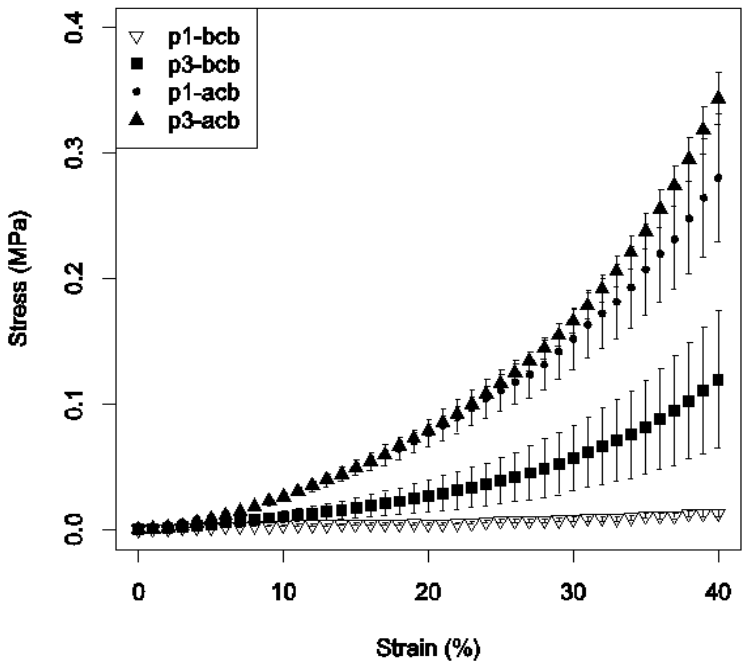

Figure 4.3: The effect of freeze-thaw cycles and coagulation treatments on PVA hydrogels (n=6).

both 1 cycle and 3 cycles PVA hydrogels, but no statistically difference was found between p1-acb and p3-acb ($p > 0.05$), where the acb designation refers to hydrogels after coagulation bath treatment.

Figures 4.4, 4.5 and 4.6 show the effect of freeze-thaw cycles and the coagulation bath on the tensile properties of PVA/Chitosan, PVA/Gelatin, and PVA/Starch hydrogels. Note that, in the labeling system used in these Figures, pc, pg, and ps refer to the PVA/Chitosan, PVA/Gelatin, and PVA/Starch compositions, respectively. The PVA/chitosan (Figure 4.4) and PVA/starch (Figure 4.6) hydrogels showed increased stiffness for the higher number of freeze-thaw cycles and after the coagulation treatment. For PVA/chitosan samples, a statistically significant difference for stress at 40% strain was found between each of the four experimental cases ($p < 0.05$). For PVA/starch hydrogels, this significant difference is also found. As for PVA/Gelatin hydrogels (Figure 4.5), the higher number of freeze-thaw cycles and the coagulation bath treatment have a similar effect on stiffness as for the other two blend systems. However, there is no significant difference between pg1-acb and pg3-bcb ($p > 0.05$).

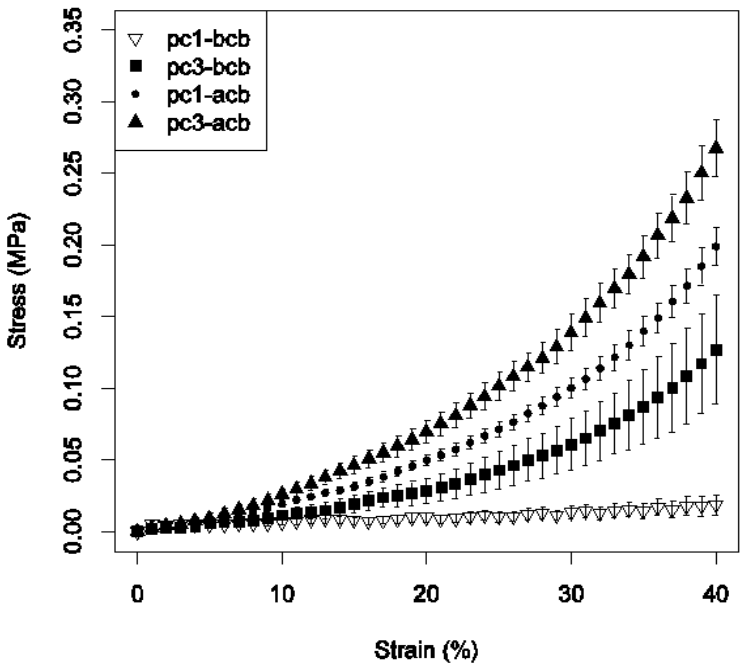

Figure 4.4: The effect of freeze-thaw cycles and coagulation treatments on PVA/Chitosan hydrogels (n=6).

Otherwise, the stiffness of the hydrogels increased according to the following order; 1-bcb, 3-bcb, 1-acb to 3-acb.

4.3 Discussion

Hydrogel grafts for vascular tissue engineering are required to have physical stability and tissue-like elasticity. In this study, the equilibrium swelling ratio (Figure 4.1) was investigated as an indicator for hydrogel structure which is confirmed for the PVA hydrogel by calculating average molecular weight between crosslinks and mesh size (Table 4.1). The uniaxial tensile test was applied to profile the stress-strain relationship of each hydrogel.

4.3.1 Preconditioning cycle

Figure 4.7 showed the effect of two preconditioning cycles (repeated loading to 60% strain and unloading to 0% strain) on the stress-strain profile of the hydrogel. In the

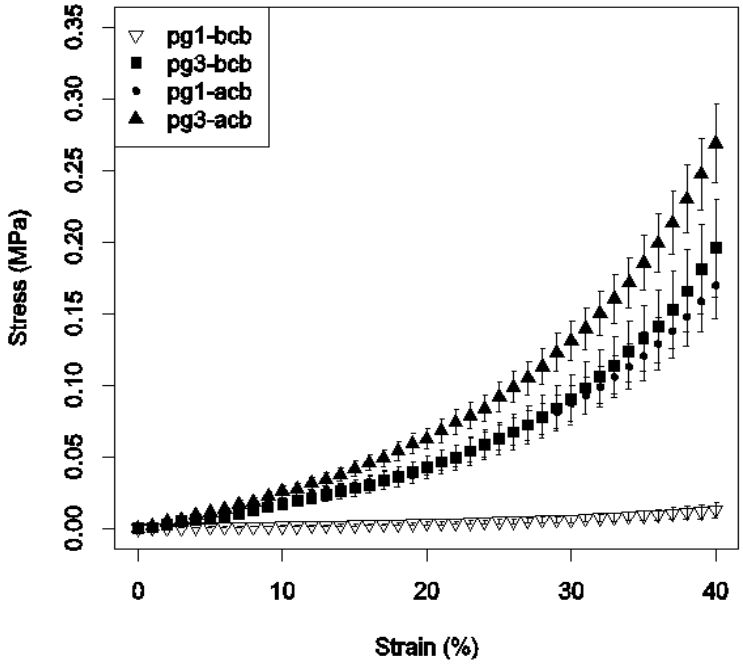

Figure 4.5: The effect of freeze-thaw cycles and coagulation treatments on PVA/Gelatin hydrogels (n=6).

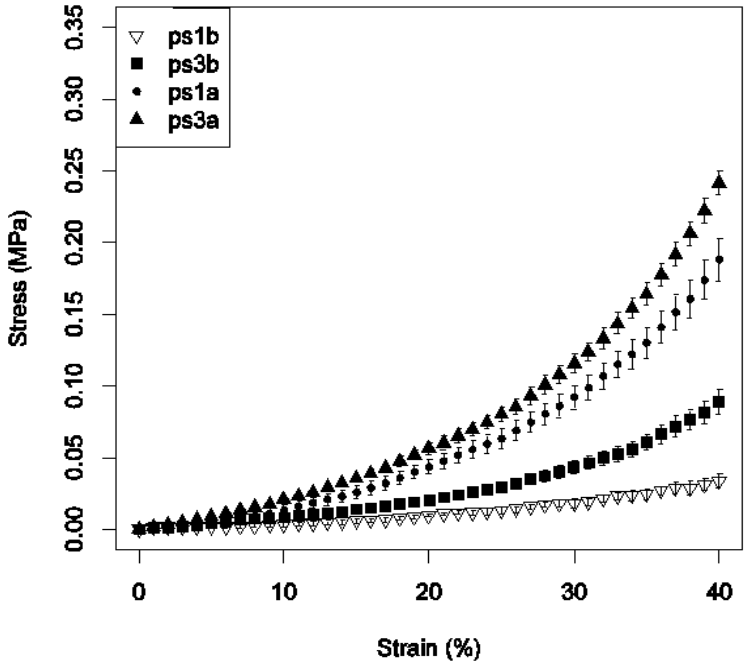

Figure 4.6: The effect of freeze-thaw cycles and coagulation treatments on PVA/Starch hydrogels (n=6).

first preconditioning cycle, the hydrogel sample is conditioned with the loading and unloading process. The unloading profile of the first preconditioning cycle overlays the unloading of the second preconditioning cycle. The loading profile of the second preconditioning cycle overlays the final loading path. If additional preconditioning cycles were performed, the profile will be the same as the second preconditioning cycle. This also means that one loading and unloading cycle is sufficient for preconditioning the hydrogel. The significant different between first loading and second loading profile represents the rearrangement of hydrogel network to the external uniaxil tensile stress.

The softening effect of the second preconditioning cycle is similar to the hysteresis effect of native arteries [151], called the hysteresis loop. The area enclosed in the loop indicates the energy lost by viscoelasticity [152], which would help to smooth the pulsatile flow.

The preconditioning cycle is able to stabilise tissue or hydrogel samples and reproduce the state of tissue sample in the physiologic condition [153]. It is therefore recommended that preconditioning cycles should be performed in tensile tests for either the hydrogels produced or for the native arteries.

4.3.2 Nonlinearity

It is well accepted that the stress-strain relationship of arteries is non-linear [152, 154, 21, 22, 23, 24, 25]. This nonlinearity is due to the main components of arteries, elastin and collagen [152, 154], see Figure 4.8. Elastin is an elastic component which can be recruited from the low strain range. Collagen is a component stiffer than elastin. Collagen fibres are initially in the coiled state. It is therefore the case that only elastin is initially employed to resist external load. When the extension passes a critical strain, the coiled collagen fibres are stretched and take a main role in response to the external load [25].

This non-linear elasticity of arteries is of extreme importance for damping out the pulsatile blood flow and allowing regular irrigation of downstream organs [155]. The

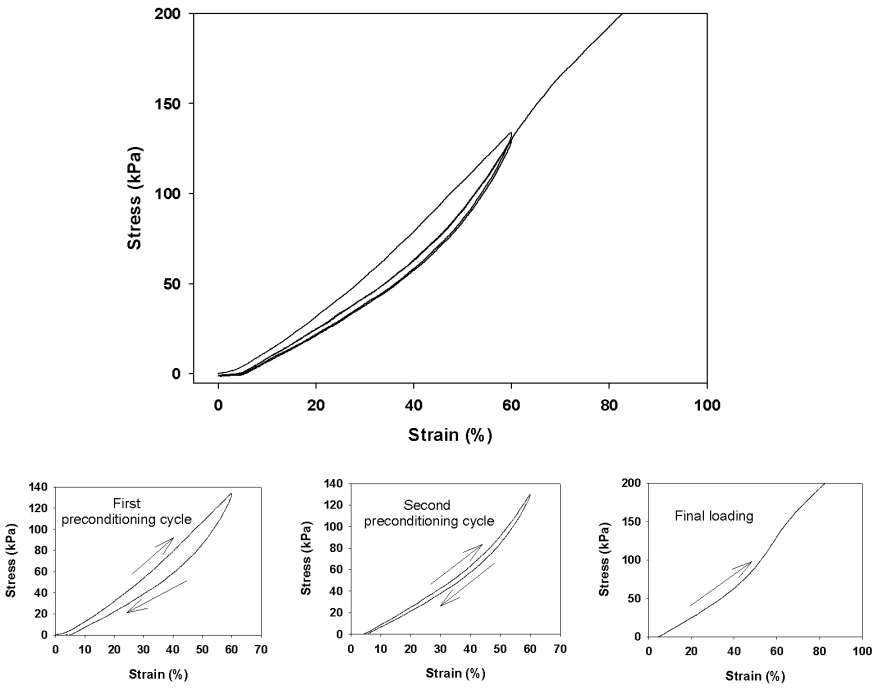

Figure 4.7: Preconditioning cycles in tensile test on a hydrogel sample. Arrows represent loading and unloading.

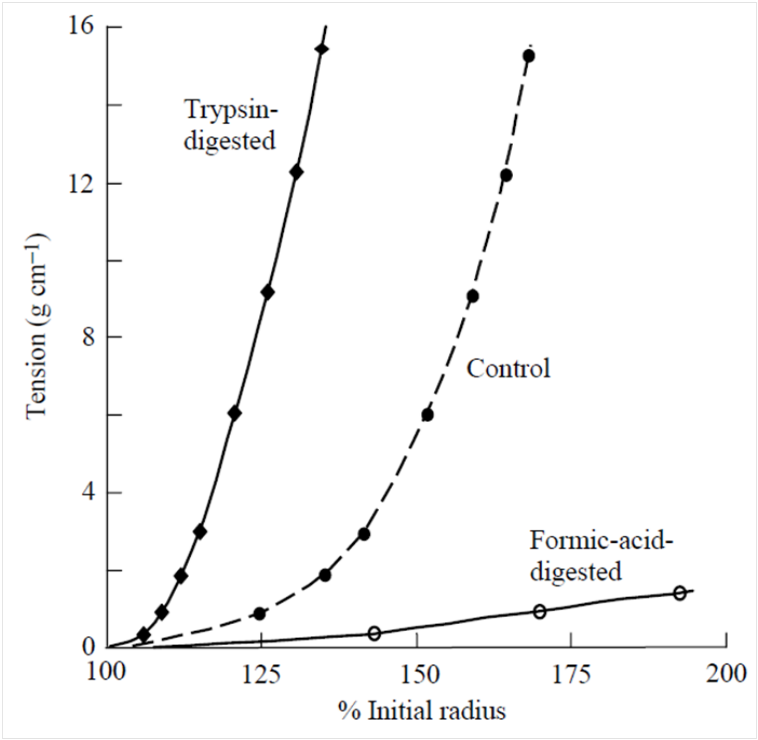

Figure 4.8: The tension-length profile of human iliac artery and its main components, elastin and collagen. Trypsin digestion removed elastin and remained collagen fibres. Formic-acid digestion removed collagen and remained elastin fibres. (data redrawn by Shadwick [152] from Roach and Burton [27])

cyclic nature of the heart pump produces cyclic increases and decreases in blood pressure which creates pulsatile blood flow [156]. This non-constant flow would result in high shear stress and irregular irrigation of organs. To address this and to smooth the blood flow, the elastic arteries serve as compliance chambers that temporarily store the stretching energy at systole (heart ejects blood) and release this energy by compressing the filled blood at diastole (heart fills with blood). Therefore the diastolic pressure in arteries does not decrease as much as in the heart. In fact, the diastolic pressure of aorta is maintained at a high value in humans. The systolic/diastolic pressure of the heart left ventricle is about 120/5 mmHg. In contrast, that of the aorta is kept at about 120/80 mmHg.

The mechanical properties of the PVA-based composite hydrogels were studied using tensile tests. All the stress-strain curves in Figures 4.3, 4.4, 4.5 and 4.6 show a nonlinear response that agrees with the nonlinear stress-strain behaviour of arteries. It is reported that elastin mainly contributes to the initial low stiffness region of the nonlinear curve, whereas collagen is responsible for the higher stiffness region at large strains [7, 157]. A similar kind of behavior might be expected for the composites used in this study. However, the mechanical properties appear to be dominated by PVA. As for the PVA hydrogel, there are three different regions that can be classified in its microstructure that would contribute to mechanical properties in a different manner: crystalline phase, amorphous phase, and water. Watase et al. [158] first investigated the effect of freezing and evacuating of PVA hydrogels on the complex Young's modulus, and concluded that the increase of the elastic modulus is due to increased crystallinity in the PVA hydrogel. Wan et al. [7] reported that the uncoiling and reorganizing of the polymer chain in PVA hydrogel under loading might contribute to the nonlinear tensile property of PVA hydrogel.

A summary of the secant modulus measurements at 40% strain is shown in Figure 4.9. All the PVA-based hydrogels showed two similar trends. First, the increase in secant modulus by increasing the number of freeze-thaw cycles without coagulation

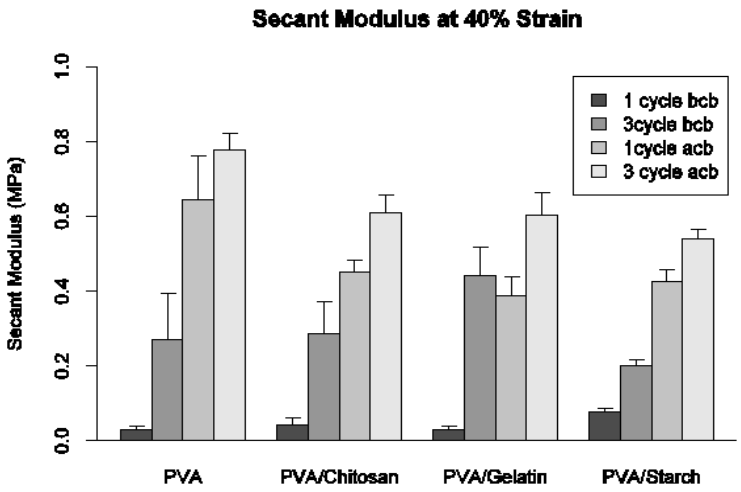

Figure 4.9: Secant modulus of PVA based hydrogels at 40% strain (n=6).

was significant. The modulus has increased 2-5-fold when the number of freeze-thaw cycle was increased from 1 to 3. This is in agreement with the previous studies for PVA hydrogels [7, 158, 159]. The second trend is that the treatment of the coagulation bath significantly increased the modulus of the hydrogels.

4.3.3 Reswelling ratio

In comparing the equilibrium swelling of the as-formed hydrogel (Figure 4.1) and of the dehydrated hydrogel (Figure 4.2), the difference between these two equilibriums can be addressed and presented as reswelling ratio (Figure 4.10). This reswelling ratio is a ratio between crosslinked polymer fraction and the total polymer fraction of the as-formed hydrogel, which indicates the physical crosslinking effect of freeze-thaw cycles and coagulation. Because these two equilibrium properties were determined for each hydrogel using separate sets of experiments, average equilibrium values were used to calculate the reswelling ratio. The dehydrated PVA-based hydrogels reswelled completely to the predehydrated level, which is consistent with other reports[88, 90]. The variation of reswelling ratios is due to the different polymer fraction applied in calculating these two equilibriums. The equilibriums of as-formed hydrogels are calculated from the polymer fraction of swollen hydrogel. The equilibriums of dehydrated

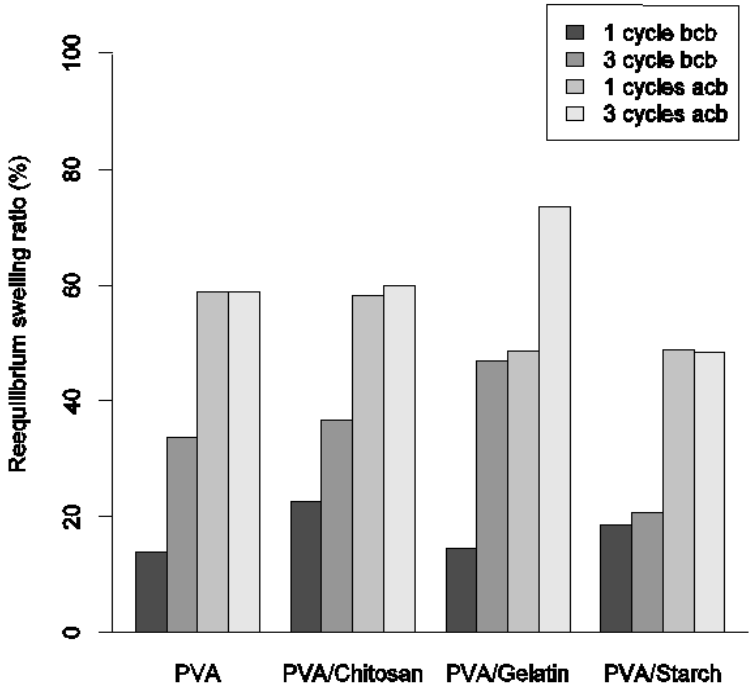

Figure 4.10: The reequilibrium swelling ratio of PVA based hydrogels.

hydrogels are calculated from the polymer fraction of as-formed hydrogel. When the noncrosslinked polymer fraction leaked out during swelling, the polymer fraction of the swollen hydrogel became lower than that of the as-formed hydrogel, which resulted in the variation of reswelling ratios. 10% polymer solution was used to prepare each hydrogel. After physical crosslinking by freeze-thaw cycles and coagulation, hydrogel networks were formed with different crosslinked polymer fraction.

The reswelling ratios (Figure 4.10) and secant modulus (Figure 4.9) of the as-prepared hydrogels are relatively consistent with each other, except for the PVA/starch hydrogels. The reswelling ratio represented the fraction of polymer crosslinked for the hydrogels in this study. The increase in reswelling ratio means more polymer has been crosslinked during freeze-thaw cycles and coagulation. In tensile tests, hydrogels were extended in one direction, and the gel network would be reorganized. With the increase in crosslinked polymer fraction, more polymer content would be applied to support the gel network and, therefore, more resistance to the extension would be generated in the tensile tests.

The freeze-thawing process has long been used as a physical crosslinking method for preparing PVA hydrogels. There are three main theories to explain the effect of the freeze-thaw process on PVA; hydrogen bonding, polymer crystallite formation, and liquid-liquid separation [7]. Combined with the model of crystalline formation during freeze-thaw cycles [160] and the model of coagulation in polymer processing [143], one hypothesis is given to explain the effect of freeze-thawing and coagulation on the property of PVA-based hydrogels. Starting from fresh polymer solution, the initial freezing step would form some ice crystals which concentrate the polymer solution in regions between the ice crystal and promote the formation of PVA crystallites. These crystallites would act as crosslinking sites for polymer chains. Upon thawing, the ice crystal would melt and create one region of polymer-rich gel which would be surrounded by another region of polymer-poor solution. During successive freeze-thawing cycles, additional formation of ice crystals would take place in the region of polymer-poor solution and the newly generated crystalline sites which further enhance the polymer crystallization in the gel,resulting in a hydrogel with smaller pore size (Table 4.1) and higher stiffness (Figure 4.9). Upon immersion of the polymer hydrogel in the coagulation bath, the region of polymer-poor solution comes in contact with the coagulant. The fast solvent-coagulant exchange across the interface of polymer solution and coagulant cause an immediate precipitation of the polymer which would results in a further enhancement of the polymer crystallization in gel network and consequently presented a further decrease in pore size (Table 4.1) and higher stiffness (Figure 4.9). Chapter 5 will describe microstructural characterisation experiments which are intended to further probe the structural formation of one of these hydrogels.

4.4 Summary

In this part of the research, the feasibility of preparing PVA-based hydrogels with controllable mechanical property was investigated. Three PVA based hydrogels were prepared by blending PVA with chitosan, gelatin and starch and by treatment with

freeze-thaw cycles and coagulation. With equilibrium swelling, reswelling and tensile testing, the synergistic crosslinking with freeze-thaw technique and coagulation was found to be able to act as versatile method to control the structure and mechanical properties of PVA-based hydrogels. The secant modulus of the hydrogels can be enhanced with the increased cycles of freeze-thaw and with the treatment of coagulation. The structural property and mechanical property were found to be closely related with each other.

A parallel study on the endothelial cell behavior on the PVA based hydrogel has been investigated by my colleague Engin Vrana [161]. It is report that endothelial cell presented highest proliferation rate on PVA/Gelatin hydrogels after culturing for 10 days. Meanwhile, PVA/Gelatin was able to form much more stable hydrogels, when comparing the ultimate tensile strength of the three composites hydrogels. For these reasons, PVA/Gelatin hydrogels were selected for further study in the following chapters.

Chapter 5

Structure formation of PVA/Gelatin hydrogels

5.1 Introduction

In last chapter, the effect of freeze-thaw cycles and coagulation bath on the structural and mechanical properties of PVA based hydrogels has been addresed. It is clear that both freeze-thaw cycle and coagulation treatments are able to enhance the stiffness of PVA/Gelatin hydrogels. However, this is an overall understanding of the relationship between processing parameters and final properties of hydrogels. To be able to explain this relationship more clearly, a study on the microsture formation of PVA/Gelatin hydrogels was necessary.

In this chapter, glass transition temperature, melting temperature, degree of crystallinity, polymer fraction and mechanical properties of PVA/Gelatin hydrogels were investigated to elucidate the structure formation of these hydrogels.

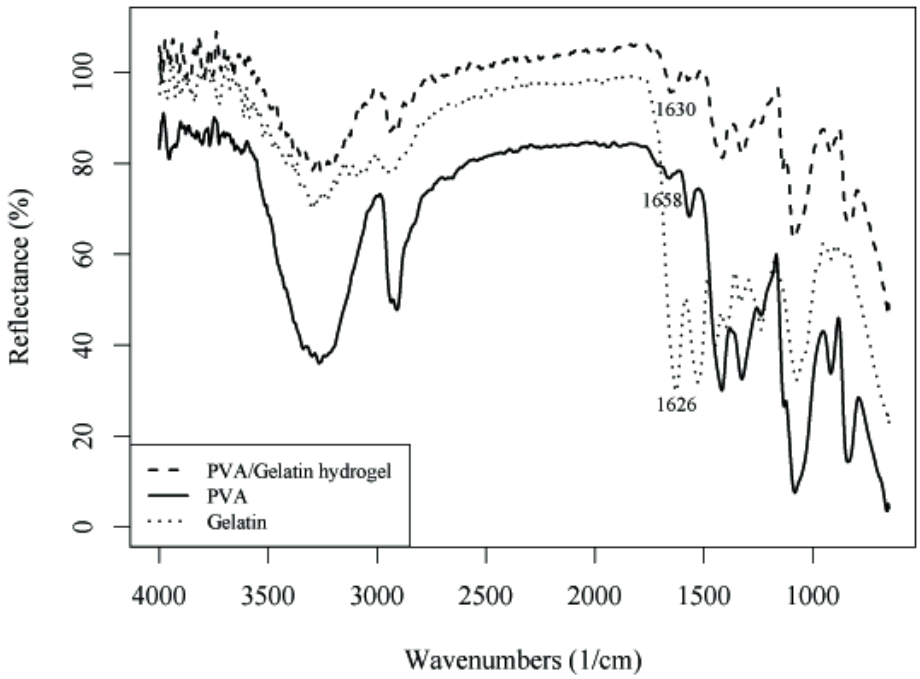

Figure 5.1: FTIR spectra of PVA, gelatin and PVA/Gelatin hydrogels.

5.2 Results

5.2.1 ATR-FTIR analysis of PVA/Gelatin hydrogels

The ATR-FTIR spectra for the PVA, gelatin and PVA/Gelatin hydrogels are shown in Figure 5.1 and the assignment of each peak of PVA and gelatin are listed in table 5.1 and 5.2. Notable differences can be found in the region of 1475-1775 cm^{-1}. The peak at 1626 cm^{-1} in the gelatin spectrum can be assigned to the C=O stretching and hydrogen bonding coupled with COO- stretching [162, 163]. As PVA only shows a small shoulder at 1658 cm^{-1} due to the water absorption, the increase in the intensity of the peak at about 1630 cm^{-1} shows the presence of gelatin in the PVA/Gelatin hydrogel. The peak shift from 1626 cm^{-1} to 1630 cm^{-1} indicates an interaction between PVA and gelatin, which represents the compatibility of PVA and gelatin blend. There is no significant difference between the other peaks of PVA and the PVA/Gelatin hydrogel.

Table 5.1: Assignment of the FTIR peak of PVA[147].

Wave number of peak (cm^{-1})	Assignment
3340	OH stretching
2942	CH_2 stretching (atactic)
1452	CH-OH bending
1336	CH-OH bending
1238	CH wagging
1095	C-O stretching
916	C-O stretching yndiotactic
843	C-C stretching

Table 5.2: Assignment of the FTIR peak of gelatin [162, 163].

wave number of peak (cm^{-1})	Assignment
3310	N-H stretching, coupled with hydrogen bonding
2924	CH_2 asymmetrical stretching
1644	C=O stretching/Hydrogen bonding coupled with COO^-
1544	N-H bending coupled with CN stretch
1451	CH_2 bending
1402	CH_2 wagging of proline
1335	CH_2 wagging of proline
1243	N-H bending coupled with CH_2 wagging of proline
1107	C-O stretching
1080-660	Skeletal stretch

5.2.2 Thermal analysis of the hydrogel systems

Figure 5.2 presents the MDSC thermograms of the PVA and PVA/Gelatin hydrogel with 1 freeze-thaw cyle. The relaxation observed at 100-200 ^oC designated as the β_c relaxation, is due to the relaxation in the PVA crystalline domains. The third relaxation in the temperature range of 200-250 ^oC is caused by the melting of the crystalline domains of PVA [164].

The MDSC thermogram of PVA/Gelatin 1FT hydrogel showed no apparent difference with that of PVA 1FT hydrogel, which is prepared using the same procedure as the PVA/Gelatin hydrogel but with 10% PVA instead of 9% PVA and 1% gelatin. The gelatin does not affect the PVA melting temperature, which indicates that no significant modification occurs in the nature of PVA crystallites because of the presence of gelatin. Cascone et al [134] reported a similar result for a PVA/dextran hydrogel system. Additionally, the PVA/Gelatin hydrogel is mainly composed of PVA. Therefore, the following discussion is based on the formation of PVA crystallites during freeze-thaw cycles and the effect of polymer coagulation.

MDSC analysis of PVA/Gelatin hydrogels (Figure 5.3) shows that the freeze-thawing and coagulation treatments affect their melting temperature (T_m). The T_m of PVA/Gelatin hydrogels increased in the order of 1FT, 3FT, 1FT-acb and 3FT-acb, with melting temperature 224 ^oC, 227 ^oC, 232 ^oC and 233 ^oC, respectively.

5.2.3 Crystallinity analysis of the hydrogel systems

The MDSC thermogram also provides information on the enthalpy of each relaxation. The heat required for melting of 100% crystalline PVA is 138.6 J/g [165, 166]. Therefore, the degree of crystallinity can be quantitatively estimated by the enthalpy of melting, which is the third relaxation in the temperature range of 200-250 ^oC.

The degrees of crystallinity of PVA/Gelatin hydrogels were calculated as 31.2%, 36.3%, 18.3% and 23.9% for 1FT, 3FT, 1FT-acb and 3FT-acb, respectively. Therefore, the treatment of freeze-thaw cycles enhanced the degree of crystallinity. In contrast,

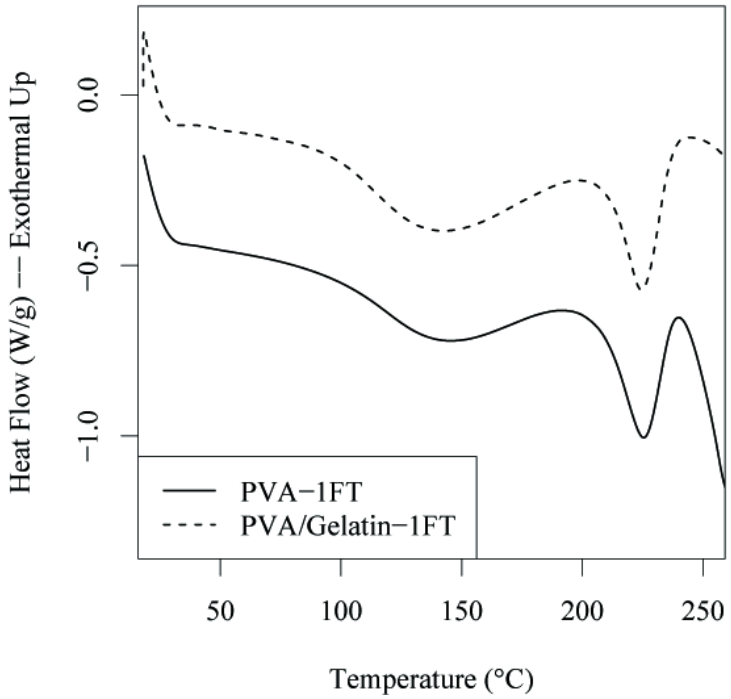

Figure 5.2: MDSC thermograms of PVA and PVA/Gelatin hydrogels with 1 freeze-thaw cycle.

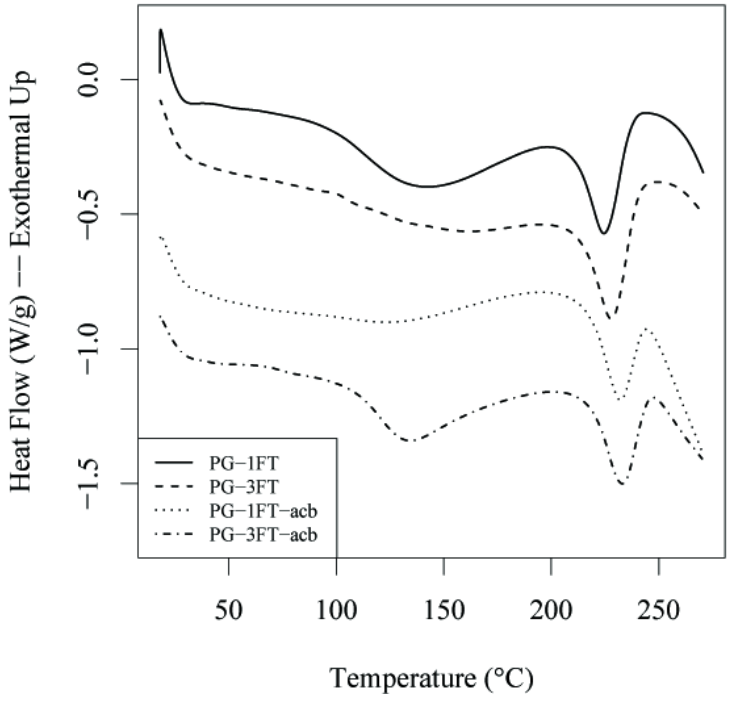

Figure 5.3: DSC thermograms of PVA/Gelatin dried hydrogels.

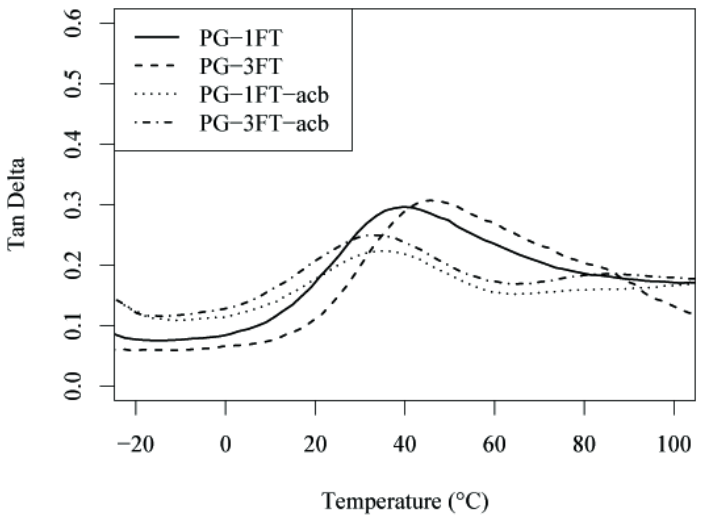

Figure 5.4: Tan delta of PVA/Gelatin dried hydrogels.

the coagulation attenuated the degree of crystallinity.

5.2.4 DMTA analysis of the hydrogel systems

DMTA was used to measure the glass transition temperature (Tg) of the PVA-based materials. Due to machine constraints, the samples were tested in their dry state, thus the modulus obtained from DMTA is not considered as an indication of a true hydrogel mechanical property. Instead, the storage modulus from rheology tests and data from ultimate strength from uniaxial tensile tests are used to evaluate the mechanical properties of these hydrogels.

From the DMTA thermograms a notable shift occurred in the Tan delta values for the hydrogels samples which correspond to the glass transition (Tg) of the gels (Figure 5.4). By increasing the freeze thaw cycle time from 1 to 3 cycles the Tg shifted from 39.7 to 45.7 ^{o}C respectively. This shift is due to the increase in the crystallinity of the hydrogel. However, in relation to the samples which were prepared using coagulation treatment, the Tg values decreased (35.6 to 33.6 ^{o}C respectively) due to the reduction in crystallinity. This finding is comparable with the MDSC crystallization analysis.

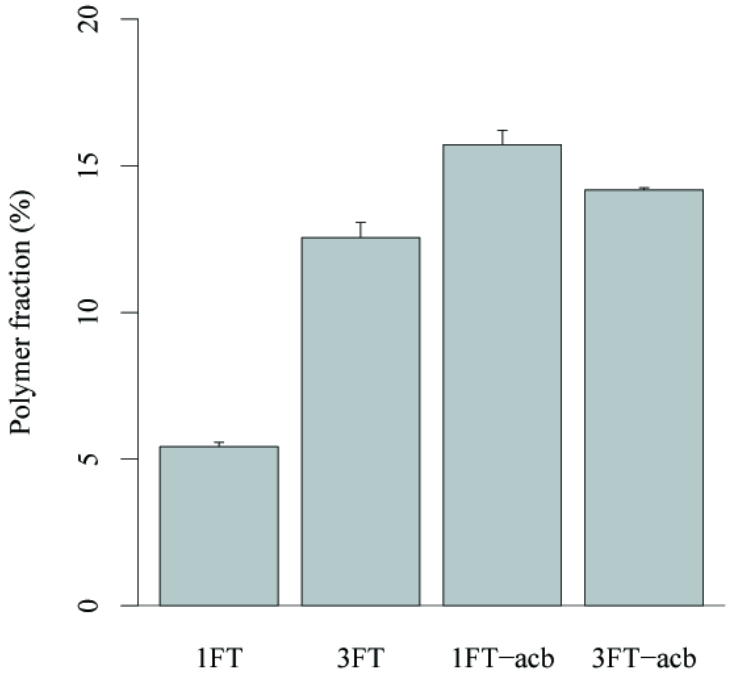

Figure 5.5: The polymer fraction of PVA/Gelatin hydrogels (n=4).

5.2.5 Polymer fraction analysis

The polymer fractions calculated for the PVA/Gelatin hydrogels are shown in Figure 5.5. Both additional thermal treatment and coagulation treatment were found to enhance the polymer fraction in the hydrogel. The polymer fraction significantly increased from 5.4% for 1FT hydrogel to 12.6% for 3FT hydrogel ($P<0.001$). When 1FT and 3FT PVA/Gelatin hydrogels were treated with coagulation, their polymer fractions further increased to 15.7% and 14.1%, respectively ($P<0.001$).

5.2.6 Mechanical analysis of the hydrogel systems

In the rheology measurements, samples were tested in triplicate, with 25 storage modulus (G‘) measurements collected for each test, which resulted in 75 data points being collected for each type of hydrogel over a narrow strain range. The average value of the 75 storage modulus data for each type of hydrogel was calculated and results are shown in Figure 5.6.

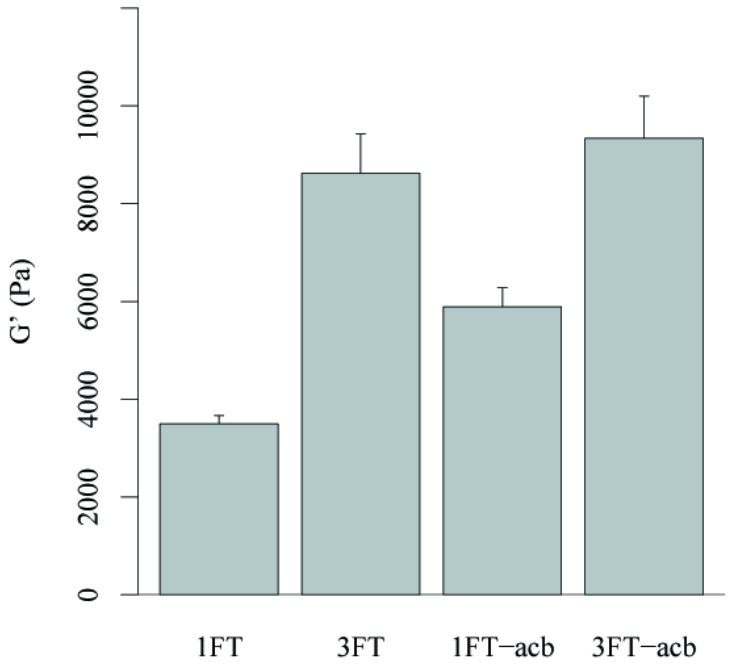

Figure 5.6: Storage modulus of PVA/Gelatin hydrogels in rheological measurement (n=3).

Both thermal treatment and coagulation treatment increased the mechanical properties of the PVA/Gelatin hydrogel. The storage modulus obtained from rheological measurement increased significantly from 3495 Pa for the 1FT hydrogel to 8616 Pa for the 3FT hydrogel ($P<0.001$). With the coagulation treatment, the G‘ of 1FT significantly increased to 5889 Pa ($P<0.05$), however, there is no significant difference between G‘ of 3FT and 3FT-acb. The trend between the storage moduli of the PVA/Gelatin hydrogels obtained from the rheological analysis agrees well with the ultimate strength trends measured from the uniaxial tensile test (Figure 5.7). A significant enhancement in ultimate strength appeared with the number of thermal cycles and the coagulation treatment, and similarly, no significant difference can be found between the ultimate strength of 3FT and 3FT-acb.

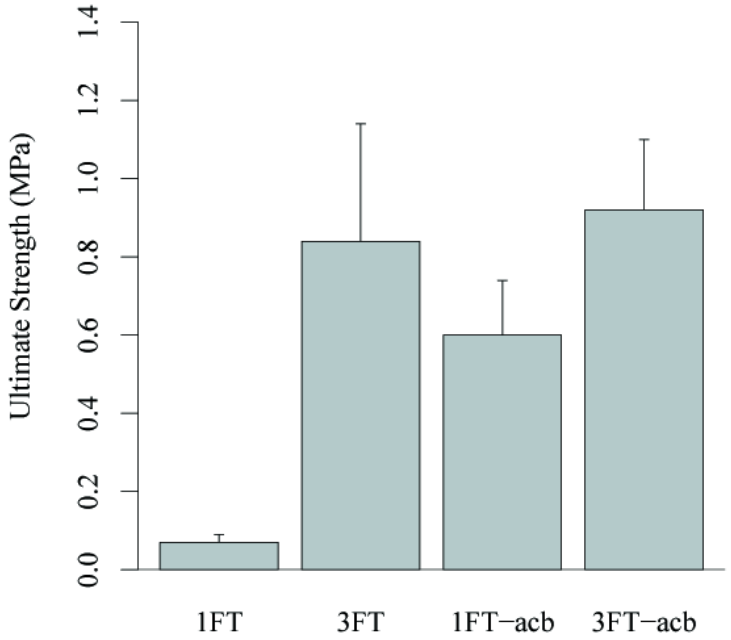

Figure 5.7: The ultimate strengths of PVA/Gelatin hydrogels in uniaxial tensile test (n=6).

5.3 Discussion

Understanding the relationship between structure and properties is always important in investigating a new material. In this study, PVA and gelatin were blended and formed into a hydrogel with thermal (freeze-thaw) treatment and coagulation treatment. The thermal behavior, degree of crystallinity, polymer fraction, storage modulus and ultimate strength of treated PVA/Gelatin hydrogels were studied in this work. The results are summarized in Table 5.3.

5.3.1 The effect of thermal treatment

The glass transition temperature, melting temperature, degree of crystallinity, polymer fraction and mechanical strength of 3FT hydrogel are all higher then that of 1FT hydrogel.

PVA polymer chains are held together by hydroxyl bonds to form a folded chain

Table 5.3: A summary of testing results.

Materials	Tm (°C)	Degree of crystallinity (%)	Tg (°C)	Polymer fraction (%)	G` modulus (Pa)	Ultimate strength (MPa)
PG-1FT	224	31.2	39.7	5.4 ± 0.2	3495 ± 173	0.07 ± 0.02
PG-3FT	227	36.3	45.7	12.6 ± 0.5	8616 ± 817	0.84 ±0.30
PG-1FT-acb	232	18.3	35.6	15.7 ± 0.5	5889 ± 394	0.60 ± 0.14
PG-3FT-acb	233	23.9	33.6	14.1 ± 0.08	9336 ± 864	0.92 ± 0.18

structure. The hydroxyl groups of PVA are able to form hydrogen bonds within chains or between chains, which lead to small crystallites scattered in an unordered, amorphous polymer matrix [80]. With additional freeze-thaw cycles, the crystalline domain grows [86] due to the strengthened hydrogen bonding, which is associated with an increase in chain stiffness. This increases the glass transition temperature of the hydrogel. Meanwhile, the crystallite domains served as crosslinks to hold the three-dimensional structure together [80] and withstand external stress, thus enhancing the G‘ modulus and ultimate strength [167].

5.3.2 The effect of coagulation treatment

For the coagulation treatment, hydrogels were immersed in the coagulation bath and vigorously stirred for 1h. After the coagulation treatment, the Tg of both 1FT and 3FT hydrogels shifted to a lower value, the melting temperature was further increased, the degree of crystallinity was depressed, and the polymer fraction was enhanced. Only the mechanical properties (modulus and strength) of 1FT were significantly strengthened with coagulation treatment.

Yokoyama et al. [89] suggested that PVA hydrogel is composed of three phases, comprising the water phase, the amorphous PVA phase and the crystal PVA phase. Mallapragada and Peppas [165] further examined the dissolution of semicrystalline PVA prepared by annealing at different temperatures. PVA crystallites are folded PVA polymer chains formed by inter-chain hydrogen bonding. When presented in water,

PVA crystallites tend to dissolve and result in a decrease in the degree of the crystallinity [80]. In the view of the increase in polymer fraction but decrease in the degree of crystallinity with coagulation in this study, two continuous processes could be proposed in the treatment of coagulation: one process is the dissolution of PVA crystallites formed during freeze-thaw cycles; the other process is the coagulation of amorphous polymer in contact with coagulants. This coagulation could produce different polymer structures among PVA crystallites, ranging from dust- to finger- to sponge-like morphologies [143]. The decreased proportion of PVA crystal phase and increased proportion of the coagulated amorphous PVA domain is associated with a reduced hydrogen bonding, which indicates decreased stiffness of the PVA chains and less constrained chain movement, and therefore a lower Tg.

The Tm increased in the following order; 1FT, 3FT, 1FT-acb and 3FT-acb. According to the Thomson-Gibbs equation [165], the melting temperature observed in DSC is proportional to the crystal lamellar thickness. An enhanced melting temperature indicates an increased crystal lamellar thickness. In this study, the Tm was enhanced with coagulation treatment. This could be explained by considering that some parts of the amorphous domains are coagulated around crystallites which increase the size of crystal domains. However, the lamellar thickness is also strongly dependent on other parameters in the Thomson-Gibbs equation, such as the value of the equilibrium melting temperature of an infinitely thick crystal and the surface free energy per unit area of the chain folds. This limitation leads to uncertainty in explaining the Tm enhancement from 1FT to 3FT.

A dramatic increase in polymer fraction indicates that more polymer phase, both amorphous and crystal, can be employed to withstand external stress, which shows in the increase of G‘ modulus and ultimate strength from 1FT to 1FT-acb. Because the polymer fractions of 3FT and 3FT-acb are closer to each other, the differences in the mass ratio between the crystal phase and amorphous phase would have a proportionally greater effect on their mechanical properties due to the different rigidity of these two

phases. The fact that no significant difference can be found between the mechanical properties of 3FT and 3FT-acb may be attributable to this effect.

5.4 Summary

This part of the research investigated the microstructure formation of PVA/Gelatin hydrogel. Infrared spectra were applied to verify the present of gelatin and PVA. The glass transition temperature, melting temperature and the crystallinity were studied by thermal analysis, including DSC and DMTA. With additional results on polymer fraction and mechanical properties of PVA/Gelatin hydrogels, the evolution of the microstructure of hydrogels was discussed in detail. Briefly, the thermal treatment (freeze-thaw cycles) increased the strength of hydrogels by growing the crystal domains in PVA matrix which acted as the crosslinks to withstand external stresses. The coagulation treatment strengthened the mechanical properties of hydrogels by increasing the polymer fraction of the hydrogels, which was resulted from the decreased portion of crystal domains and the increased portion the amorphous PVA phase within hydrogel matrix.

Chapter 6

Fabrication of PVA-SbQ fibres by electrospinning and photocrosslinking

6.1 Introduction

Electrospinning is a highly versatile method that can produce fibres on the micro- or nano-scale. Electrospun fibre mats have a large surface-to-volume ratio, tunable porosity, and relatively high production rates, and possess the potential for use in many technological areas [96, 98]. In the biomaterials field, electrospun fibres have been successfully applied in wound dressing, in artificial blood vessels, and as vehicles for controlled drug delivery [168].

Polyvinyl alcohol (PVA), a synthetic polymer, has attracted great attention due to its hydrophilicity, good physical properties, biocompatibility and chemical resistance [169]. PVA electrospun fibres could potentially have the merits of both the polymer and the nano-fibrous architecture. However, high hydrophilicity contributes to the dissolution of PVA fibres, which limits its application in some areas, especially in biomedical engineering. There have been several studies related to the crosslinking of PVA [170, 171, 172]. Gohil et al [170] crosslinked PVA using maleic acid with heat treatment. Ding et al [171] crosslinked electrospun PVA/glyoxal fibres by heat treatment. Zeng et al [172] synthesised a PVA derivative containing thienyl acrylate groups and

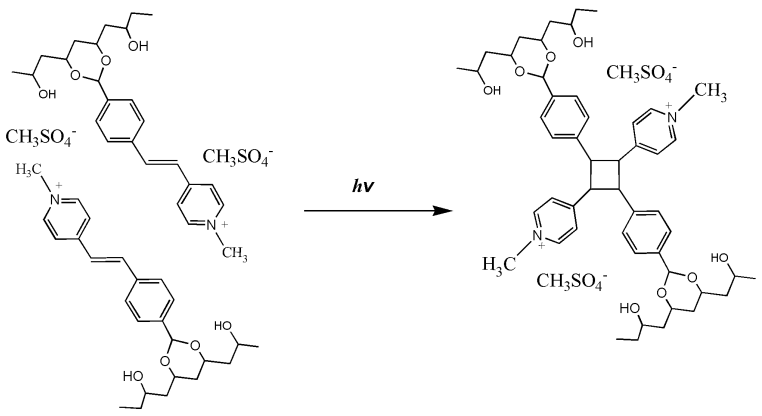

Figure 6.1: Schematic of the [2+2] cycloaddition reation of PVA-SbQ

photocrosslinked PVA-Thio electrospun fibres with UV irradiation. The crosslinked PVA in these studies showed less water solubility than non-crosslinked PVA. Another PVA derivative, PVA with pendent styrylpyridinium groups (SbQ), has been widely used as a photocrosslinkable material due to its water stability, high photosensitivity and good storage stability [173]. The photocrosslinking behaviour and mechanism of PVA-SbQ have been systematically investigated by Ichimura et al [173, 174], Shindo et al [175, 176, 177] and Cockburn et al [178]. The SbQ pendant groups undergo [2+2]-cycloaddition reactions which crosslink the PVA backbones (Figure 6.1). The present study is the first to use PVA-SbQ as a photocrosslinkable polymer to prepare water-insoluble electrospun fibres. PVA-SbQ fibres were fabricated by the electrospinning process and then photocrosslinked with UV irradiation. The photoactivation, water resistance, and morphology of PVA-SbQ fibres were investigated in this study.

6.2 Results and discussion

6.2.1 Preliminary experiment of electrospun fibres

PVA has been used as a preliminary material for exploiting the electrospun technique. PVA fibres showed good morphology and sub-micron fibre size (Figure 6.2A). However, upon being immersed in water and dried immediately, the PVA fibres dissolved quickly and formed a crispy film (Figure 6.2B). The need for a PVA based fibre that

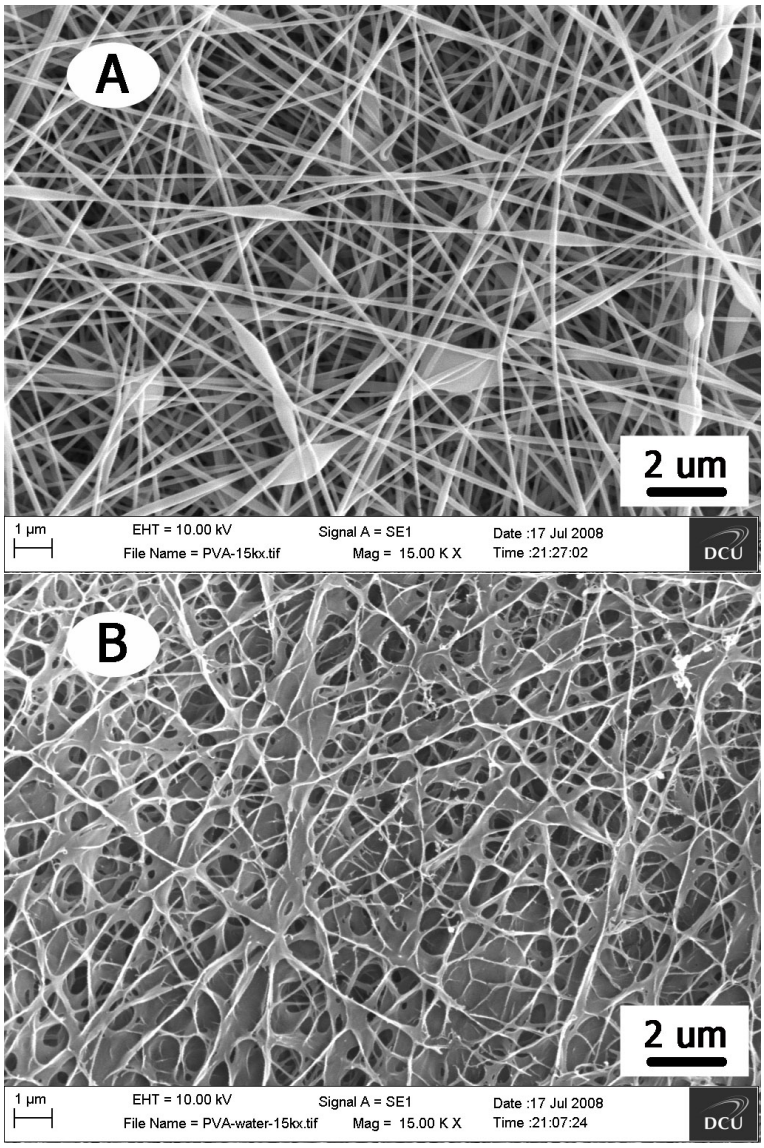

Figure 6.2: Morphology of PVA electrospun fibres. (A) Without contact with water; (B) Briefly immersed in water and dried out immediately.

would be stable in water leads to the following studies of photocrosslinkable PVA, PVA-SbQ, as a material for electrospinning technique.

6.2.2 Photosensitivity of PVA-SbQ

6.2.2.1 UV-VIS Spectrum

The spectral change of PVA bearing 4.1 mol% 4-styrylpyridinium groups (SbQ) in aqueous solutions is shown in Figure 6.3. When 3.3% and 10% PVA-SbQ solutions

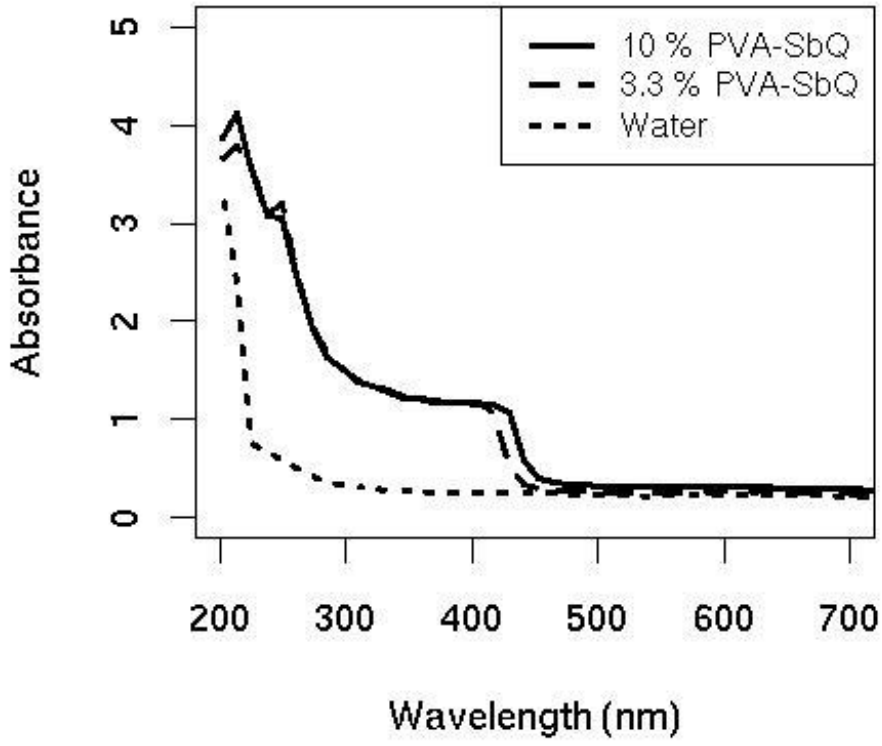

Figure 6.3: Absorption spectra of 3.3% PVA-SbQ and 10% PVA-SbQ.

were exposed to 200~700nm light in measurement, a dramatically wide absorption band occurs at 200~411 nm for 3.3% PVA-SbQ and 200~428 nm for 10% PVA-SbQ, which can be attributed to the presence of the SbQ group on the PVA backbone. Interestingly, the absorption value is not affected by the difference in PVA-SbQ concentration.

Ichimura et al. reported that the photosensitivity of PVA-SbQ was high in spite of the extraordinarily low content of the styrylpyridinium group [174]. It was reported that PVA with 1 mol% SbQ was about 10 times more sensitive than PVA that contained 6 wt% of ammonium dichromate. When the SbQ content was increased to 1.9 mol%, it exhibited about 80 times more sensitivity than the dichromated PVA. Therefore, the dramatically wide absorption band could be a result of the much higher content of

SbQ on the PVA backbone, 4.1 mol%, in this study. As PVA-SbQ is sensitive to a wide range of wavelengths, light sources with various wavelengths could be used to irradiate the SbQ group to crosslink the PVA-SbQ. In the present work, a 365-nm high intensity UV lamp was used to irradiate PVA-SbQ fibres after electrospinning.

6.2.2.2 FTIR

The photocrosslinking reaction has been tracked by the FTIR analysis of PVA-SbQ fibres without UV exposure and with UV exposure for 5 min and 10 min (Figure 6.4). PVA (Sigma) fibre was applied as a control to the PVA-SbQ fibres. Two absorption bands, 1652 cm^{-1} and 1626 cm^{-1}, are of the most interest. PVA fibres have no obvious absorption in between 1580 cm^{-1} and 1680 cm^{-1}. PVA-SbQ fibres without UV exposure have a strong absorption at 1626 cm^{-1} and a small shoulder band at 1652 cm^{-1}. Upon being exposed to UV light for 5 min, PVA-SbQ fibres showed an enhanced absorption at 1652 cm^{-1} and a significantly decreased absorption at 1626 cm^{-1}. When extending exposure time to 10 min, the spectrum of PVA-SbQ fibre showed no difference with that of the fibres with 5-min UV exposure. Therefore, the band at 1626 cm^{-1} was assigned to the C=C bonds of styrylpyridinium pendent groups and the band at 1652 cm^{-1} was assigned to the result of [2+2] cycloaddition reaction.

6.2.3 Weight loss measurement

To evaluate water resistance, as-prepared PVA, PVA-SbQ and PVA-SbQ-hv fibres were immersed in 37 ^{o}C distilled water for 5 days. The average mass loss and standard deviation of these fibres are shown in Figure 6.5. PVA fibres and PVA-SbQ fibres were soluble in water and are therefore represented as 100 % mass loss. UV irradiation significantly decreases the water solubility of PVA-SbQ-hv fibres and lowers its mass loss to about 17.5 % ($p<0.001$). In fact, the mass of PVA-SbQ-hv fibres reduced to approximately 17.5% in the first day immersion (data not shown) and then stabilised. Therefore, this mass loss is attributed to the dissolution of non-crosslinked PVA-SbQ.

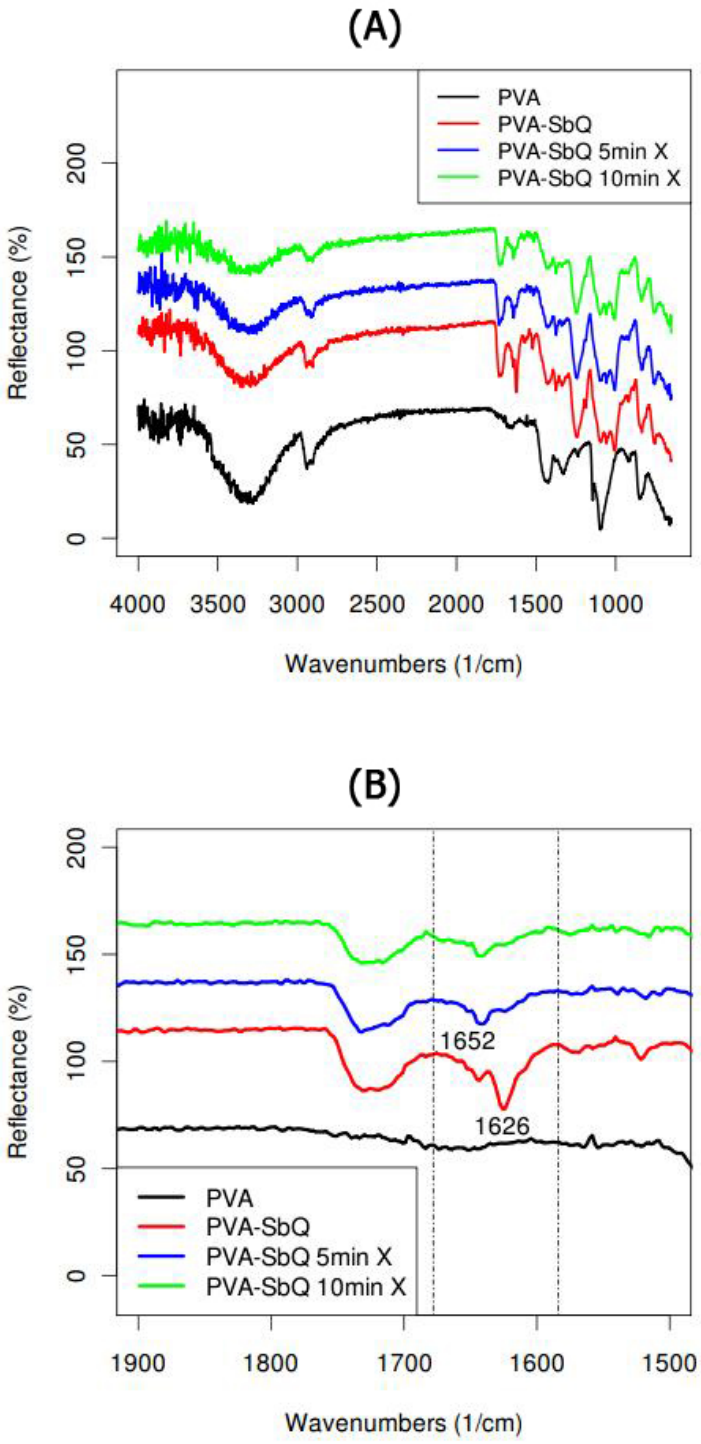

Figure 6.4: ATR-FTIR spectra of PVA fibre exposed to UV light for 0 min, 5 min and 10 min. PVA has been shown as control. (A) IR spectra in 4000-400 cm^{-1}; (B) IR spectra in 1500-900 cm^{-1}. The band of at 1626 cm^{-1} was assigned to the C=C bonds of styrylpyridinium pendent groups and the enhancement at band 1652 cm^{-1} indicated the reaction of [2+2] cycloaddition.

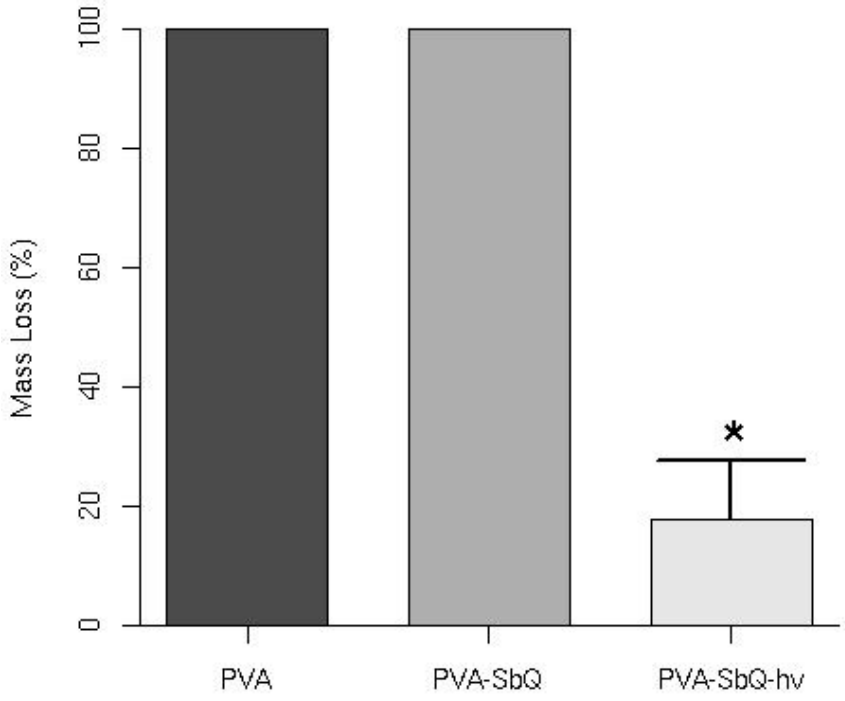

Figure 6.5: Mass loss of PVA, PVA-SbQ and PVA-SbQ-hv fibres (n=4). Data are presented as mean ± S.D. *p<0.001, significant differences from the PVA and PVA-SbQ fibres.

6.2.4 Fibre morphology

The morphology changes of PVA, PVA-SbQ and PVA-SbQ-hv fibres were observed by SEM (Figure 6.6). Upon water immersion for 5 days, the PVA fibres and PVA-SbQ fibres totally dissolved in water. Actually, the PVA and PVA-SbQ fibres dissolved immediately upon coming into contact with water. This would clearly present a problem in vivo. This was shown by dropping water onto these two fibre mats. The trace of water drops on the fibre mats are shown in Figure 6.6 A and B. With the exposure to UV light, PVA-SbQ-hv did not change its morphology during water immersion (Figure 6.6 C), and hence remains a viable prospect for in vivo applications.

PVA-SbQ was supplied in a water solution (Polysciences Inc.). Within the electrospinning process, the applied voltages moved the PVA-SbQ solution jet towards the counter grounded collector with the water evaporating on the way to the collector. Upon UV irradiation, PVA-SbQ-hv dramatically decreased its solubility. Consistent with the mass loss result and morphology observation, irradiation is assumed to result in the formation of cyclobutane rings which leads to the crosslinking of the PVA chains and their consequently being water-durable [179].

6.2.5 Optimization of electrospinning parameters

Many studies have addressed the processing/property relationships in electrospun polymer fibres [180, 181]. It is clear that the structure and morphology of electrospun fibre are determined by a synergetic effect of solution parameters and process parameters, such as viscosity, surface tension, concentration of polymer, solution feed rate and the applied voltage. The relationship between the parameters and fibre properties identified in one polymer system may not be suitable for other systems. Therefore, it is necessary to optimize the electrospinning parameters for PVA-SbQ. This work focused on the two main parameters of electrospinning technique, applied voltage and feeding rate. Please note that the fibre collector in this optimization is assembled by parellel wires, see Figure 6.7. The using of this collector not only helped in optimizing the

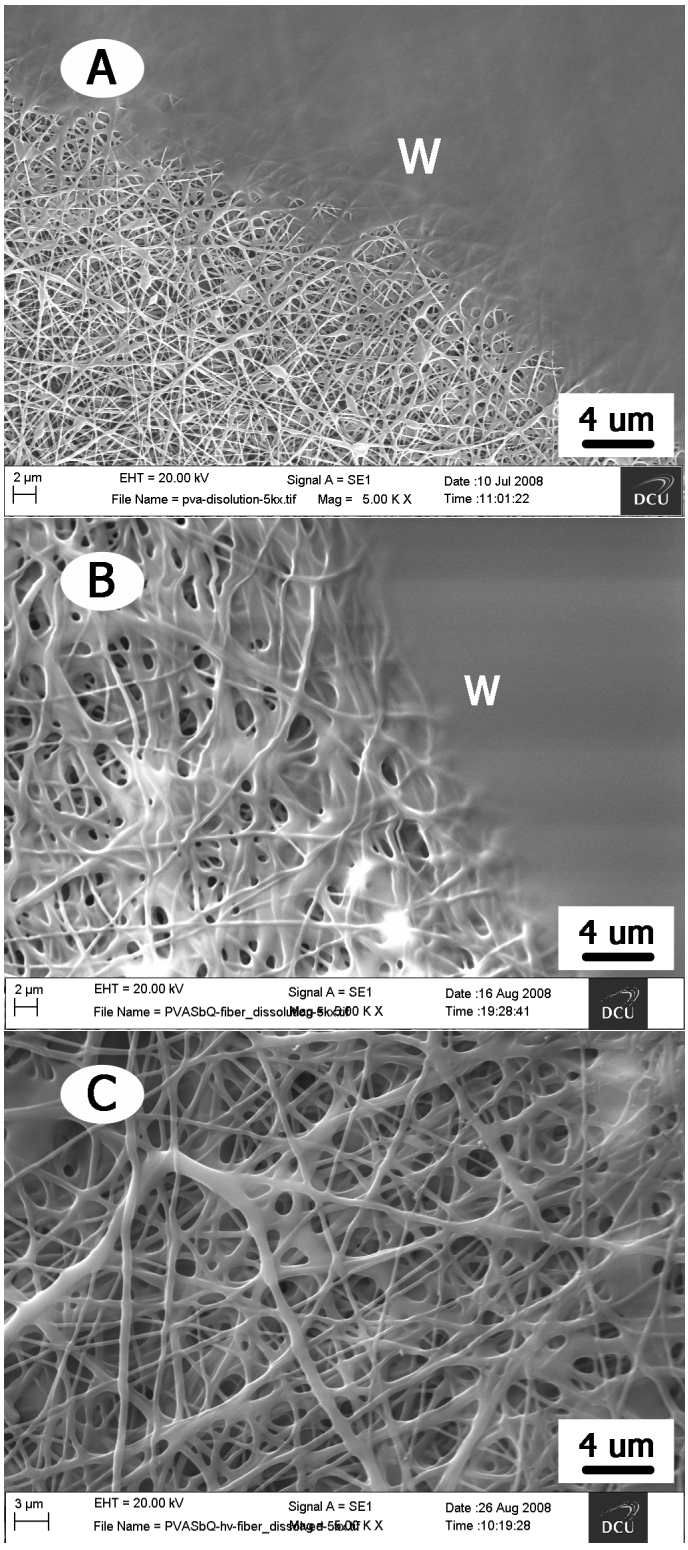

Figure 6.6: SEM micrographs of PVA, PVA-SbQ and PVA-SbQ-hv fibres. (A) PVA fibres with a trace of water drop, (B) PVA-SbQ fibres with a trace of water drop, (C) PVA-SbQ-hv fibres during water immersion (label "W" refers to the position of the trace of water drop) .

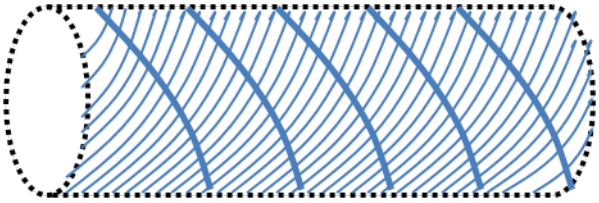

Figure 6.7: The schematic of wired assembled collector. Solid lines are wires and the dot line represent the edge of collector.

electrospinning parameters for PVA-SbQ, it also indicated the possibility of assembling PVA-SbQ fibres with helical alignment. One electrospinning experiment was carried out for each case, and multiple samples were obtained from each experiment.

6.2.5.1 Effect of the applied voltage

In this PVA-SbQ/water system, the applied voltage significantly changed the morphology of electrospun fibres. 5kV did not reach the jet initiating point, which resulted in no deposition on the collector. When 10kV voltage was applied, the PVA-SbQ fibre showed as defect-free and deposited both on wires and in between wires (Figure 6.8 A, C and E). The alignment of the fibres in between wires was relaxed during sample preparation for the scanning electron microscope, but the predominant alignment of the fibres is clearly evident (Figure 6.9). The fibre changed to a highly disordered fibre morphology at a voltage of 15kV (Figure 6.8 B, D and F). As the voltage increases, there is a shift from circular fibres (Figure 6.9 A) to flat fibres (Figure 6.9 B). Extensive coiling can also be observed when applied voltage reach 15kV (Figure 6.9 B), which indicate the splitting and splaying of jet due to the bending instability [182]. This effect of applied voltage on the electrospun fibre morphology agreed with Deitzel's study in PEO/Water system [181]. It was shown that an increase in applied voltage causes a change in the shape of the jet initiating point, and a consequent change on the morphology of electrospun fibre [181].

6.2.5.2 Effect of feeding rate

The feeding rate of PVA-SbQ solution had no significant effect on the morphology of electrospun fibres (Figure 6.9). As the feeding rate of PVA-SbQ solution was increased, there was an enhancement of the deposition of PVA-SbQ fibres on the collector. However, with higher feeding rate, the polymer solution tended to accumulate at the nozzle of syringe and resulted in dripping of solution. For this wire collector, the dripping effect is apparent at the feeding rate of 0.35 ml/h and 0.5 ml/h. To prevent wasting of polymer solution, 0.2 ml/h was considered to be the suitable feeding rate for electrospinning of PVA-SbQ with the wire collector. However, if a plane collector (surface collect area higher than that of wire collector) should be applied, 0.35 ml/h will be a better feeding rate to ensure the productivity of PVA-SbQ fibres.

6.2.6 Cell attachment on PVA-SbQ fibres

After endothelial cells were cultured on PVA-SbQ fibres for 1 day, the initial cell attachment was characterized by immunofluoresence staining and the cell morphology on PVA-SbQ fibres were observed by scanning electron microscopy. Figure 9B showed the immunofluoresence staining result. The nucleii of endothelial cells were stained by DAPI and can be seen as a blue colour. Both F-Actin of endothelial cells and PVA-SbQ fibres were stained by FITC-Phaloidin and can be seen as green colour. When comparing the immunofluoresence image (Figure 6.10 A) with the image of light microscopy Figure 6.10 B), the attached cells can be easily distinguished from PVA-SbQ fibres. With initial seeding density of 2×10^5 cells/ml, the density of attached cells on fibres can also been seen from a lower magnification by light microscopy (Figure 6.11 A) and scanning electron microscopy (Figure 6.11 B). It is apparent that endothelials cells preferably attached to the PVA-SbQ fibres. Some cells spread across PVA-SbQ fibres and other cells remain in round shape due to the short culture duration (1 day). The cell-cell contacts can be easily found from Figure 6.11 B.

Another advantage of fibres for cell attachment is that the electrospun fibre could

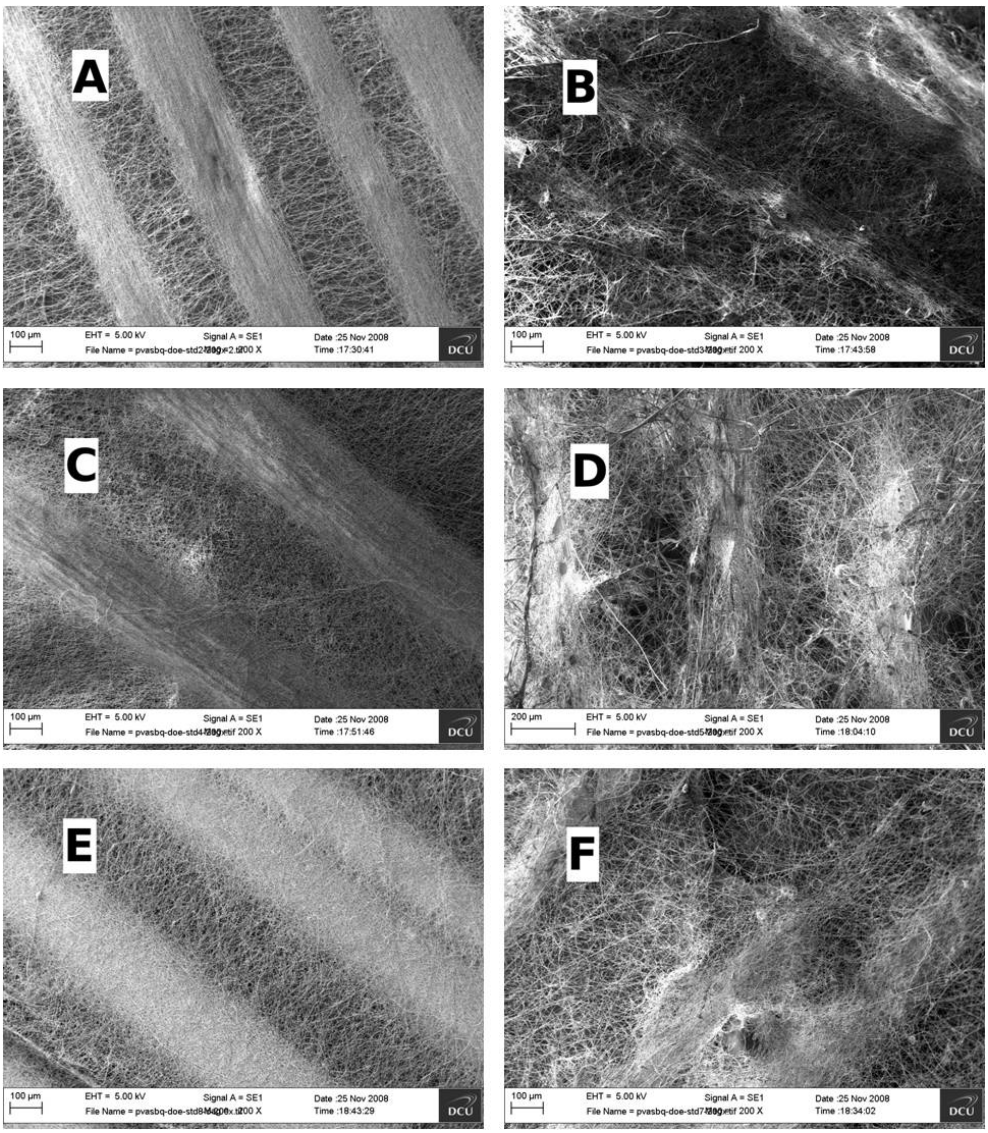

Figure 6.8: SEM micrographs of each run of the design of experiment, bar=100µm. (A)Run 2, 10kV, 0.2 mL/h; (B) Run 3, 15kV, 0.2 mL/h; (C) Run 5, 10kV, 0.35mL/h; (D) Run 6, 15kV, 0.35mL/h; (E) Run 8, 10kV, 0.5 mL/h; (F) Run 9, 15kV, 0.5 mL/h.

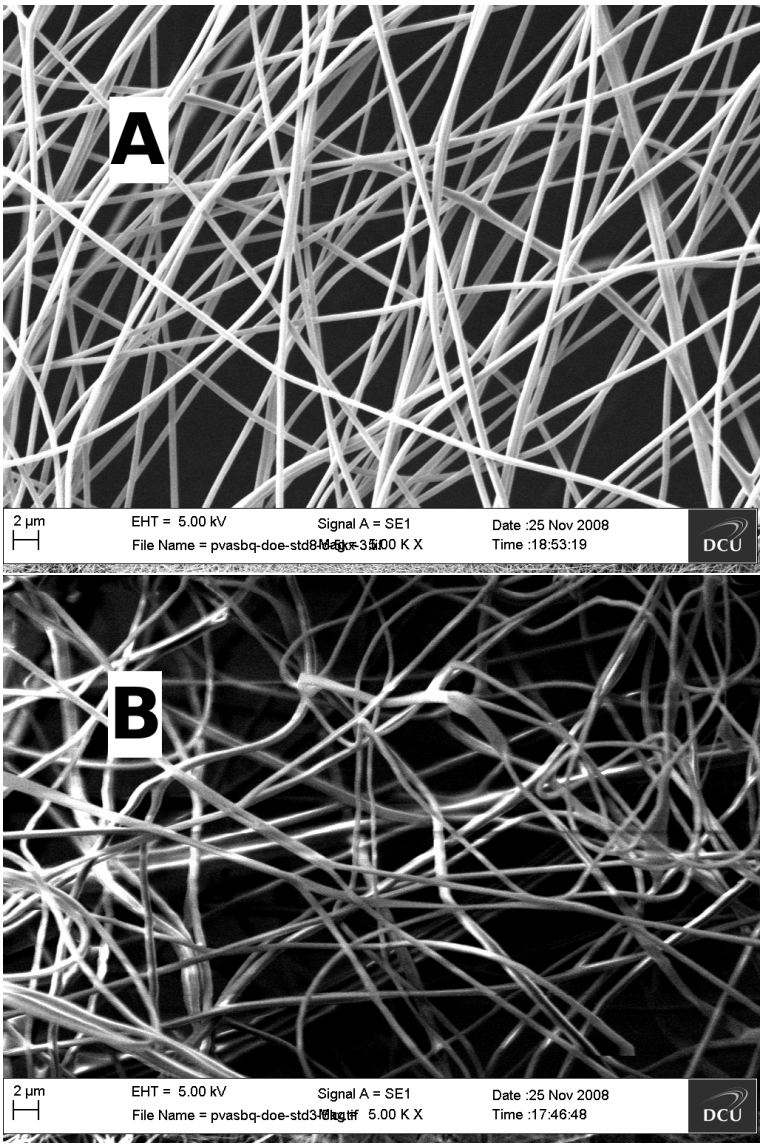

Figure 6.9: SEM micrographs showing the effect of applied voltage on the structure in the electrospun PVA-SbQ fibres. (A) 10kV; (B) 15kV.

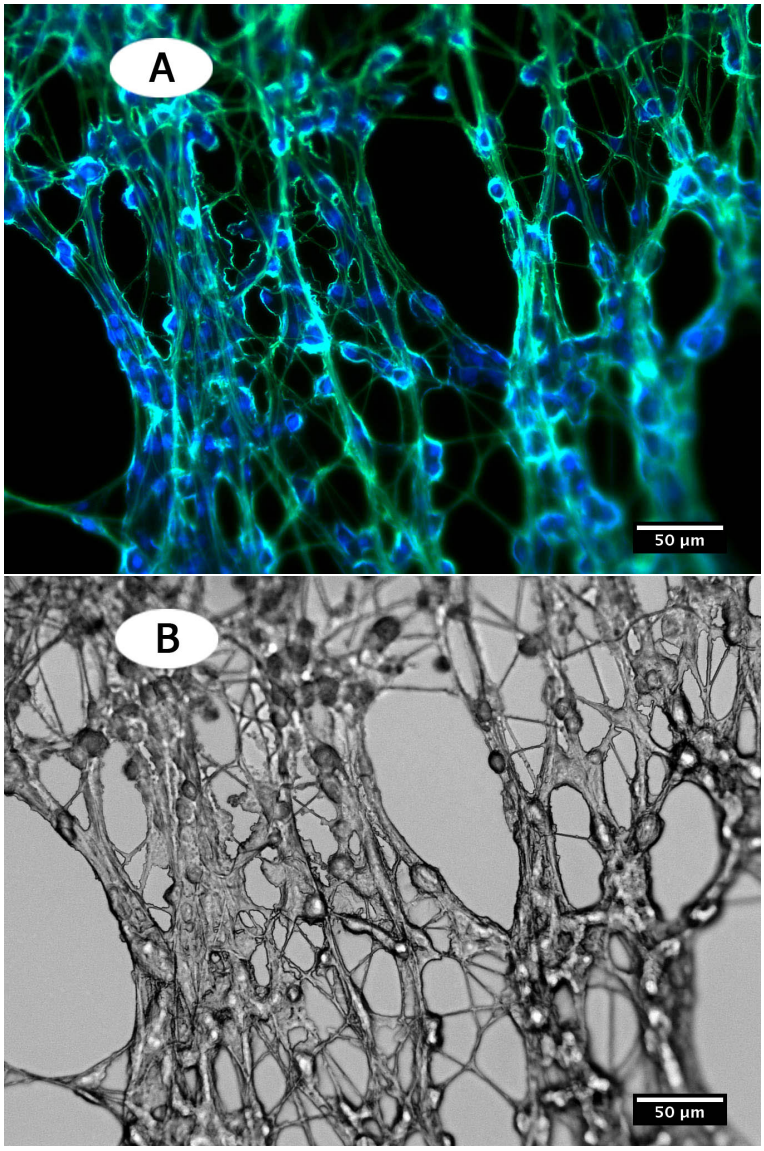

Figure 6.10: Immunofluoresence staining of endothelial cell attachment on PVA-SbQ fibres (bar=50 μm). (A) Immunofluoresence stainning image, DAPI stains cell nucleus in blue and Phalloidin-FITC stains F-actin and electrospun fibre in green. (B) Light microscope image, as control.

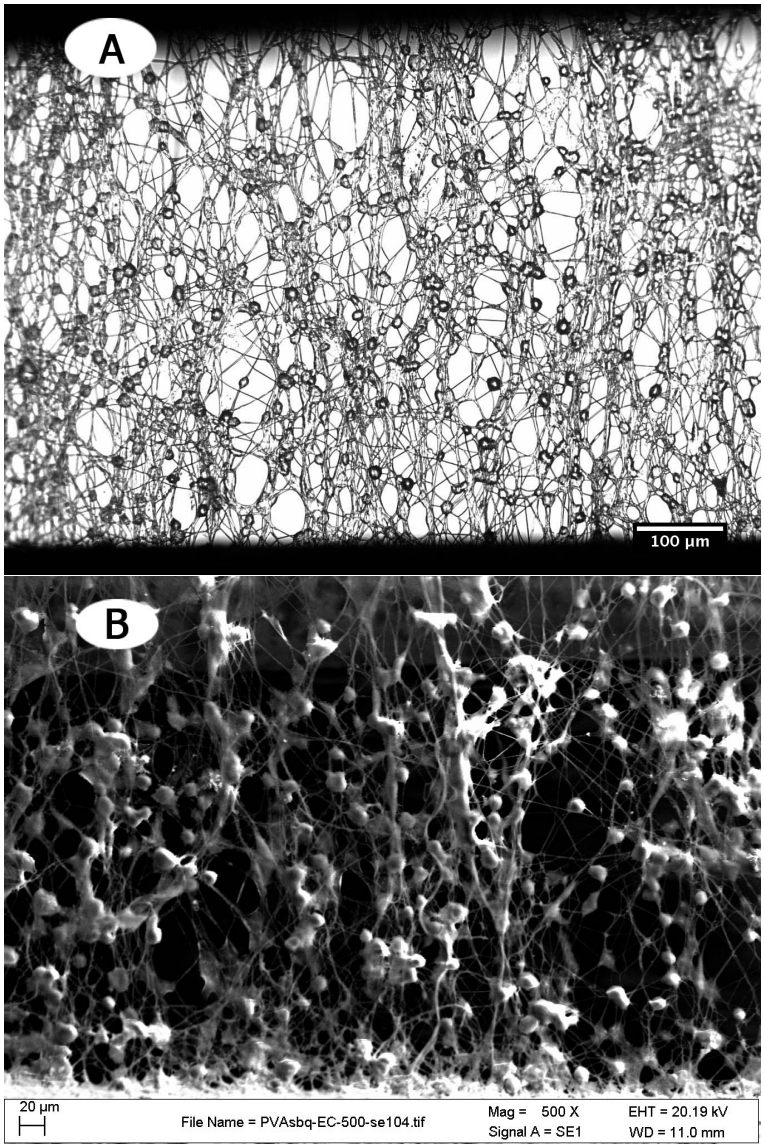

Figure 6.11: Morphology of endothelial cell attached on PVA-SbQ fibres. (A) light microscope image; (B) scanning electronic microscopy image.

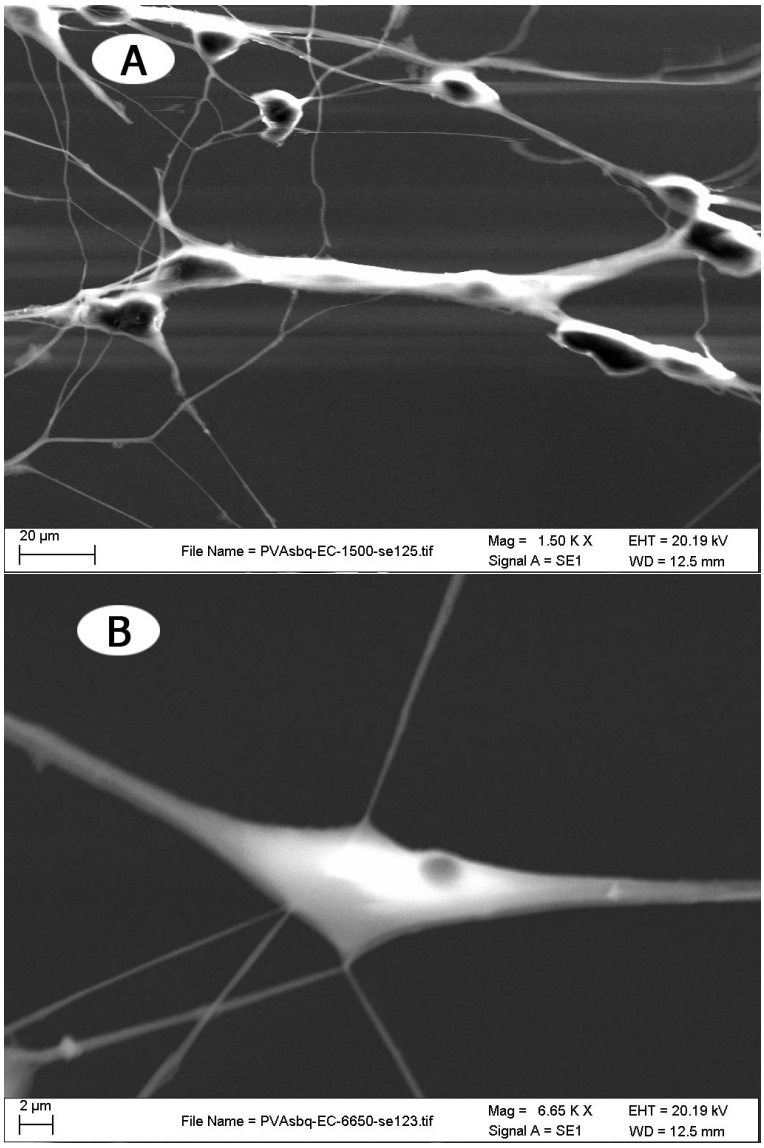

Figure 6.12: Morphology of the endothelial cell attached on PVA-SbQ electrospun fibres. (A) Cell-cell contact on fibres; (B) Cell hanging on fibres.

act as the guidance for cell growth. In this cell culture experiment, some cells have been found to grow along the fibres to contact with other cells (figure 6.12 A) and some other cells are seem to be hanging on fibres (figure 6.12 B), which is evidence that PVA-SbQ fibres could be applied to guide the growth of endothelial cells.

The present work appears to be the first to use PVA-SbQ as a photocrosslinkable material for use in the electrospinning process. Ichimura [174] investigated the immobilization of biocatalysts, like enzymes, in PVA-SbQ. The SbQ photosensitive units provided a promising way to entrap biocatalysts due to the prevention of photochemi-

cal modification on the biomolecules during photodimerization. Meanwhile, with the low content of SbQ substitution on the PVA backbone, the physical properties of PVA, especially the mechanical properties, are likely to be only slightly affected. Together with the mild crosslinking conditions, PVA-SbQ photocrosslinked electrospun fibres could act as good candidates for biomedical or tissue engineering scaffold applications.

It should be noted that this is a preliminary evaluation of cell attachment and that a comprehensive study would be required to evaluate proliferation at various durations, such as 1day, 3days, 5days, 7days and longer.

6.3 Summary

This part of the research focused on fabricating PVA-SbQ fibres by electrospinning and photocrosslinking techniques. The PVA-SbQ showed high photosensitivity in the spectroscopic study. The photocrosslinked PVA-SbQ fibre presented water-insoluble property in the study of water immersion and the analysis of Secondary Electronic Microscopy. Electrospinning parameters, including applied voltage and polymer feeding rate, were optimized to obtained fibres with good morphology and deposition. The attachment of endothelial cells showed the potential of PVA-SbQ fibres as a substrate for endothelial cell lining.

Chapter 7

PVA based hydrogel and fibres duo-layer construct

7.1 Introduction

The structure and mechanical properties of PVA/Gelatin hydrogel have been investigated in Chapters 4 and 5. The results showed the mechanical properties of the hydrogel can be controlled by the treatment of freeze-thawing cycles and coagulation. Chapter 6 presented the preparation of PVA-SbQ fibres with electrospinning and photocrosslinking techniques. The attachment of endothelial cells to the fibres has been demonstrated.

In this chapter, the PVA/Gelatin hydrogel and PVA-SbQ fibres were finally constructed as duo-layer vascular graft to take advantage of the merits of both the hydrogels and the fibres. PVA/Gelatin hydrogels with one freeze-thaw cycle were prepared to provide the main mechanical support for the duo-layer construct. The PVA-SbQ fibres were laminated onto the luminal surface of the graft to supply a favourable surface for endothelial cell attachment.

By understanding the overall effect of the coagulation treatment on the properties of PVA/Gelatin hydrogel (chapter 5), coagulation parameters (including coagulation duration, static or dynamic coagulation bath) were applied to control the mechanical

properties of PVA/Gelatin hydrogels and consequently the duo-layer construct. The thickness of hydrogels affects the permeability of coagulants through the gel matrix, which would vary the affect of coagulation treatment on the properties of hydrogels. This is why the constructs with two different thickness (1mm and 2mm) were compared in this study (see Table 3.2 in section 3.2.5.3).

The mechanical properties of the constructs are of the main concern. Both uniaxial tensile tests and compliance tests helped to elucidate the effect of the coagulation bath and the layer of fibres on the mechanical properties. Especially, the compliance property is an essential mechanical property of an artery. The compliance property of grafts has been closely related with long-term patency rate [68, 70, 183, 184, 185, 186, 187]. In the study, the elasticity or compliance of the final duo-layer graft closely match with that of native arteries.

7.2 Results

7.2.1 Uniaxial tensile test

Figure 7.1, 7.2 and 7.3 presented the stress-strain profile of the 1mm thick PG1FT (PVA/Gelatin hydrogel with one freeze-thaw cycle) with a coagulation time of 15min, 30min and 60min, respectively. Upon submersion in a dynamic coagulation bath, all hydrogels behaved as elastic materials, especially at the low strain range (0-40%). The stiffness of the hydrogels with 15-min coagulation was lower than that of the hydrogels with 30-min coagulation. When the coagulation time was increased to 60min, the stiffness barely changed.

Figure 7.4, 7.5 and 7.6 presented the stress-strain profile of the 2mm thick PG1FT hydrogel with coagulation time of 15min, 30min and 60min. The dynamic coagulation bath gradually increased the stiffness of these 2mm thick hydrogels when extending coagulation duration from 15min to 30min and 60min. The stress-strain profiles of these hydrogels showed a linear response within the strain range of 0-40% and a non-

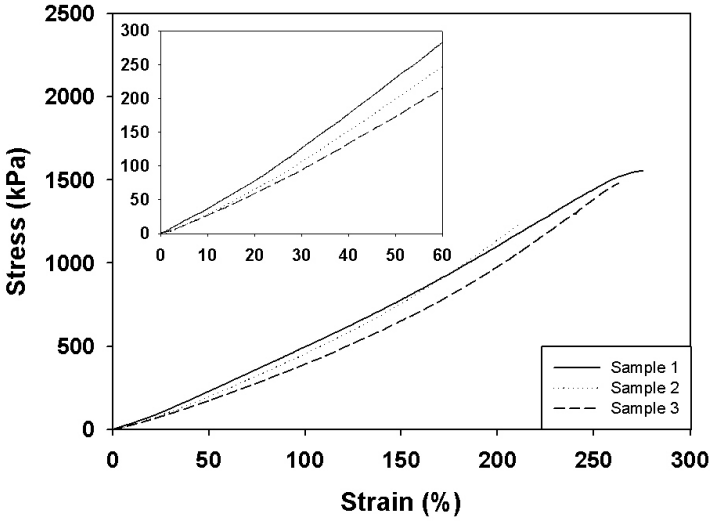

Figure 7.1: Stress-strain profile of 1mm thick PG hydrogel with 1freeze-thaw cycle and 15 min coagulation.

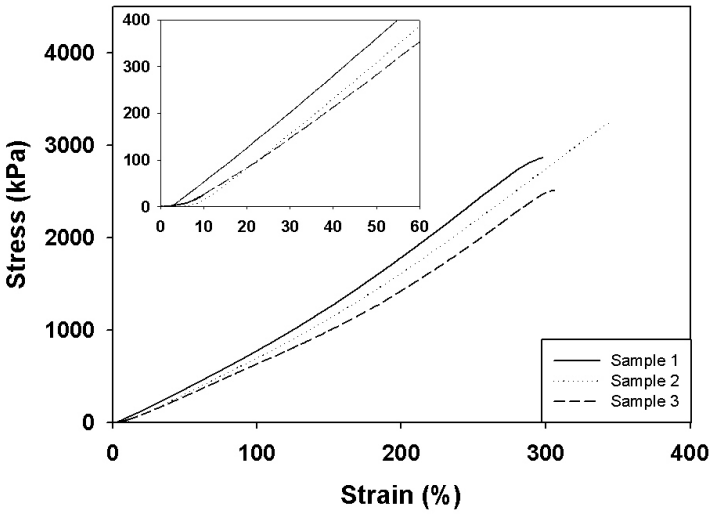

Figure 7.2: Stress-strain profile of 1mm thick PG hydrogel with 1 freeze-thaw cycle and 30 min coagulation.

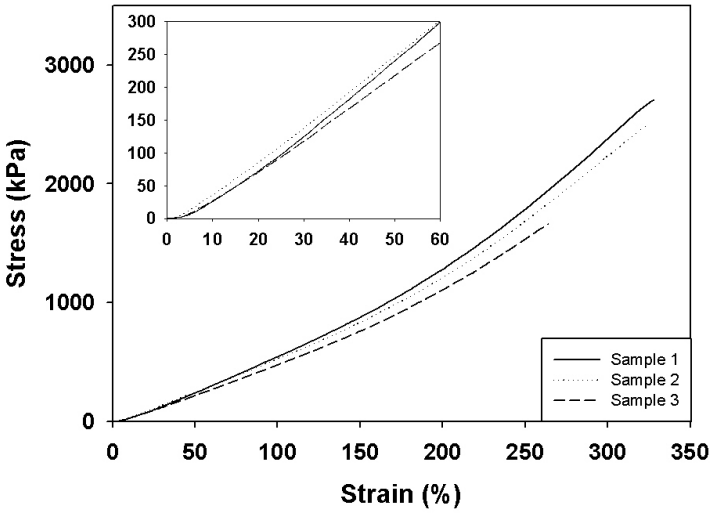

Figure 7.3: Stress-strain profile of 1 mm thick PG hydrogel with 1 freeze-thaw cycle and 60 min coagulation.

linear curve at the strains higher than 40%.

Figure 7.7 presented the stress-strain profile of the 2mm thick PG1FT hydrogel/fibre composite with coagulation duration of 60min. The stress-strain profiles were non-linear in the strain range of 0-60%, which covered the physiological strain range of arteries. In the strain range of 0-40%, the stress-strain profiles showed as a linear response and there was no apparent difference of stiffness between hydrogel/fibre and the hydrogel (Figure 7.6) in this strain range. When the hydrogel/fibre construct extended to the strain range of 40-60%, the stress-strain profile became non-linear and the stiffness of the hydrogel/fibre construct was higher than that of single hydrogel construct shown in Figure 7.6.

7.2.2 Compliance test

Figure 7.8 presents the compliance results for PVA/Gelatin hydrogels with 1 freeze-thaw cycle and 1h dynamic coagulation. The three samples were prepared by freeze-thawing PVA/Gelatin hydrogel for one cycle and then the as formed hydrogel was further treated with stirred coagulation bath for 1h.

As can be seen from the compliance profile of each of the three samples, there is

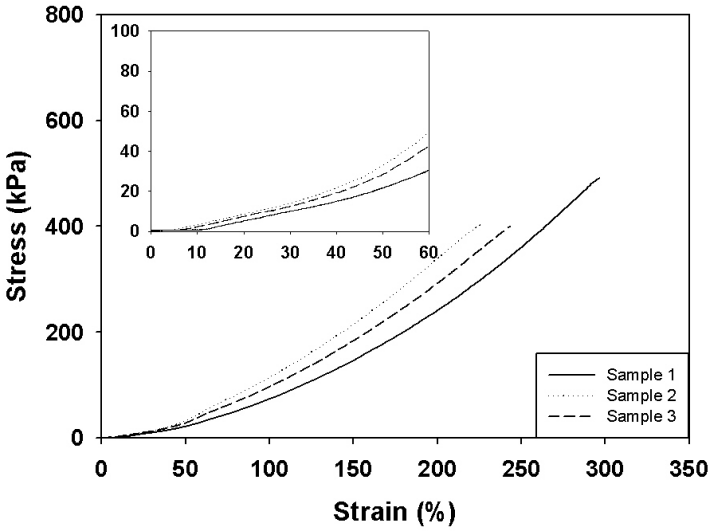

Figure 7.4: Stress-strain profile of 2 mm thick PG hydrogel with1 freeze-thaw cycle and 15 min coagulation.

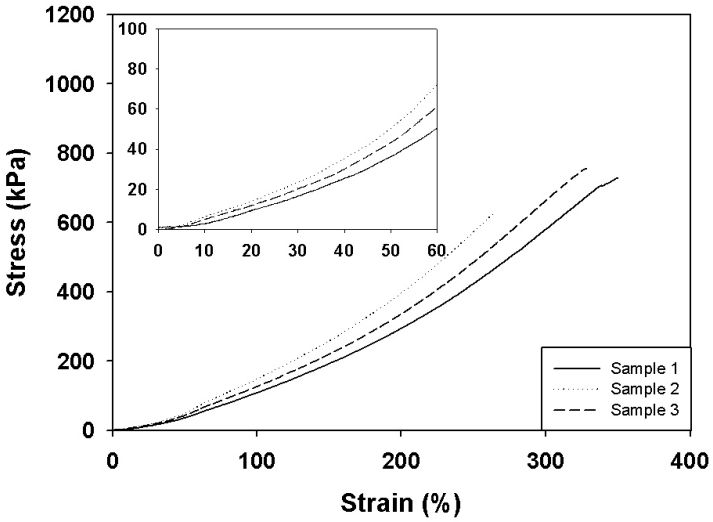

Figure 7.5: Stress-strain profile of 2 mm thick PG hydrogel with 1 freeze-thaw cycle and 30 min coagulation.

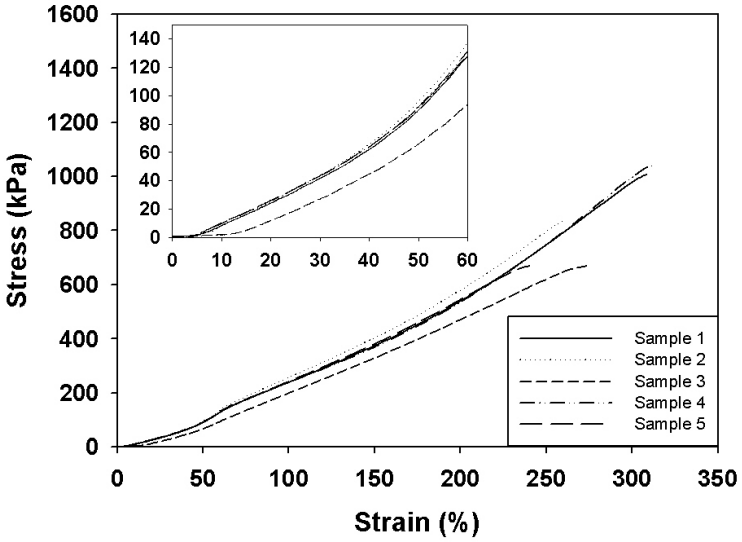

Figure 7.6: Stress-strain profile of 2 mm thick PG hydrogel with 1 freeze-thaw cycle and 60 min coagulation.

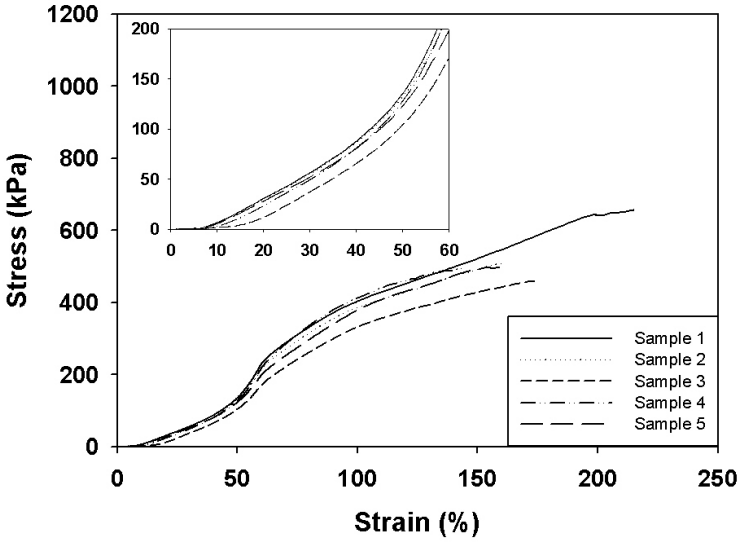

Figure 7.7: Stress-strain profile of 2 mm hydrogel/fibre duo-layer construct with 1 freeze-thaw cycle and 60 min coagulation.

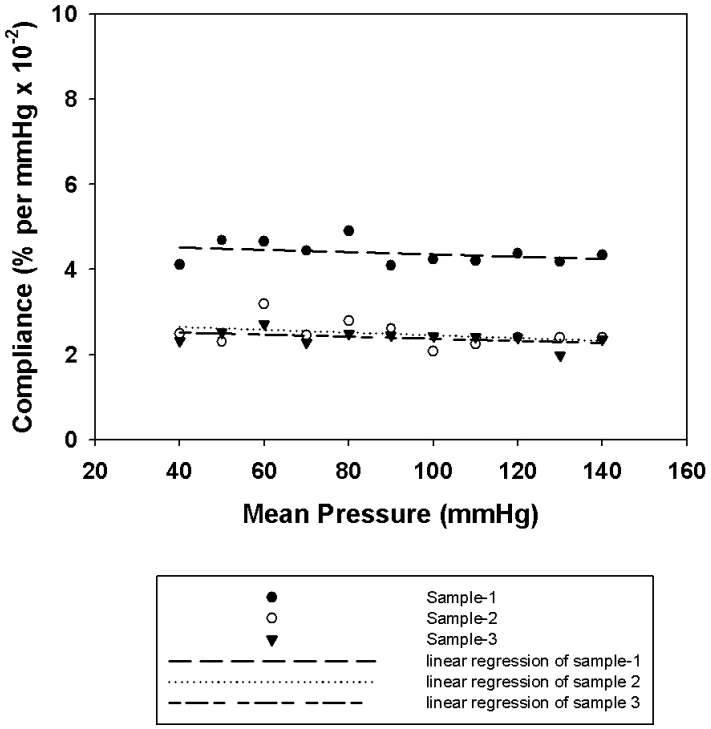

Figure 7.8: Compliance-mean pressure profile of PG hydrogel with 1freeze-thaw cycle and 60 min dynamic coagulation.

no apparent change in the compliance values over the mean pressure range of 40-140 mmHg. The compliance value among samples varied from about 2.4 to 4.2 per cent per mmHg$\times 10^{-2}$.

Note that the dynamic coagulation treatment was performed by using magnetic stirrer to the coagulation bath. The vigorous flow of the bath is able to increase the precipitation rate of polymer by bursting coagulating agent into the PVA/Gelatin hydrogel matrix generated primarily by freeze-thawing treatment. However, the stirrer imparts limitations on controlling the flow rate of the bath, which may consequently lead to inconsistent results. Therefore the following compliance tests were performed on the graft with static coagulation treatment.

Figure 7.9 shows that compliance values of samples of PG hydrogel and a PG hydrogel/fibre composites. PG hydrogel samples were prepared by 1 freeze-thaw cycle and 1h static coagulation treatment. PG hydrogel/fibre samples were prepared by freeze-thawing a PVA/Gelatin solution with photocrosslinked PVA-SbQ fibres for 1

cycle and then treated with static coagulation bath for 1h.

PG hydrogels samples generally have a linearly decreased compliance values in response to increases in mean pressure (Figure 7.9A). The compliance values among samples spread in a wide range of 8 – 26.6 per cent per mmHg$\times 10^{-2}$. The range of compliance values at each mean pressure among samples was confined to a smaller range as the the mean pressure was increased.

Similar to PG hydrogels, PG hydrogel/fibre samples showed decreased compliance values in response to increases in mean pressure (Figure 7.9B). At low mean pressure, the compliance value reached as high as 9.1. The compliance gradually decreased to as low as 2.5 at the high mean pressure of 140 mmHg. The linear regression in Figure 7.9 clearly showed that the dynamic compliance changes in response to increases in the mean pressure.

7.3 Discussion

7.3.1 Nonlinearity

All the hydrogels or hydrogel/fibre composites with thicknesses of 2mm exhibit non-linear stress-strain profiles at high strains. This is one of the critical properties of a vascular graft because it could store a part of the pulsatile energy in systole and restore it in diastole to the circulation [21]. The modulus of 2mm thick hydrogels with coagulation for 15min, 30min and 60min are all within the range of the modulus of pig aortas (Figure 7.10).

It is notable that the variations of elasticity among pig aortas are significant, which could be due to the multiple components in elastin and collagen matrices [151]. Elastin can be composed of microfibrillar and amorphous components. Collagen structure can be different depending on the composition of differing amino acids. At different arterial sites or in different species, it is possible that the collagen and elastin matrices may be composed of different ratios of these components, which may result in differences

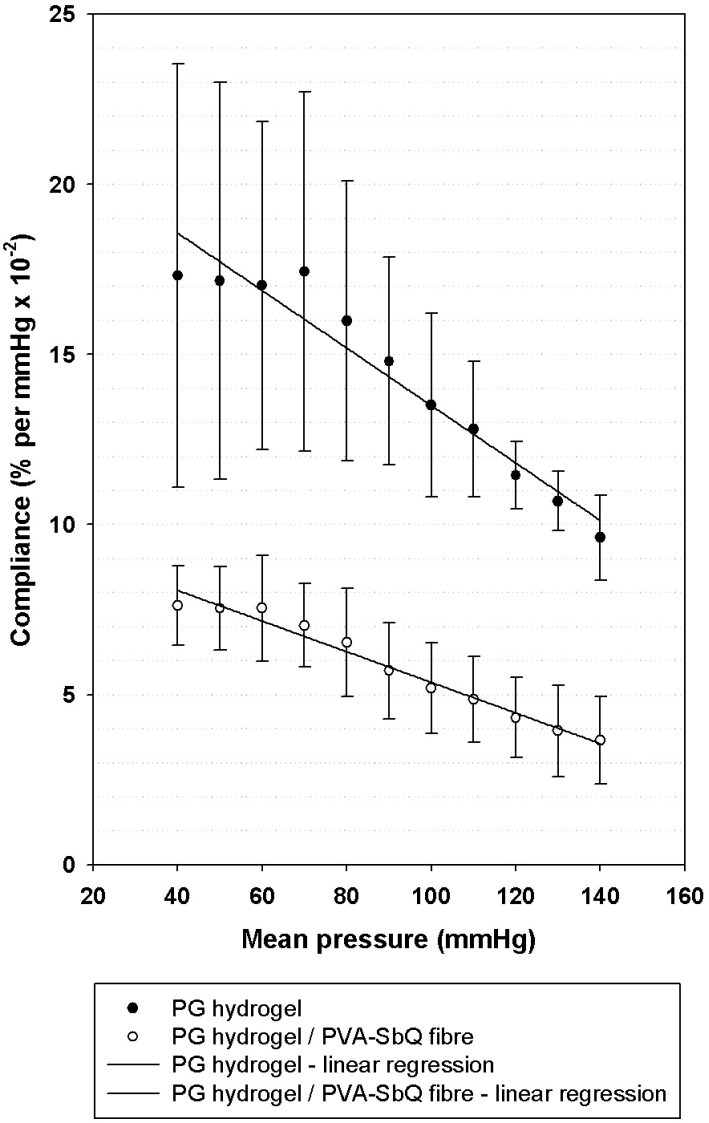

Figure 7.9: Compliance-mean pressure profile of PG hydrogel and hydrogel/fibre duo-layer vessels.

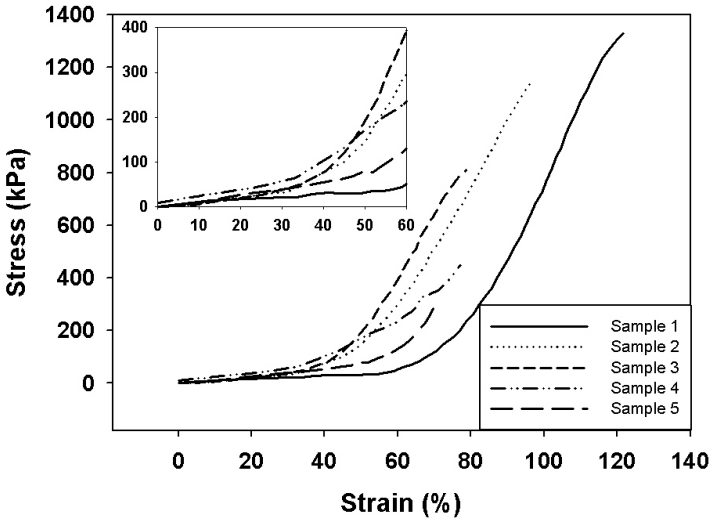

Figure 7.10: Stress-strain profile of five pig aortas. (data redrawn from Prendergast et al. [188])

in the arrangement and linkages and consequent significant differences in the overall mechanics of blood vessels [153].

7.3.2 Effect of coagulation treatment

The coagulation bath applied in this study is composed of 7.5% KOH and 1M Na_2SO_4, which is basically a non-solvent system for PVA and gelatin. This non-solvent system can be any over-saturated basic water-soluble salt solution. The coagulation treatment is intended to stabilise the gelatin within the PVA physically crosslinked (by freeze-thaw cycle) matrix. Another polymer solution phase exists in the PVA crosslinked matrix, namely the PVA solution phase, which is the part of the PVA solution have not been physically crosslinked during freeze-thaw cycle. This part of PVA solution can be stabilised and precipitated when treated with the coagulation bath. This is why coagulation treatment increased the polymer fractions and improved the mechanical properties of hydrogels in Chapter 5. In this chapter, a similar effect of coagulation can be found from Figure 7.1, 7.2, 7.3, 7.4, 7.5 and 7.6. It is obviously that the coagulation treatment increased the stiffness of the hydrogels. Meanwhile, these data shows the possibility of controlling coagulation effect by the duration of submerging

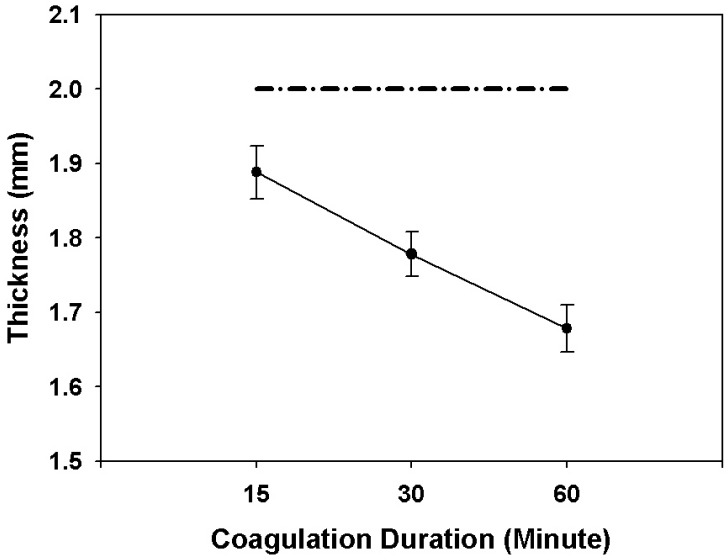

Figure 7.11: Thickness of hydrogel changed when increasing coagulation duration. The thickness of hydrogel before submerging in coagulation bath was 2 mm (dash-dot line).

in coagulation bath.

The effect of coagulation on the thickness of hydrogel is evident in Figure 7.11. When the coagulation duration increased from 15min to 30min and 60min, a linearly decreasing thickness was found. This is due to the precipitation of polymer solution around PVA crystal domain, which expelled free water from the gel matrix.

Meanwhile, coagulation has a different effect on the hydrogel with different thickness. For those hydrogels with 1mm thickness (Figure 7.1, 7.2 and 7.3), the stress-strain curves were almost linear. The hydrogels with 2mm thickness displayed non-linear stress-strain curves. This could due to the saturation of the coagulation effect. For thinner hydrogels, the coagulants can easily permeate through and coagulate the polymer solution within the gel matrix. In contrast, a thicker hydrogel would take more time to coagulate all the parts of the polymer solution. The remaining polymer solution phase in the gel structure would contribute a viscous effect to the overall mechanics of hydrogel.

It is noteworthy that the colour of the PVA-SbQ fibre of the hydrogel/fibre composite changed to green and became darker green with increasing coagulation time. This

green coloured PVA-SbQ fibre became lighter following rinsing of the hydrogel/fibre composite in deionised water. After keeping these coloured composites in a refrigerator (dark enviroment) for 1 week, the colour changed to pink. This colour variation of PVA-SbQ fibres could be due the reaction of remaining uncrosslinked SbQ group with chemicals in coagulation bath. Light in the lab could also affect the SbQ group. Interestingly, as the fibres colour changed in coagulation bath, it gives a way to visualise the PVA-SbQ fibres of the hydrogel/fibre comoposite. However, this is an issue of system stability that may require further investigation.

7.3.3 Effect of fibres layer

When comparing Figure 7.6 and 7.7, the effect of a layer of PVA-SbQ fibres can be easily found. The hydrogels, with or without the fibre layer, show linear stress-strain profile at the strain range of 0-40% and non-linear profile at the strain range of 40%-60%. The fibre layer does not affect the modulus of hydrogel in the low strain range (0-40%). However, at a higher strain range (40% - 60%), the fibres significantly increase the modulus up to about two-fold. This result clearly shows that the PVA-SbQ fibres only recruit at higher strain range, which play a similar role to the collagen fibres in the native arteries. However, the modulus of this hydrogel/fibre composite (Figure 7.7) seems too high when compared with the modulus of pig aortas (Figure 7.10). This means that coagulation effect is too strong when coagulating with 7.5% KOH, 1M Na_2SO_4 for 60min in a dynamic coagulation bath stirred by a magnetic stirrer. To decrease the coagulation effect, several options could be addressed: firstly, a decrease in the concentration of KOH and Na_2SO_4; secondly, a decrease in the submerging duration; lastly, submerging in a static coagulation bath (without stirring by magnetic bars).

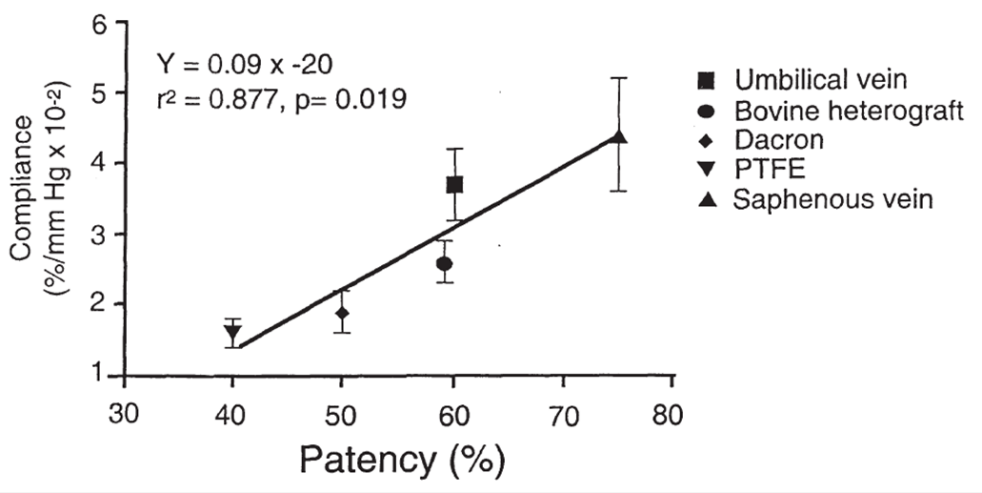

Figure 7.12: The relationship between the compliance of various vascular grafts versus patency rate. (data from Salacinski et al. [190])

7.3.4 Compliance test

This compliance property of arteries is an essential factor in the storage of energy during systole and the release of energy during diastole. As a result, compliant arteries are able to damp out the pulsatile arterial flow to smooth the venous flow and to decrease the blood pressure progressively from the heart to the irrigated organs [189, 155]. Some synthetic grafts have been developed as substitute arteries for bypass surgery. Dacron and ePTFE are the two vascular grafts which are clinically dominant. However, Dacron and ePTFE have the disadvantage of compliance mismatch with native arteries. This mismatch of compliance at the anastomosis site (at which the artery connects to the vascular graft) tends to invoke a variation on normal blood flow, which increases the risk of thrombosis and intimal hyperplasia and consequently results in unsatisfactory long-term patency [68, 70, 183, 184, 185, 186, 187]. Salacinski et al. have summarized the compliance of grafts and their patency rates [190]. Their study showed a linear relationship between compliance and patency rates (Figure 7.12). It is therefore possible that a better the patency rate can be maintained when more compliant graft is applied.

Recently, a compliant vascular graft, poly(carbonate)polyurethane (CPU), has been developed [6]. CPU shows a static compliance value of 8.1 % per mmHg $\times 10^{-2}$over

a range of mean pressure, 30-100 mmHg. The compliance of CPU matched with that of artery in the pressure range of 30-60 mmHg. However, a significant compliance mismatch can be found at mean pressures higher than 60 mmHg. Taking into account the fact that physiological blood pressure of 120/80 mmHg, a new vascular graft is desired to match the compliance artery over a wide range of pressure. This has led to the study of a PVA/Gelatin hydrogel and PVA-SbQ fibre duo-layer constructed graft.

The PVA/Gelatin hydrogel single layer graft was much more compliant than arteries (Figure 7.13 B) over the whole pressure range (Figure 7.9). When the PVA-SbQ fibres were assembled on the luminal surface of PVA/Gelatin hydrogel, the as-prepared duo-layer graft exhibit a close compliance match to the arterty over the whole pressure range (Figure 7.13). One of the most significant properties is that this hydrogel/fibre duo-layer graft behaves with a variable pattern of compliance. A higher compliance value is found at the lower mean pressure. This is important to impart pulsatile energy to the blood flow in the case of low blood pressure, such as shock [190]. Decreased lower compliance can be found at higher pressure, which helps to prevent vessel burst at high pressures.

The compliance of PG hydrogels can be controlled by the treatment of freeze-thawing and coagulation. The effect of coagulation on the compliance can be seen from Figure 7.8 and 7.9. With stirring in the coagulation bath, the coagulation effect on the PG hydrogel was enhanced and resulted in lower compliance values. This agrees with coagulation effect observed in uniaxial tensile test experiments, where the coagulation effect was enhanced by prolonging the coagulation time (Figure 7.4, 7.5 and 7.6). The compliance of PG hydrogels can also be controlled by the number of freeze-thaw cycles and the thawing rate [81].

When PG hydrogels were constructed with PVA-SbQ fibres, the compliance of the duo-layer graft dramatically reduced to the physiological range of the compliant artery. It clearly showed that the fibres increased the elastic modulus which agrees with the tensile test results (Figure 7.6 and 7.7).

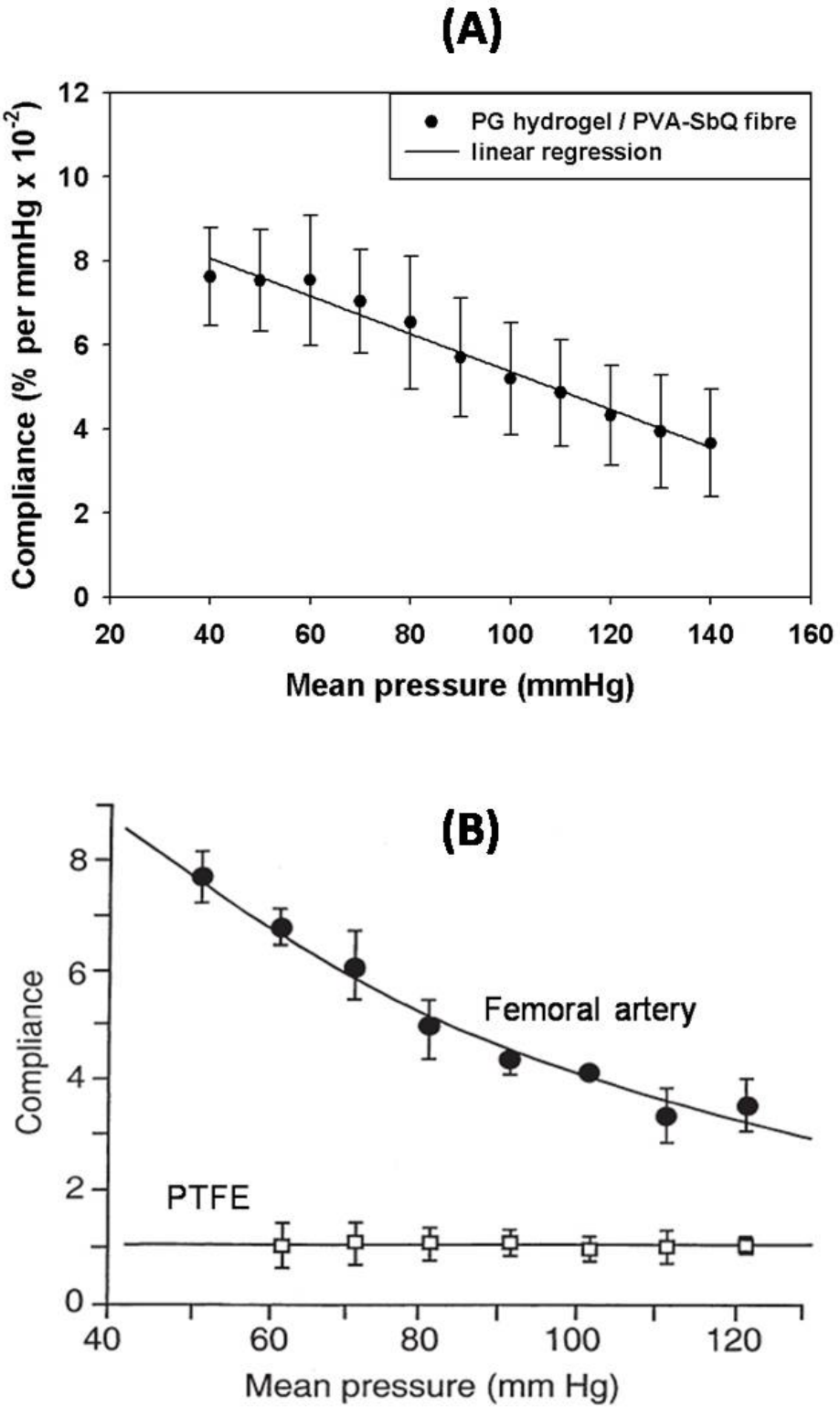

Figure 7.13: The comparison of compliance-mean pressure profile of the hydrogel/fibre duo-layer graft, human femoral artery and PTFE graft. (A) PG hydrogel/PVA-SbQ fibre duo-layer graft. (B) Human femoral artery and PTFE graft (data is adapted from Salacinski et al. [190]).

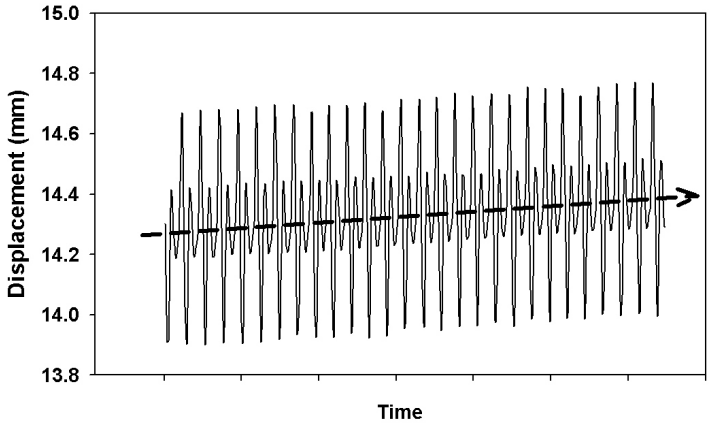

Figure 7.14: Creeping of statically coagulated PG hydrogel at the mean pressure of 140 mmHg. The control on the frequency of pusatile flow was of concern and therefore the displacement-time profile were ploted without specific time on x-axis.

Fibres not only help to control the elasticity of the duo-layer graft, they also eliminate the creeping effect, which is significant for statically coagulated PG hydrogel at mean pressure of 140 mmHg (Figure 7.14). Another advantages is that the PVA-SbQ fibres are favourable for endothelial cell attachment, and could be further immobilized with molecules like RGDs to regulate cell behaviour on the fibres. Meanwhile, the fibres can also be applied as reservoir for various drugs, which would give benefits of anti-infection and curing vascular disease.

7.4 Summary

In this last part of the research, a duo-layer vascular graft was designed and constructed by a layer of PVA/Gelatin hydrogel and another layer of PVA-SbQ fibres. The result of uniaxial tensile tests showed the preconditioning effect, non-linear stress-strain profile and the effect of coagulation treatment and additional layer of fibres on the elasticity of constructs. It is clear that both extension of the coagulation duration and addition of the fibre layer increase the elastic modulus of the constructs. The compliance results show that the compliance of the duo-layer graft closely matches with that of native artery over a wide range of pressure (mean pressure at 40-140 mmHg). A significant

conclusion that can be addressed from the uniaxial tensile test and the compliance test is that the mechanical properties of the as-prepared duo-layer graft closely match with that of native artery. This superiority in mechanical properties is coupled with the advantages of fibre layers in conducting the endothelial cell lining and potentially delivering growth factors or drugs. All these merits make the duo-layer graft a very promising candidate for potential applications in vascular tissue engineering.

Chapter 8

Conclusions and future work

8.1 Conclusions

This research involved in the development and evaluation of a duo-layer vascular graft to mimic the structure and function of the native artery. The contributions to the knowledge gained from this study are summarized as follows:

1. Soft-tissue like PVA-based hydrogels with controllable structural and mechanical properties were developed by physical crosslinking methods, specifically freeze-thawing and coagulation. These methods provide the possibility to tailor the mechanical property of PVA based hydrogels to fit the needs of vascular graft applications.

2. With the findings on the effect of physical crosslinking methods on the glass transition temperature, melting temperature, crystallinity, polymer fraction and mechanical properties of hydrogels, the current study developed a comprehensive understanding of the formation of hydrogel microstructures and provided fundamental knowledge concerning the control of the mechanical properties (especially the compliance property) of the final duo-layer graft. This finding also filled a gap in the literature in terms of a micro-structural study on the effect of coagulation treatment on the properties of hydrogels.

3. Endothelial cell attachment favourable fibres were fabricated by electrospinning and photocrosslinking. To the best of our knowledge, this was the first time that PVA-SbQ was applied as a material for the electrospinning technique. With photo-activation, PVA-SbQ fibres provide promising water insolubility and conduciveness to the attachment of endothelial cells.

4. The most significant contribution of the current study is that the novel duo-layer construct has the most suitable compliance characteristics for vascular graft applications, compared to all prototype grafts described in the literature to our best knowledge. This finding inspires a platform method to develop vascular grafts to mimic the multiple-layer structure of native arteries by compositing hydrogel and fibrous layers.

8.2 Perspectives and future work

8.2.1 Duo-layer constructs as vascular grafts

The design of the duo-layer graft was inspired by the layered structure of native arteries. The media layer plays a dominant role in the mechanical properties of arteries. The intima layer provides a basal membrane to conduct the lining of endothelial cells, and a subendothelial connective tissue to support the basal membrane. Accordingly, a duo-layer graft was designed in this research. Firstly, PVA/Gelatin hydrogels with controllable mechanical properties were formed by physical crosslinking methods. Taken with the parallel study [191] on the encapsulation of smooth muscle cells, PVA/Gelatin hydrogels evidently have the potential to mimic the role of the media layer of arteries in providing the main mechanical support and in encapsulating smooth muscle cells. Secondly, the PVA-SbQ fibres were fabricated by electrospinning and photocrosslinking techniques. PVA-SbQ was employed as a material to fabricate electrospun fibres due to its photocurable property, which is a superior approach to chemical crosslinking methods when considering the issue of chemical residuals. The preliminary result on

the attachment of endothelial cells showed the possibility of PVA-SbQ to play the role of intima to facilitate the lining of endothelial cells. As the mild conditions of electrospinning and photocrosslinking, the PVA-SbQ fibres give the possibility to preserve functionalities of proteins which could invoke future application as a delivery system for process-sensitive substances, such as growth factors and medicines. The capability of PVA-SbQ to preserve the functions of enzymes was proved by Ichimura [174]. More interestingly, the thin PVA-SbQ fibre layer was able to affect the overall mechanical properties of the duo-layer construct. Actually, the layer of PVA/Gelatin hydrogel (with the reported preparation process) presented an overly high compliance value and the PVA-SbQ fibre layer helped to tailor the mechanical property of vascular graft to match with that of native artery. Therefore the electrospinning and photocrosslinking processes are also important factors when trying to obtain suitable mechanical properties for vascular graft application.

Apart from obtaining a graft with suitable mechanical properties, this duo-layer design also inspired a platform method, which is the fabrication of the multilayer structure vascular graft with one layer to provide mechanical support, and another layer to conduct endothelial cell behaviour and to modify the mechanical properties.

The hydrogel layer can be made from compliant materials, such as PVA based hydrogels in this study and possibly other materials, such as bacterial cellulose [192]. PVA and bacterial cellulose can also be blended to form a composite hydrogel layer [193]. Importantly, the mechanical property of this layer is of the first concern for the entire design. Jeong et al. [118] fabricated a duo-layer graft with a porous collagen porous scaffold and an inner layer of PLGA fibres. However, the collagen scaffold is too weak to supply mechanical support, which leads to a deficit of mechanical strength of the final graft.

The fibrous layer in this study is made from PVA-SbQ, which could possibly be replaced by other materials that can be prepared as fibre form, such as collagen [109] and photocrosslinkable PEG [194]. Fibres coated with cell conducive material [195]

Figure 8.1: VWR thermal circulator 1187P.

could be another candidate for this layer. Meanwhile, as the physiological strain is typically lower than 5%, the addition of the thin stiffer layer could also account for the overall mechanical characteristics of the final duo-layer graft. Therefore, the influence of the fibrous layer on the overall mechanical property of the vascular graft is worthy of further investigation.

8.2.2 PVA based hydrogel developments

PVA based hydrogels were fabricated with freeze-thaw cycles and coagulation treatments. Both of these effectively contributed to the final mechanical characteristics of the hydrogels. The effect of the number of freeze-thaw cycles, the duration of the coagulation treatment and either static or dynamic coagulation bath conditions were investigated. There are still some other factors available to further control the mechanical properties of final gels. The rate of thawing is another important factor in the freeze-thaw process. For pure PVA gels, a stronger gel can be formed by a slower thawing process [81]. More specifically, there may be a temperature range (around -2.5 $^{\circ}C$) optimum for the formation of the gel network [81]. The longer the temperature resides in this range, the stronger the gel will be. Therefore, it will be worth to control the thawing rate by a thermal circulator (such as VWR Circulator 1187P, see Figure 8.1).

The aortic tissue has an anisotropic pattern of mechanical response. The elastic modulus of the circumferential direction is higher than that of the axial direction of

the aortic tissue [9]. In the current study, the compliance of duo-layer graft closely matched that of native artery. However, the non-linearity of compliance with respect to mean blood pressure was not apparent. This is may be improved by replacing the currently used isotropic hydrogels with anisotropic hydrogels, which can be developed by stretching the hydrogel during the freeze-thawing process for PVA hydrogels[9].

8.2.3 Alignment of electrospun fibres

Various methods have been developed to assemble oriented fibres in electrospinning, (see Figure 2.13). A novel wire collector (Figure 6.7) has been designed to obtain helical aligned fibres, in order to simulate the helical alignment of fibrous bundles in the media layer of the artery [16]. With a preliminary study on the electrospinning of the PVA with this new collector, the alignment of PVA fibres was successfully fabricated, as described in section 6.2.5 (Figure 8.2). The fibres were aligned both on the wires and across the wires. this also offers the possibility to redesign the collector to obtain fibrous tubes with luminal alignment which would facilitate the attachment or migration of endothelial cells on the fibres. A stent with a suitable pattern, like Figure 8.3, could possibly be used as a collector for electrospinning. A drum collector with rotation controller has been developed in our group as part of this project, which would also help to obtain the alignment of fibres in future.

8.2.4 Biocompatibility testing

The current study presented promising mechanical characteristics of the duo-layer graft. Some future work on other mechanical properties and biocompatibility testing still needs to be performed to ensure successful application as vascular graft.

In compliance test, our duo-layer graft was able to withstand flow pressure as high as 140 mmHg, however, a burst pressure experiment (ASTM D6797-07) would still be necessary to ensure the potential use of this graft in vivo. A suture retension strength would be required to approve the suture holding capacities [47].

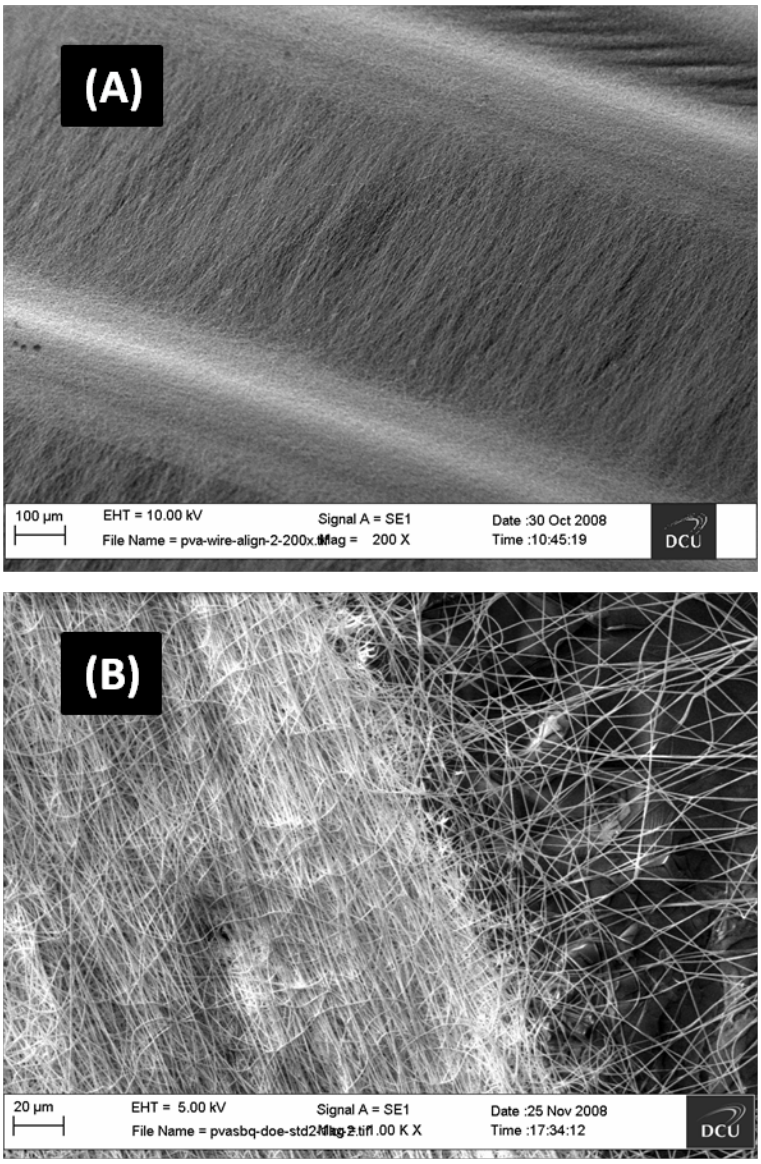

Figure 8.2: Aligned fibres on wire collector of electrospinning. (A) 200 magnification; (B) 5000 magnification.

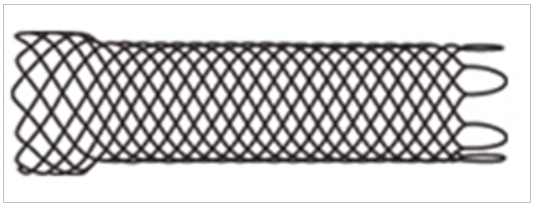

Figure 8.3: A helically assembled stent. (Image obtained from www. bostonscientific. com)

As to the in vitro cell compatibility testing, the viability of endothelial cell and smooth muscle cell can be tested by neutral red dye. The cell proliferation can be tested using the mitochondrial metabolic (MTT) activity assay or the Alamar blue assay. The cell attachment can be observed by scanning electron microscopy or analysed by immunofluoresence staining, where using anti-alpha smooth muscle actin and anti-CD-31 to visualize the smooth muscle cell and endothelial cell , respectively [119].

In vivo biocompatibility testing can be performed on animals, such as mice, pig and sheep. Micro computed tomography (CT) can be employed to evaluate the wall of grafts and arteries in vivo [196]. Smooth muscle cells and endothelial cells can be distinguished by Hematoxylin and Eosin (H&E) staining or by immunofluoresence staining as the same method in vitro. Especially, the behaviour of endothelial cells on the luminal surface can also be analysed by the synthesis of Prostacyclin (PGI2) , a potent inhibitor of platelet aggregation [38]. The production of collagen and elastin can be tracked by Masson trichrome and Verhoeff staining, respectively.

Bibliography

[1] Lloyd-Jones D, Adams R, Carnethon M, Simone GD, Ferguson TB, Greenlund K, et al. Heart Disease and Stroke Statistics - 2009 update: A Report From the American Heart Association Statistics Committee and Stroke Statistics Subcommittee. Circulation. 2009;119:e21–e181.

[2] Mortality and burden of disease: cardiovascular disease in ireland. WHO statistical Information System. 2002;.

[3] Petersen S, Peto V, Rayner M, Leal J, Luengo-Fernandez R, Gray A. European cardiovascular disease statistics. British Heart Foundation. 2005;.

[4] Ouriel K. Peripheral arterial disease. Lancet. 2001;358:1257–1264.

[5] Baguneid MS, Seifalian AM, Salacinski HJ, Murray D, Hamilton G, Walker MG. Tissue engineering of blood vessels. British Journal of Surgery. 2006;93(3):282–290.

[6] Tai NR, Salacinski HJ, Edwards A, Hamilton G, Seifalian AM. Compliance properties of conduits used in vascular reconstruction. British Journal of Surgery. 2000;87(11):1516–1524.

[7] Wan WK, Campbell G, Zhang ZF, Hui AJ, Boughner DR. Optimizing the tensile properties of polyvinyl alcohol hydrogel for the construction of a bioprosthetic heart valve stent. Journal of Biomedical Materials Research. 2002;63(6):854–861.

[8] Chu KC, Rutt BK. Polyvinyl alcohol cryogel: an ideal phantom material for MR studies of arterial flow and elasticity. Magnetic resonance in medicine : official journal of the Society of Magnetic Resonance in Medicine / Society of Magnetic Resonance in Medicine. 1997;37(2):314–319.

[9] Millon LE, Nieh MP, Hutter JL, Wan WK. SANS characterization of an anisotropic poly(vinyl alcohol) hydrogel with vascular applications. Macromolecules. 2007;40(10):3655–3662.

[10] Mathews DT, Birney YA, Cahill PA, McGuinness GB. Mechanical and morphological characteristics of poly(vinyl alcohol)/chitosan hydrogels. Journal of Applied Polymer Science. 2008;109(2):1129–1137.

[11] Mathews DT, Birney YA, Cahill PA, McGuinness GB. Vascular Cell Viability on Polyvinyl Alcohol Hydrogels Modified With Water-Soluble and -Insoluble Chitosan. Journal of Biomedical Materials Research Part B-Applied Biomaterials. 2008;84B:531–540.

[12] Holzapfel G, Gasser T, Ogden R. A new constitutive framework for arterial wall mechanics and a comparative study of material models. Journal of Elasticity. 2000;61(1):1–48.

[13] Sarkar S, Schmitz-Rixen T, Hamilton G, Seifalian AM. Achieving the ideal properties for vascular bypass grafts using a tissue engineered approach: a review. Medical & Biological Engineering & Computing. 2007;45(4):327–336.

[14] Yao L, Liu J, Andreadis S. Composite Fibrin Scaffolds Increase Mechanical Strength and Preserve Contractility of Tissue Engineered Blood Vessels. Pharmaceutical Research. 2008;25(5):1212–1221.

[15] Thomas V, Zhang X, Vohra YK. A biomimetic tubular scaffold with spatially designed nanofibers of protein/PDS(R) bio-blends. Biotechnology and Bioengineering. 2009;.

[16] Rhodin JA, Bohr DF. Architecture of the vessel wall. In: Handbook of Physiology. Section 2: The Cardiovascular System. Vol II. Vascular Smooth Muscle. American Physiological Society; 1980. p. 1–31.

[17] Clark J, Glagov S. Structural integration of the arterial wall. I. Relationships and attachments of medial smooth muscle cells in normally distended and hyperdistended aortas. Laboratory investigation; a journal of technical methods and pathology. 1979;40(5):587.

[18] Silver FH, Christiansen DL, Buntin CM. Mechanical properties of the aorta: a review. Critical Reviews in Biomedical Engineering. 1989;17(4):323–358.

[19] Schmedlen RH, Elbjeirami WM, Gobin AS, West JL, Fisher JP, Mikos AG, et al. Tissue Engineered Vascular Grafts. In: Tissue Engineering. U.S.A: Taylor & Francis Group, LLC; 2007. p. 434–446.

[20] Seifalian AM, Giudiceandrea A, Schmitz-Rixen T, Hamilton G, P GHPZ. Noncompliance: The silent Acceptance of a Villain. In: Tissue engineering of vascular prosthetic grafts. U.S.A: R.G. Landes Company; 1999. p. 45–58.

[21] Sarkar S, Salacinski HJ, Hamilton G, Seifalian AM. The mechanical properties of infrainguinal vascular bypass grafts: Their role in influencing patency. European Journal of Vascular and Endovascular Surgery. 2006;31(6):627–636.

[22] Wu SG, Lee GC, Tseng NT. Nonlinear elastic analysis of blood vessels. Journal of Biomechanical Engineering. 1984;106(4):376–383.

[23] Wu SG, Lee GC. On nonlinear viscoelastic properties of arterial tissue. Journal of Biomechanical Engineering. 1984;106(1):42–47.

[24] von Maltzahn WW, Warriyar RG, Keitzer WF. Experimental measurements of elastic properties of media and adventitia of bovine carotid arteries. Journal of Biomechanics. 1984;17(11):839–847.

[25] Sharma MG. Viscoelastic behavior of conduit arteries. Biorheology. 1974;11(4):279–91.

[26] Holzapfel G, Schulze-Bauer C, Stadler M. Mechanics of angioplasty: Wall, balloon and stent. ASME Applied Mechanics Division-Publications-AMD. 2000;242:141–156.

[27] Roach MR, Burton AC. The Reason for the Shape of the Distensibility Curves of Arteries. Canadian Journal of Biochemistry and Physiology. 1957;35(8):681–690.

[28] ASTM. Stand Test Method for Tensile Properties of Plastics D638-00). 2000;.

[29] Yow KH, Ingram J, Korossis SA, Ingham E, Homer-Vanniasinkam S. Tissue engineering of vascular conduits. British Journal of Surgery. 2006;93(6):652–661.

[30] Schaner PJ, Martin ND, Tulenko TN, Shapiro IM, Tarola NA, Leichter RF, et al. Decellularized vein as a potential scaffold for vascular tissue engineering. Journal of Vascular Surgery. 2004;40(1):146–153.

[31] Conklin BS, Richter ER, Kreutziger KL, Zhong DS, Chen C. Development and evaluation of a novel decellularized vascular xenograft. Medical Engineering & Physics. 2002;24(3):173–183.

[32] Teebken OE, Bader A, Steinhoff G, Haverich A. Tissue engineering of vascular grafts: human cell seeding of decellularised porcine matrix. European Journal of Vascular and Endovascular Surgery. 2000;19(4):381–386.

[33] Kaushal S, Amiel GE, Guleserian KJ, Shapira OM, Perry T, Sutherland FW, et al. Functional small-diameter neovessels created using endothelial progenitor cells expanded ex vivo. Nature Medicine. 2001;7(9):1035–1040.

[34] Lantz GC, Badylak SF, Hiles MC, Coffey AC, Geddes LA, Kokini K, et al. Small intestinal submucosa as a vascular graft: a review. Journal of Investigative Surgery. 1993;6(3):297–310.

[35] Clarke DR, Lust RM, Sun YS, Black KS, Ollerenshaw JD. Transformation of nonvascular acellular tissue matrices into durable vascular conduits. The Annals of Thoracic Surgery. 2001;71(5 Suppl):S433–S436.

[36] Huynh T, Abraham G, Murray J, Brockbank K, Hagen PO, Sullivan S. Remodeling of an acellular collagen graft into a physiologically responsive neovessel. Nature Biotechnology. 1999;17(11):1083–1086.

[37] Weinberg CB, Bell E. A blood vessel model constructed from collagen and cultured vascular cells. Science. 1986;231(4736):397–400.

[38] L'Heureux N, Paquet S, Labbe R, Germain L, Auger FA. A completely biological tissue-engineered human blood vessel. The FASEB Journal. 1998;12(1):47–56.

[39] Koyama H, Raines EW, Bornfeldt KE, Roberts JM, Ross R. Fibrillar collagen inhibits arterial smooth muscle proliferation through regulation of Cdk2 inhibitors. Cell. 1996;87(6):1069–1078.

[40] Li DY, Brooke B, Davis EC, Mecham RP, Sorensen LK, Boak BB, et al. Elastin is an essential determinant of arterial morphogenesis. Nature. 1998;393(6682):276–280.

[41] Wight TN. Cell biology of arterial proteoglycans. Arteriosclerosis. 1989;9(1):1–20.

[42] Bingley JA, Hayward IP, Campbell JH, Campbell GR. Arterial heparan sulfate proteoglycans inhibit vascular smooth muscle cell proliferation and phenotype change in vitro and neointimal formation in vivo. Journal of Vascular Surgery. 1998;28(2):308–318.

[43] Voytik-Harbin SL, Brightman AO, Kraine MR, Waisner B, Badylak SF. Identification of extractable growth factors from small intestinal submucosa. Journal of Cellular Biochemistry. 1997;67(4):478–491.

[44] Gillis C, Bengtsson L, Wilman B, Haegerstrand A. Secretion of prostacyclin, tissue plasminogen activator and its inhibitor by cultured adult human endothelial cells grown on different matrices. European Journal of Vascular and Endovascular Surgery. 1996;11(2):127–133.

[45] Kallenbach K, Leyh RG, Lefik E, Walles T, Wilhelmi M, Cebotari S, et al. Guided tissue regeneration: porcine matrix does not transmit PERV. Biomaterials. 2004;25(17):3613–3620.

[46] Martin U, Winkler ME, Id M, Radeke H, Arseniev L, Takeuchi Y, et al. Productive infection of primary human endothelial cells by pig endogenous retrovirus (PERV). Xenotransplantation. 2000;7(2):138–142.

[47] L'Heureux N, Dusserre N, Konig G, Victor B, Keire P, Wight TN, et al. Human tissue-engineered blood vessels for adult arterial revascularization. Nature medicine. 2006;12:361–365.

[48] Greisler HP, Petsikas D, Cziperle DJ, Murchan PM, Henderson SC, Lam TM. Dacron stimulation of macrophage transforming growth factor-beta release. Cardiovascular Surgery. 1996;4(2):169–173.

[49] Marois Y, Chakfe N, Guidoin R, Duhamel RC, Roy R, Marois M, et al. An albumin-coated polyester arterial graft: in vivo assessment of biocompatibility and healing characteristics. Biomaterials. 1996;17(1):3–14.

[50] Fournier N, Doillon CJ. Biological molecule-impregnated polyester: an in vivo angiogenesis study. Biomaterials. 1996;17(17):1659–1665.

[51] Demiri EC, Iordanidis SL, Mantinaos CF. Experimental use of prosthetic grafts in microvascular surgery. Handchir Mikrochir Plast Chir. 1999;31(2):102–106.

[52] Camiade C, Maher A, Ricco JB, Roumy J, Febrer G, Marchand C, et al. Carotid bypass with polytetrafluoroethylene grafts: a study of 110 consecutive patients. Journal of Vascular Surgery. 2003;38(5):1031–7; discussion 1038.

[53] Sala F, Hassen-Khodja R, Lecis A, Bouillanne PJ, Declemy S, Batt M. Long-term outcome of femoral above-knee popliteal artery bypass using autologous saphenous vein versus expanded polytetrafluoroethylene grafts. Annals of Vascular Surgery. 2003;17(4):401–407.

[54] Kannan RY, Salacinski HJ, Butler PE, Hamilton G, Seifalian AM. Current status of prosthetic bypass grafts: a review. Journal of Biomedical Materials Research - Part B Applied Biomaterials. 2005;74(1):570–581.

[55] Coury AJ, P GHPZ. Biostable polymers as durable scaffolds for tissue engineered vascular prostheses. In: Tissue engineering of vascular prosthetic grafts. U.S.A: R.G. Landes Company; 1999. p. 469–480.

[56] Deutsch M, Meinhart J, Fischlein T, Preiss P, Zilla P. Clinical autologous in vitro endothelialization of infrainguinal ePTFE grafts in 100 patients: a 9-year experience. Surgery. 1999;126(5):847–855.

[57] Stankus JJ, Guan JJ, Fujimoto K, Wagner WR. Microintegrating smooth muscle cells into a biodegradable, elastomeric fiber matrix. Biomaterials. 2006;27(5):735–744.

[58] Stankus JJ, Soletti L, Fujimoto K, Hong Y, Vorp DA, Wagner WR. Fabrication of cell microintegrated blood vessel constructs through electrohydrodynamic atomization. Biomaterials. 2007;28(17):2738–2746.

[59] Zhang Z, Marois Y, Guidoin RG, Bull P, Marois M, How T, et al. Vascugraft polyurethane arterial prosthesis as femoro-popliteal and femoro-peroneal bypasses in humans: pathological, structural and chemical analyses of four excised grafts. Biomaterials. 1997;18(2):113–124.

[60] Mathur AB, Collier TO, Kao WJ, Wiggins M, Schubert MA, Hiltner A, et al. In vivo biocompatibility and biostability of modified polyurethanes. Journal of Biomedical Materials Research. 1997;36(2):246–257.

[61] Salacinski HJ, Odlyha M, Hamilton G, Seifalian AM. Thermo-mechanical analysis of a compliant poly(carbonate-urea)urethane after exposure to hydrolytic, oxidative, peroxidative and biological solutions. Biomaterials. 2002;23(10):2231–2240.

[62] Rashid ST, Salacinski HJ, Button MJ, Fuller B, Hamilton G, Seifalian AM. Cellular engineering of conduits for coronary and lower limb bypass surgery: role of cell attachment peptides and pre-conditioning in optimising smooth muscle cells (SMC) adherence to compliant poly(carbonate-urea)urethane (MyoLink) scaffolds. European Journal of Vascular and Endovascular Surgery. 2004;27(6):608–616.

[63] Tiwari A, Salacinski HJ, Punshon G, Hamilton G, Seifalian AM. Development of a hybrid cardiovascular graft using a tissue engineering approach. The FASEB Journal. 2002;16(8):791–6.

[64] Tang YW, Labow RS, Santerre JP. Enzyme-induced biodegradation of polycarbonate polyurethanes: dependence on hard-segment concentration. Journal of Biomedical Materials Research. 2001;56(4):516–528.

[65] Lemson MS, Tordoir JH, Daemen MJ, Kitslaar PJ. Intimal hyperplasia in vascular grafts. European Journal of Vascular and Endovascular Surgery. 2000;19(4):336–350.

[66] Perktold K, Leuprecht A, Prosi M, Berk T, Czerny M, Trubel W, et al. Fluid dynamics, wall mechanics, and oxygen transfer in peripheral bypass anastomoses. Annals of Biomedical Engineering. 2002;30(4):447–460.

[67] Stewart SF, Lyman DJ. Effects of a vascular graft/natural artery compliance mismatch on pulsatile flow. Journal of Biomechanics. 1992;25(3):297–310.

[68] Weston MW, Rhee K, Tarbell JM. Compliance and diameter mismatch affect the wall shear rate distribution near an end-to-end anastomosis. Journal of Biomechanics. 1996;29(2):187–198.

[69] Fry DL. Acute vascular endothelial changes associated with increased blood velocity gradients. Circulation Research. 1968;22(2):165–197.

[70] Walden R, L'Italien GJ, Megerman J, Abbott WM. Matched elastic properties and successful arterial grafting. Archives of Surgery. 1980;115(10):1166–1169.

[71] O'Flynn P, Roche E, Pandit A. Generating an Ex Vivo Vascular Model. American society for artificial internal organs. 2005;51(4):426–433.

[72] Millon LE, Mohammadi H, Wan WK. Anisotropic polyvinyl alcohol hydrogel for cardiovascular applications. Journal of Biomedical Materials Research Part B-Applied Biomaterials. 2006;79B(2):305–311.

[73] Marten FL. In: Vinyl alcohol polymers. Wiley-Interscience; 2003. p. 399–437.

[74] Sundararajan PR, Mark JE, Anonymous. Poly(vinyl alcohol). In: Polymer Data Handbook. Oxford University Press; 1999. p. 890–909.

[75] Vidal MB, Gil MH. Swelling and thermal properties of poly(vinyl alcohol) containing hemoglobin membranes. Journal of Bioactive and Compatible Polymers. 1999;14(3):243–257.

[76] Clough R. High-energy radiation and polymers: A review of commercial processes and emerging applications. Nuclear Inst and Methods in Physics Research, B. 2001;185(1-4):8–33.

[77] Hennink WE, van Nostrum CF. Novel crosslinking methods to design hydrogels. Advanced Drug Delivery Reviews. 2002;54(1):13–36.

[78] Peppas N, Merrill E. Crosslinked poly (vinyl alcohol) hydrogels as swollen elastic networks. Journal of Applied Polymer Science. 1977;21(7):1763–1770.

[79] Zhao L, Mitomo H, Zhai ML, Yoshii F, Nagasawa N, Kume T. Synthesis of antibacterial PVA/CM-chitosan blend hydrogels with electron beam irradiation. Carbohydrate Polymers. 2003;53(4):439–446.

[80] Hassan CM, Peppas NA. Structure and Applications of Poly (vinyl alcohol) Hydrogels Produced by Conventional Crosslinking or by Freezing/Thawing Methods. Advances in Polymer Science. 2000;153:37–66.

[81] Lozinsky VI. Cryotropic gelation of poly (vinyl alcohol) solutions. Russian Chemical Reviews. 1998;67(7):573–586.

[82] Peppas NA, Huang Y, Torres-Lugo M, Ward JH, Zhang J. Physicochemical foundations and structural design of hydrogels in medicine and biology. Annual Review of Biomedical Engineering. 2000;2:9–29.

[83] Peppas NA, Wright SL. Drug diffusion and binding in ionizable interpenetrating networks from poly(vinyl alcohol) and poly(acrylic acid). European Journal of Pharmaceutics and Biopharmacutics. 1998;46(1):15–29.

[84] Fergg F, Keil FJ, Quader H. Investigations of the microscopic structure of poly(vinyl alcohol) hydrogels by confocal laser scanning microscopy. Colloid and Polymer Science. 2001;279(1):61–67.

[85] Willcox P, Jr DH, Schmidt-Rohr K, Hoagland D, Gido S, Pudjijanto S, et al. Microstructure of poly (vinyl alcohol) hydrogels produced by freeze/thaw cycling. Journal of Polymer Science Part B: Polymer Physics. 1999;37(24):3438–3454.

[86] Ricciardi R, Auriemma F, Gaillet C, Rosa CD, Laupretre F. Investigation of the crystallinity of freeze/thaw poly (vinyl alcohol) hydrogels by different techniques. Macromolecules. 2004;37(25):9510–9516.

[87] Ricciardi R, Gaillet C, Ducouret G, Lafuma F, Laupretre F. Investigation of the relationships between the chain organization and rheological properties of atactic poly(vinyl alcohol) hydrogels. Polymer. 2003;44(11):3375–3380.

[88] Ricciardi R, D'Errico G, Auriemma F, Ducouret G, Tedeschi AM, Rosa CD, et al. Short time dynamics of solvent molecules and supramolecular organization of poly (vinyl alcohol) hydrogels obtained by freeze/thaw techniques. Macromolecules. 2005;38(15):6629–6639.

[89] Yokoyama F, Masada I, Shimamura K, Ikawa T, Monobe K. Morphology and structure of highly elastic poly (vinyl alcohol) hydrogel prepared by repeated freezing-and-melting. Colloid and Polymer Science. 1986;264(7):595–601.

[90] Ricciardi R, Mangiapia G, Celso FL, Paduano L, Triolo R, Auriemma F, et al. Structural organization of poly(vinyl alcohol) hydrogels obtained by freezing and thawing techniques: A SANS study. Chemistry of Materials. 2005;17(5):1183–1189.

[91] Kanaya T, Ohkura M, Takeshita H, Kaji K, Furusaka M, Yamaoka H, et al. Gelation Process of Poly(Vinyl Alcohol) as Studied by Small-Angle Neutron and Light-Scattering. Macromolecules. 1995;28(9):3168–3174.

[92] Kanaya T, Takeshita H, Nishikoji Y, Ohkura M, Nishida K, Kaji K. Micro- and mesoscopic structure of poly(vinyl alcohol) gels determined by neutron and light scattering. Supramolecular Science. 1998;5(3-4):215–221.

[93] Takeshita H, Kanaya T, Nishida H, Kaji K. Gelation process and phase separation of PVA solutions as studied by a light scattering technique. Macromolecules. 1999;32(23):7815–7819.

[94] Takeshita H, Kanaya T, Nishida K, Kaji K, Takahashi T, Hashimoto M. Ultra-small-angle neutron scattering studies on phase separation of poly(vinyl alcohol) gels. Physical Review E. 2000;61(2):2125–2128.

[95] Kanaya T, Ohkura M, Kaji K, Furusaka M, Misawa M. Structure of Poly(Vinyl Alcohol) Gels Studied by Wide-Angle and Small-Angle Neutron-Scattering. Macromolecules. 1994;27(20):5609–5615.

[96] Ramakrishna S, Fujihara K, Teo WE, Yong T, Ma ZW, Ramaseshan R. Electrospun nanofibers: solving global issues. Materials Today. 2006;9(3):40–50.

[97] Huang ZM, Zhang YZ, Kotaki M, Ramakrishna S. A review on polymer nanofibers by electrospinning and their applications in nanocomposites. Composites Science and Technology. 2003;63(15):2223–2253.

[98] Greiner A, Wendorff JH. Electrospinning: A fascinating method for the preparation of ultrathin fibres. Angewandte Chemie-International Edition. 2007;46(30):5670–5703.

[99] Taylor G. Studies in Electrohydrodynamics. I. The Circulation Produced in a Drop by Electrical Field. Proceedings of the Royal Society of London Series A, Mathematical and Physical Sciences. 1966;291(1425):159–166.

[100] Yarin AL, Koombhongse S, Reneker DH. Bending instability in electrospinning of nanofibers. Journal of Applied Physics. 2001;89(5):3018–3026.

[101] Yarin AL, Koombhongse S, Reneker DH. Taylor cone and jetting from liquid droplets in electrospinning of nanofibers. Journal of Applied Physics. 2001;90(9):4836–4846.

[102] Ramakrishna S, Fujihara K, Teo WE, Lim TC, Ma ZW, editors. An introduction to electrospinning and nanofibers. Singpore: World Scientific Publishing Company; 2005.

[103] Tan SH, Inai R, Kotaki M, Ramakrishna S. Systematic parameter study for ultrafine fiber fabrication via electrospinning process. Polymer. 2005;46(16):6128–6134.

[104] Supaphol P, Mit-uppatham C, Nithitanakul M. Ultrafine electrospun polyamide-6 fibers: Effects of solvent system and emitting electrode polarity on morphology and average fiber diameter. Macromolecular Materials and Engineering. 2005;290(9):933–942.

[105] Mit-uppatham C, Nithitanakul M, Supaphol P. Ultratine electrospun polyamide-6 fibers: Effect of solution conditions on morphology and average fiber diameter. Macromolecular Chemistry and Physics. 2004;205(17):2327–2338.

[106] Teo WE, Ramakrishna S. A review on electrospinning design and nanofibre assemblies. Nanotechnology. 2006;17(14):R89–R106.

[107] Li D, Wang YL, Xia YN. Electrospinning of polymeric and ceramic nanofibers as uniaxially aligned arrays. Nano Letters. 2003;3(8):1167–1171.

[108] Chew SY, Wen J, Yim EKF, Leong KW. Sustained release of proteins from electrospun biodegradable fibers. Biomacromolecules. 2005;6(4):2017–2024.

[109] Matthews JA, Wnek GE, Simpson DG, Bowlin GL. Electrospinning of collagen nanofibers. Biomacromolecules. 2002;3(2):232–238.

[110] Kim KW, Lee KH, Khil MS, Ho YS, Kim HY. The effect of molecular weight and the linear velocity of drum surface on the properties of electrospun poly(ethylene terephthalate) nonwovens. Fibers and Polymers. 2004;5(2):122–127.

[111] Wannatong L, Sirivat A, Supaphol P. Effects of solvents on electrospun polymeric fibers: preliminary study on polystyrene. Polymer International. 2004;53(11):1851–1859.

[112] Katta P, Alessandro M, Ramsier RD, Chase GG. Continuous electrospinning of aligned polymer nanofibers onto a wire drum collector. Nano Letters. 2004;4(11):2215–2218.

[113] Bhattarai N, Edmondson D, Veiseh O, Matsen FA, Zhang MQ. Electrospun chitosan-based nanofibers and their cellular compatibility. Biomaterials. 2005;26(31):6176–6184.

[114] Teo WE, Kotaki M, Mo XM, Ramakrishna S. Porous tubular structures with controlled fibre orientation using a modified electrospinning method. Nanotechnology. 2005;16(6):918–924.

[115] Xu CY, Inai R, Kotaki M, Ramakrishna S. Aligned biodegradable nanotibrous structure: a potential scaffold for blood vessel engineering. Biomaterials. 2004;25(5):877–886.

[116] Drilling S, Gaumer J, Lannutti J. Fabrication of burst pressure competent vascular grafts via electrospinning: Effects of microstructure. Journal of Biomedical Materials Research Part A. 2009;88A(4):923–934.

[117] Williamson MR, Black R, Kielty C. PCL-PU composite vascular scaffold production for vascular tissue engineering: Attachment, proliferation and bioactivity of human vascular endothelial cells. Biomaterials. 2006;27(19):3608–3616.

[118] Jeong SI, Kim SY, Cho SK, Chong MS, Kim KS, Kim H, et al. Tissue-engineered vascular grafts composed of marine collagen and PLGA fibers using pulsatile perfusion bioreactors. Biomaterials. 2007;28(6):1115–1122.

[119] Stitzel J, Liu L, Lee SJ, Komura M, Berry J, Soker S, et al. Controlled fabrication of a biological vascular substitute. Biomaterials. 2006;27:1088–1094.

[120] Mo XM, Xu CY, Kotaki M, Ramakrishna S. Electrospun P(LLA-CL) nanofiber: a biomimetic extracellular matrix for smooth muscle cell and endothelial cell proliferation. Biomaterials. 2004;25(10):1883–1890.

[121] Sun DH, Chang C, Li S, Lin LW. Near-field electrospinning. Nano Letters. 2006;6(4):839–842.

[122] Kessick R, Fenn J, Tepper G. The use of AC potentials in electrospraying and electrospinning processes. Polymer. 2004;45(9):2981–2984.

[123] Zhang DM, Chang J. Electrospinning of Three-Dimensional Nanofibrous Tubes with Controllable Architectures. Nano Letters. 2008;8(10):3283–3287.

[124] Ekaputra AK, Prestwich GD, Cool SM, Hutmacher DW. Combining electrospun scaffolds with electrosprayed hydrogels leads to three-dimensional cellularization of hybrid constructs. Biomacromolecules. 2008;9(8):2097–2103.

[125] Im JS, Park SJ, Lee YS. Preparation and characteristics of electrospun activated carbon materials having meso- and macropores. Journal of Colloid and Interface Science. 2007;314(1):32–37.

[126] Townsend-Nicholson A, Jayasinghe SN. Cell electrospinning: a unique biotechnique for encapsulating living organisms for generating active biological microthreads/scaffolds. Biomacromolecules. 2006;7(12):3364–3369.

[127] Kempski H, Austin N, Roe A, Chatters S, Jayasinghe SN. Pilot study to investigate the possibility of cytogenetic and physiological changes in bio-electrosprayed human lymphocyte cells. Regenerative Medicine. 2008;3(3):343–349.

[128] Stuart B, editor. Infrared Spectroscopy: Fundamentals and Applications. John Wiley & Sons, Ltd; 2004.

[129] Cheremisinoff NP, editor. Polymer Characterization - Laboratory Techniques and Analysis. Westwood, New Jersey, U.S.A.: Noyes Publications; 1996.

[130] Cines DB, Pollak ES, Buck CA, Loscalzo J, Zimmerman GA, McEver RP, et al. Endothelial cells in physiology and in the pathophysiology of vascular disorders. Blood. 1998;91(10):3527.

[131] Cascone MG, Sim B, Sandra D. Blends of synthetic and natural polymers as drug delivery systems for growth hormone. Biomaterials. 1995;16(7):569–574.

[132] Cascone MG, Maltinti S, Barbani N, Laus M. Effect of chitosan and dextran on the properties of poly (vinyl alcohol) hydrogels. Journal of Materials Science: Materials in Medicine. 1999;10(7):431–435.

[133] Cascone MG, Lazzeri L, Sparvoli E, Scatena M, Serino LP, Danti S. Morphological evaluation of bioartificial hydrogels as potential tissue engineering scaffolds. Journal of Materials Science: Materials in Medicine. 2004;15(12):1309–1313.

[134] Cascone MG, Barbani N, Pgiusti CC, Ciardelli G, Lazzeri L. Bioartificial polymeric materials based on polysaccharides. Journal of Biomaterials Science, Polymer Edition. 2001;12(3):267–281.

[135] Chuang WY, Young TH, Yao CH, Chiu WY. Properties of the poly (vinyl alcohol)/chitosan blend and its effect on the culture of fibroblast in vitro. 1999;.

[136] Koyano T, Minoura N, Nagura M, Kobayashi K. Attachment and growth of cultured fibroblast cells on PVA/chitosan-blended hydrogels. Journal of Biomedical Materials Research. 1998;39(3):486–490.

[137] Awad HA, Wickham MQ, Leddy HA, Gimble JM, Guilak F. Chondrogenic differentiation of adipose-derived adult stem cells in agarose, alginate, and gelatin scaffolds. Biomaterials. 2004;25(16):3211–3222.

[138] Moscato S, Mattii L, D'Alessandro D, Cascone MG, Lazzeri L, Serino LP, et al. Interaction of human gingival fibroblasts with PVA/gelatine sponges. Micron. 2008;39(5):569–579.

[139] Zekorn D. Intravascular retention, dispersal, excretion and break-down of gelatin plasma substitutes. Bibliotheca haematologica. 1969;33:131.

[140] Fan H, Hu Y, Zhang C, Li X, Lv R, Qin L, et al. Cartilage regeneration using mesenchymal stem cells and a PLGA gelatin/chondroitin/hyaluronate hybrid scaffold. Biomaterials. 2006;27(26):4573–4580.

[141] Bastioli C, Bellotti V, Camia M, Giudice LD, Rallis A. Starch/vinyl-alcohol copolymer interactions. Studies in Polymer Science. 1994;12:200–200.

[142] Tudorachi N, Cascaval CN, Rusu M, Pruteanu M. Testing of polyvinyl alcohol and starch mixtures as biodegradable polymeric materials. Polymer Testing. 2000;19(7):785–799.

[143] Termonia Y. Fundamentals of polymer coagulation. Journal of Polymer Science Part B: Polymer Physics. 1995;33(2):279–288.

[144] Peppas NA, Bures P, Leobandung W, Ichikawa H. Hydrogels in pharmaceutical formulations. European Journal of Pharmaceutics and Biopharmaceutics. 2000;50(1):27–46.

[145] Hassan CM, Peppas NA. Structure and Morphology of Freeze/Thawed PVA Hydrogels. Macromolecules. 2000;33(7):2472–2479.

[146] Flory PJ, Jr JR. Statistical Mechanics of Cross Linked Polymer Networks I. Rubberlike Elasticity. The Journal of Chemical Physics. 1943;11:512.

[147] Mark JE, editor. Polymer Data Handbook. Oxford University Press; 1999.

[148] Trieu HH. The processing/structure/property relationships of polyvinyl alcohol hydrogels. Case Western Reserve University,; 1995. Ph.D.

[149] Bajpai AK, Saini R. Preparation and characterization of biocompatible spongy cryogels of poly(vinyl alcohol)-gelatin and study of water sorption behaviour. Polymer International. 2005;54(9):1233–1242.

[150] Hansen B, Menkis AH, Vesely I. Longitudinal and radial distensibility of the porcine aortic root. The Annals of Thoracic Surgery. 1995;60(2):384–390.

[151] Cox RH. Passive mechanics and connective tissue composition of canine arteries. American Physiological Society. 1978;234(5):H533–H541.

[152] Shadwick RE. Mechanical design in arteries. The Journal of Experimental Biology. 1999;202(Pt 23):3305–3313.

[153] Bergel D. The static elastic properties of the arterial wall. Journal of Physiology. 1961;1961:445–457.

[154] Burton AC. Relation of structure to function of the tissues of the wall of blood vessels. Physiological Reviews. 1954;34(4):619–642.

[155] Faury G. Function-structure relationship of elastic arteries in evolution: from microfibrils to elastin and elastic fibres. Pathologie-biologie. 2001;49(4):310–325.

[156] Ku DN. Blood flow in arteries. Annual Review of Fluid Mechanics. 1997;29:399–434.

[157] Fung YC, Fronek K, Patitucci P. Pseudoelasticity of Arteries and the Choice of Its Mathematical Expression. American Journal of Physiology. 1979;237(5):H620–H631.

[158] Watase M, Nishinari K. Anomalous rheological behaviour of poly(vinyl alcohol) gels. Polymer communications. 1983;24(9):270–273.

[159] Peppas NA, Stauffer SR. Reinforced uncrosslinked poly (vinyl alcohol) gels produced by cyclic freezing-thawing processes: a short review. Journal of Controlled Release. 1991;16:305–310.

[160] Wang T, Turhan M, Gunasekaran S. Selected properties of pH-sensitive, biodegradable chitosan-poly (vinyl alcohol) hydrogel. Polymer International. 2004;53(7):911–918.

[161] Vrana NE. PhD Thesis: Use of PVA cryogelation for Tissue Engineering: Composites, Scaffold Formation and Cell Encapsulation. Vrana NE, editor. Dublin City University; 2009.

[162] Jackson M, Choo LP, Watson PH, Halliday WC, Mantsch HH. Beware of connective tissue proteins: Assignment and implications of collagen absorptions in infrared spectra of human tissues. BBA-Molecular Basis of Disease. 1995;1270(1):1–6.

[163] Muyonga JH, Cole CGB, Duodu KG. Fourier transform infrared (FTIR) spectroscopic study of acid soluble collagen and gelatin from skins and bones of young and adult Nile perch (Lates niloticus). Food Chemistry. 2004;86(3):325–332.

[164] Park JS, Park JW, Ruckenstein E. Thermal and dynamic mechanical analysis of PVA/MC blend hydrogels. Polymer. 2001;42(9):4271–4280.

[165] Mallapragada SK, Peppas NA. Dissolution mechanism of semicrystalline poly (vinyl alcohol) in water. Journal of Polymer Science Part B Polymer Physics. 1996;34:1339–1346.

[166] Peppas NA, Merrill EW. Differential scanning calorimetry of crystallized PVA hydrogels. Journal of Applied Polymer Science. 1976;20(6):1457–1465.

[167] Anseth KS, Bowman CN, Brannon-Peppas L. Mechanical properties of hydrogels and their experimental determination. Biomaterials. 1996;17(17):1647–1657.

[168] Liang D, Hsiao BS, Chu B. Functional electrospun nanofibrous scaffolds for biomedical applications. Advanced Drug Delivery Reviews. 2007;59(14):1392–1412.

[169] Yang E, Qin X, Wang S. Electrospun crosslinked polyvinyl alcohol membrane. Materials Letters. 2008;62(20):3555–3557.

[170] Gohil JM, Bhattacharya A, Ray P. Studies On The Crosslinking Of Poly (Vinyl Alcohol). Journal of Polymer Research. 2006;13(2):161–169.

[171] Ding B, Kim HY, Lee SC, Lee DR, Choi KJ. Preparation and characterization of nanoscaled poly (vinyl alcohol) fibers via electrospinning. Fibers and Polymers. 2002;3(2):73–79.

[172] Zeng J, Hou H, Wendorff JH, Greiner A. Photo-induced solid-state crosslinking of electrospun poly (vinyl alcohol) fibers. Macromolecular Rapid Communications. 2005;26(19).

[173] Ichimura K, Watanabe S. Preparation and characteristics of photocross-linkable poly (vinyl alcohol). Journal of Polymer Science: Polymer Chemistry Edition. 1982;20(6).

[174] Ichimura K. Photocrosslinkable poly (vinyl alcohols): preparation, properties and applications. Heterogeneous Chemistry Reviews. 1996;3:419–442.

[175] Shindo Y, Morikawa S, Hasegawa M, Sugimura T, Adachi D. Photocrosslinking Reaction and Dynamic Viscoelastic Properties of Photosensitive Poly (vinyl alcohol). Journal of Photopolymer Science and Technology. 1995;8(1):125–128.

[176] Shindo Y, Hasegawa M, Kawanobe J, Inoue K. Water Resistance of Photosensitive Poly (Vinyl Alcohol) Films. Journal of Photopolymer Science and Technology. 2001;14(2):293–294.

[177] Shindo Y, Yamada Y, Kawanobe J, Inoue K. Reactivities and Thermal Mechanical Properties of Poly (vinyl alcohol) and Poly (vinyl-b-acrylic acid) with Pendant Styrylpyridinium Groups. Journal of Photopolymer Science and Technology. 2002;15(1):153–157.

[178] Cockburn ES, Davidson RS, Pratt JE. The photocrosslinking of styrylpyridinium salts via a [2+ 2]-cycloaddition reaction. Journal of Photochemistry and Photobiology A: Chemistry. 1996;94(1):83–88.

[179] Ichimura K. Photocrosslinking behavior of poly(vinyl alcohol)s with pendent styrylpyridinium or styrylquinolinium groups. Makromolekulare Chemie. 1987;188:2973–2982.

[180] Subbiah T, Bhat GS, Tock RW, Parameswaran S, Ramkumar SS. Electrospinning of nanofibers. Journal of Applied Polymer Science. 2005;96(2):557–569.

[181] Deitzel JM, Kleinmeyer J, Harris D, Tan NCB. The effect of processing variables on the morphology of electrospun nanofibers and textiles. Polymer. 2001;42(1):261–272.

[182] Koski A, Yim K, Shivkumar S. Effect of molecular weight on fibrous PVA produced by electrospinning. Materials Letters. 2004;58(3-4):493–497.

[183] Trubel W, Schima H, Moritz A, Raderer F, Windisch A, Ullrich R, et al. Compliance mismatch and formation of distal anastomotic intimal hyperplasia in externally stiffened and lumen-adapted venous grafts. European Journal of Vascular and Endovascular Surgery. 1995;10(4):415–423.

[184] Trubel W, Moritz A, Schima H, Raderer F, Scherer R, Ullrich R, et al. Compliance and formation of distal anastomotic intimal hyperplasia in Dacron mesh tube constricted veins used as arterial bypass grafts. ASAIO Journal. 1994;40(3):M273–M278.

[185] Lyman DJ, Fazzio FJ, Voorhees H, Robinson G, Albo D. Compliance as a factor effecting the patency of a copolyurethane vascular graft. Journal of Biomedical Materials Research. 1978;12(3):337–345.

[186] Kidson IG. The effect of wall mechanical properties on patency of arterial grafts. Annals of the Royal College of Surgeons of England. 1983;65(1):24–29.

[187] Ballyk PD, Walsh C, Butany J, Ojha M. Compliance mismatch may promote graft-artery intimal hyperplasia by altering suture-line stresses. Journal of Biomechanics. 1998;31(3):229–237.

[188] Prendergast PJ, Lally C, Daly S, Reid AJ, Lee TC, Quinn D, et al. Analysis of prolapse in cardiovascular stents: a constitutive equation for vascular tissue and finite-element modelling. Journal of Biomechanical Engineering. 2003;125(5):692–699.

[189] Baird RN, Abbott WM. Pulsatile blood-flow in arterial grafts. Lancet. 1976;2(7992):948–950.

[190] Salacinski HJ, Goldner S, Giudiceandrea A, Hamilton G, Seifalian AM, Edwards A, et al. The Mechanical Behavior of Vascular Grafts: A Review. Journal of Biomaterials Applications. 2001;15(3):241.

[191] Vrana NE, O'Grady A, Kay E, Cahill PA, McGuinness GB. Cell encapsulation within PVA-based hydrogels via freeze-thawing: a one-step scaffold formation and cell storage technique. Journal of Tissue Engineering and Regenerative Medicine. 2009;3:567–572.

[192] Iguchi M, Yamanaka S, Budhiono A. Bacterial cellulose - a masterpiece of nature's arts. journal of materials science. 2000;35:261–270.

[193] Millon LE, Wan WK. The polyvinyl alcohol-bacterial cellulose system as a new nanocomposite for biomedical applications. Journal of Biomedical Materials Research Part B-Applied Biomaterials. 2006;79B(2):245–253.

[194] Ko H, Kameoka J. Photo-crosslinked porous PEG hydrogel membrane via electrospinning. Journal of Photopolymer Science and Technology. 2006;19(3):413–418.

[195] He W, Ma Z, Yong T, Teo WE, Ramakrishna S. Fabrication of collagen-coated biodegradable polymer nanofibre mesh and its potential for endothelial cells growth. Biomaterials. 2005;26:7606–7615.

[196] Langheinrich AC, Bohle RM, Greschus S, Hackstein N, Walker G, v Gerlach S, et al. Atherosclerotic lesions at microCT: feasibility for analysis of coronary artery wall in autopsy specimens. Radiology. 2004;231:675–681.

Appendix

The mould used for fabricating duo-layer graft

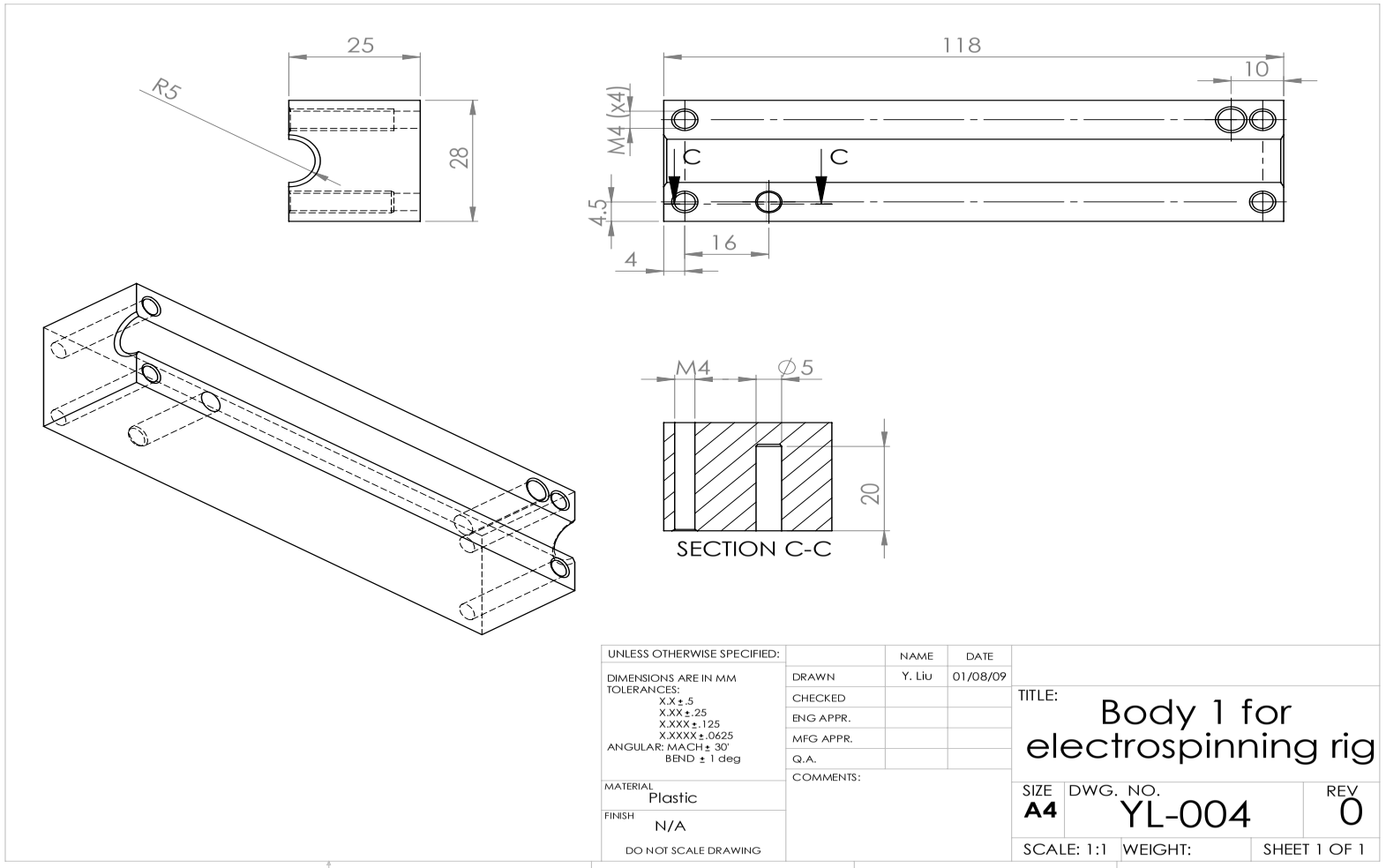
25
R5
28
118
10
M4 (X4)
C
C
4.5
16
4
M4
∅5
20
SECTION C-C
UNLESS OTHERWISE SPECIFIED:
DIMENSIONS ARE IN MM
TOLERANCES:
X.X ± .5
X.XX ± .25
X.XXX ± .125
X.XXXX ± .0625
ANGULAR: MACH ± 30'
BEND ± 1 deg
MATERIAL
Plastic
FINISH
N/A
DO NOT SCALE DRAWING
NAME
DATE
DRAWN
Y. Liu
01/08/09
CHECKED
ENG APPR.
MFG APPR.
Q.A.
COMMENTS:
TITLE:
Body 1 for electrospinning rig
SIZE
A4
DWG. NO.
YL-004
REV
0
SCALE: 1:1
WEIGHT:
SHEET 1 OF 1
5
4
3
2
1

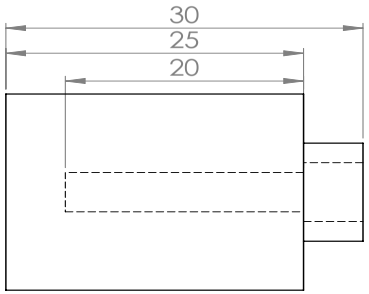

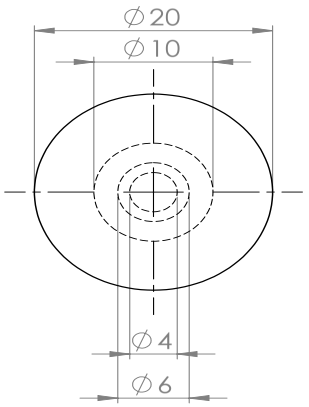

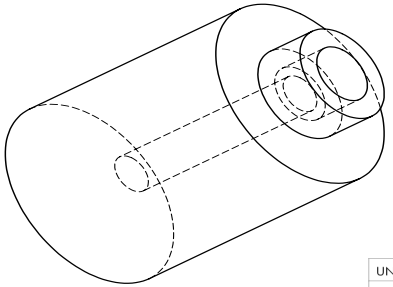

UNLESS OTHERWISE SPECIFIED:		NAME	DATE
DIMENSIONS ARE IN MM TOLERANCES: X.X ± .5 X.XX ± .25 X.XXX ± .125 X.XXXX ± .0625 ANGULAR: MACH ± 30' BEND ± 1 deg	DRAWN	Y. Liu	01/08/09
	CHECKED		
	ENG APPR.		
	MFG APPR.		
	Q.A.		
MATERIAL Plastic	COMMENTS:		
FINISH N/A			
DO NOT SCALE DRAWING			

TITLE: Cap 1 for electrospinning rig

SIZE	DWG. NO.	REV
A4	YL-002	0
SCALE: 1:1	WEIGHT:	SHEET 1 OF 1

5 4 3 2 1

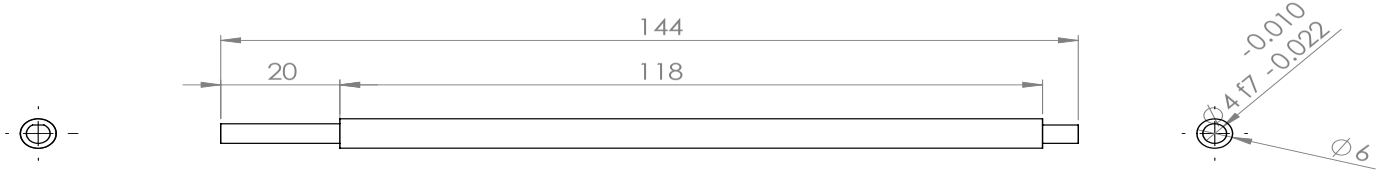

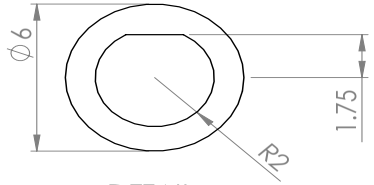

DETAIL
SCALE 5 : 1

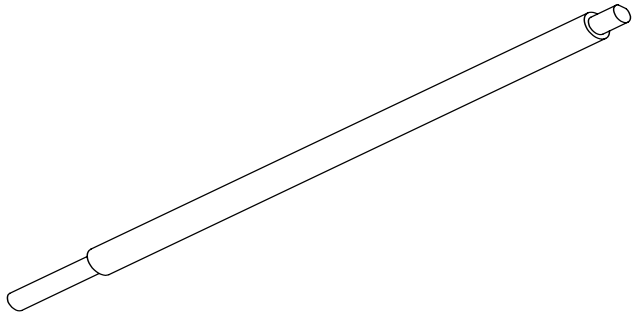

		NAME	DATE
UNLESS OTHERWISE SPECIFIED:			
DIMENSIONS ARE IN MM TOLERANCES: X.X ± .5 X.XX ± .25 X.XXX ± .125 X.XXXX ± .0625 ANGULAR: MACH ± 30' BEND ± 1 deg	DRAWN	Y. Liu	01/08/09
	CHECKED		
	ENG APPR.		
	MFG APPR.		
	Q.A.		
MATERIAL: Stainless steel	COMMENTS:		
FINISH: N/A			
DO NOT SCALE DRAWING			

TITLE: Drum for electrospinning rig

SIZE	DWG. NO.	REV
A4	YL-001	0
SCALE: 1:1	WEIGHT:	SHEET 1 OF 1

5 4 3 2 1